Local Self-Renewing of Microglia after Genetic Ablation is Dependent on Interleukin-1 Signaling

Dissertation

Zur Erlangung des Grades

Doktor der Naturwissenschaften

Am Fachbereich Biologie

Der Johannes Gutenberg-Universität Mainz

Vorgelegt von

Julia Bruttger

geb. am 14. Juni 1984 in Bad Kreuznach, Deutschland

Mainz, 2015

Tag der mündlichen Prüfung: __25.01.2016_____

Für Sven

Table of Contents

Abbreviations

BBB	blood brain barrier
BM	bone marrow
BM MΦ	bone marrow derived macrophages
BrdU	5-bromo-2'deoxyuridine
HSVTK	herpes simplex virus thymidine kinase
CNS	central nervous system
CSF-1	colony stimulating factor 1
CSF-1R	colony stimulating factor 1 receptor
Cx_3Cr1	CX3C chemokine receptor 1 or Fractalkine receptor
DE	differentially expressed
DT	diphtheria toxin
DTR^{MG}	diphtheria toxin receptor expression on microglia
E9	embryonic day 9 of development
EAE	experimental autoimmune encephalomyelitis
EMPs	eythromyeloid progenitors
ESC	embryonic stem cells
ETS	E-twenty six
FACS	flurescence activated cell sorting
FLT3	Fms-like tyrosine kinase 3
PDGFR	Platelet-derived growth factor receptor
KIT	tyrosine-protein kinase Kit
GCV	ganciclovir
HSCs	hematopoietic stem cells
Iba1	ionized calcium binding adaptor molecule 1
IL-1R1	Interleukin-1 receptor type 1
$IL\text{-}1R1^{MG}$	Interleukin-1 receptor type 1 conditional K.O. on microglia

IL-1RA	Interleukin-1 receptor antagonist
IL-12β	Interleukin 12-beta
IL-34	Interleukin 34
i.c.v.	intra-cerebro-ventricular
iDTR	inducible diphtheria toxin receptor
i.p.	intra-peritoneal
i.v.	intra-veneously
Irf8	interferon regulatory factor 8
Mac-1	macrophage-1 antigen or CD11b
MFI	mean Fluorescence Intensity
MS	multiple sclerosis
Myb	myeloblastosis oncogene
Nos2	inducible nitric oxide synthase 2
PCA	principle component analysis
PNS	peripheral nervous system
R26	Rosa-26 gene locus
Runx1	runt-related transcription factor I
TAM	tamoxifen
TGFβ1	transforming growth factor beta 1
YFP	yellow fluorescent protein
YS	yolk sac

1 Introduction

1.1 Microglia – the Link between Nervous System and Immune System

1.1.1 Glia Cells and the Central Nervous System

The human nervous system consists of the central nervous system (CNS) and the peripheral nervous system (PNS). The CNS is composed of the brain and spinal cord, whereas the PNS encompasses the nervous tissues outside of the CNS. The human brain is highly complex, consisting of approximately 1 x 10^{12} neurons, where one neuron can form as many as 1000 synaptic connections. This constitutes anything from simple motor controls to more sophisticated emotional and cognitive behavior. Supporting these functions, the spinal cord integrates responses to different types of stimuli that are conveyed to and from the brain. The PNS is essential for monitoring the internal environment, by relaying information to the CNS.

The term “Glia” was introduced by Rudolf Virchow in 1859 and implies “nerve glue”. It was believed that glial cells only serve as an agglutinative unit giving structural support. In fact, glia cells provide a much more crucial role in the CNS than just structural support. They outnumber the neurons by tenfold, maintaining the functionality of this intricate neuronal network in many different ways (Baumann and Pham-Dinh, 2001). Glia cells are divided into two groups: the macroglia consisiting of astrocytes, oligodendrocytes, and oligodendrocyte precursor cells, and the microglia (Fig. 1). Astrocytes supply neurons with nutrients from the blood circulation. They regulate the extracellular ion concentration, are capable of recycling neurotramsmitters (Miller, 2002) and they support synaptogenesis and the blood-brain barrier (Ballabh et al., 2004). Oligodendrocytes form the myelin sheath around the axons. In the CNS, one oligodendrocyte is able to myelinate up to 50 axonal segments (Bjartmar et al., 1994) whereas one Schwann cell in the PNS typically myelinates only a single axon (Salzer, 2003). During myelination the oligodendrocyte ensheaths the axon several times, resulting in electrical

insulation, thereby helping to accelerate the neuronal signal conduction. Nodes of Ranvier arise in between the single myelinated segments allowing the signals to jump from node to node (internodes) resulting in what is known as saltatory conduction. In contrast to their progeny, oligodendrocyte precursor cells are much less understood. Besides generating mature oligodendrocytes, they are the only known glial cells that can form functional synapses with neurons. The reason why they form these synapses is still elusive, but is believed to help maintaining neuronal network functionality (Trotter et al., 2010). Microglia are the smallest cells among the glial cells. They are CNS-resident myeloid cells that adopt various different functions. Robertson (1900) and Nissl (1898) were the first to report these cells, describing them as “rod cells” (“Stäbchenzellen” in German) because of their rod-like shape, and noting their accumulation near inflammatory lesions in the CNS. Robertson was also the first to describe the phagocytic function of microglia: using Scharlach Red and hematoxylin staining, he was able to visualize fatty degeneration products that most likely resulted from destroyed myelin and neurons inside microglia. In 1919, Pio del Rio-Hortega, a Spanish scientist considered by many to be “the father of microglia”, provided an exceptional visualization of nervous tissue by inventing the silver carbonate method. He was also the first to name these cells “microglia” or the “third element”. Del Rio-Hortega was not only capable of distinguishing microglia from oligodendrocytes and astrocytes, he also discovered their potential to change morphology from ramified to amoeboid under pathological conditions (Del Rio-Hortega, 1932; Kettenmann et al., 2011; Samokhvalov et al., 2007).

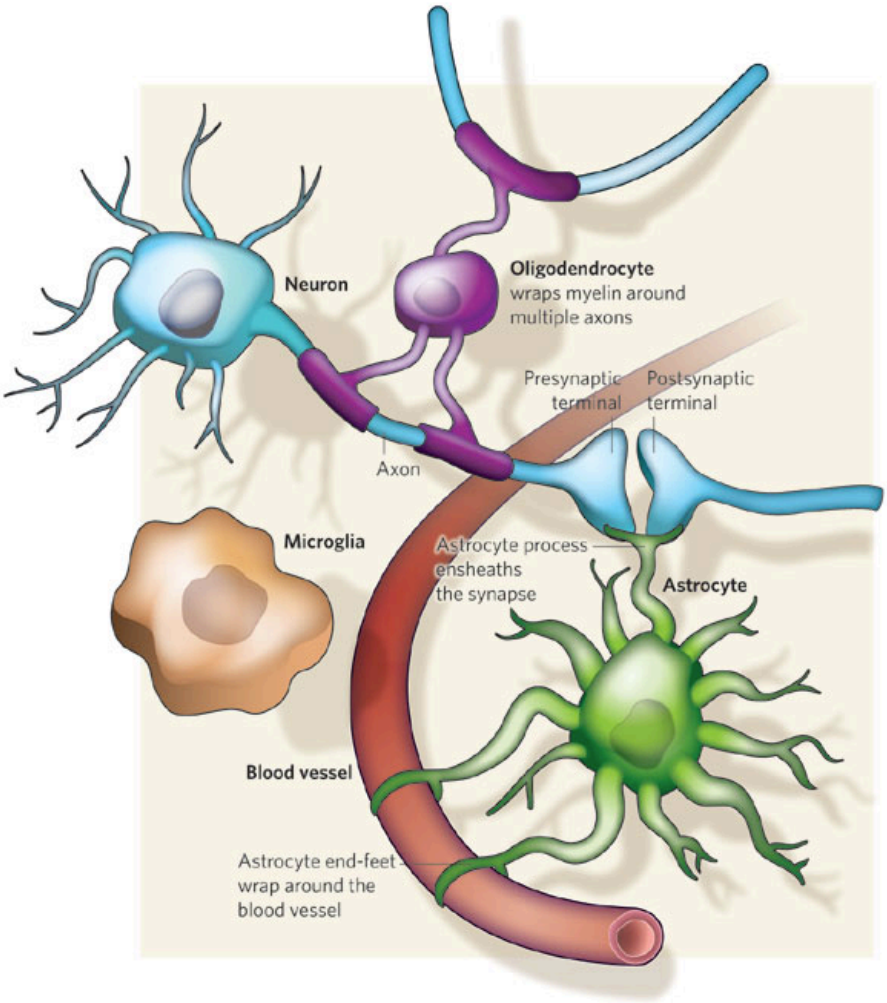

Figure 1 Glia- neuron interactions (Allen and Barres, 2009)
Different types of glia cells interacting with each other are shown. Neurons form synapses, which are controlled by astrocytes. On the other hand astrocytes are in contact with blood vessels. Oligodendrocytes form the myelin sheath by wrapping around the axons. Microglia survey the brain for damage or infection.

1.1.2 Microglia and their Role in the Immune System

Microglia, as tissue resident macrophages, have crucial roles in tissue homeostasis and immunity. They are the only immune cells present in the healthy CNS parenchyma and are thus the first responders to any environmental change. Under conditions of CNS tissue damage, such as bacterial or viral infections, microglia play a critical role in clearing debris, leading to restoration of the CNS homeostasis (Koizumi et al., 2007; Sierra et al., 2010). Microglia function not only as innate immune cells in pathological conditions, but they also maintain tissue integrity in non-inflammatory

conditions, such as secreting growth factors and anti-inflammatory molecules to helo in regeneration of damaged tissue (Davalos et al., 2005b; Kettenmann et al., 2011; Nimmerjahn et al., 2005; Prinz and Priller, 2014). It is clear that microglia are anything but “resting” in steady state: for immune surveillance they constantly extend and retract their processes to monitor their proximal environment for tissue damage or foreign invaders (Davalos et al., 2005a; Nimmerjahn et al., 2005). In addition, emerging data reveal new and fundamental roles for microglia in the control of neuronal proliferation, differentiation and maintaining neuronal network integrity in the form of supporting synaptogenesis/ synaptic pruning (Paolicelli et al., 2011). This way, microglia are involved in building up the neuronal network, especially during brain development, and are capable to engulf and clear malformed synapses.

1.2 Microglia - Factors on which they Depend on

In previous studies the role of microglia in development, maintenance and inflammation, among other aspects, has been analyzed. Various molecules, such as transcription factors, chemokines and their receptors and growth factors are involved in shaping microglial phenotypes (Fig. 2). The following chapter will summarize the published knowledge about microglia in health and disease accompanied by known key factors controlling microglial genesis and homeostasis.

Endogenous transcription factors play critical roles in microglia development. During embryogenesis, maturation and differentiation states of microglia are transcriptionally controlled by Runt-related transcription factor I (Runx1), interferon regulatory factor 8 (Irf8) and ETS (E-twenty six) family transcription factor PU.1 (Kierdorf and Prinz, 2013). Runx1 has a crucial role in definitive hematopoiesis since it is expressed early on by hematopoietic stem cells (HSCs) in the yolk sac (Ginhoux et al., 2010). Runx1 deficient mice completely lack HSCs and the deletion is embryonically lethal at the developmental stage E12.5. Runx1 is therefore considered as the major transcription factor driving the lineage of hematopoiesis, including microglia

development. However, the function of Runx1 in microglia homeostasis in the adult CNS is still elusive. Postnatal, it is responsible for regulating microglia proliferation and activation status (Zusso et al., 2012). Runx1 also interacts with the other myeloid specific factors PU.1 and IRF8. PU.1 is essential for adult myelopoiesis (Hoeffel et al., 2015) and is expressed on early microglial progenitors, but is dispensable for proper HSC development (Schulz et al., 2012b). PU.1 deficiency leads to a lack of B cells along with complete suppression of myeloid cells including tissue macrophages like Kupffer cells or microglia. Thus, PU.1-deficient mice die shortly after birth. Furthermore, a deletion of PU.1 leads to down-regulation of Irf8 (Kierdorf et al., 2013c). Additionally, PU.1 and Irf8 can act simultaneously as hetero-dimerization partners or Irf8 can function as downstream target of PU.1. However, there is no direct evidence if PU.1 is also involved in normal homeostasis of adult microglia.

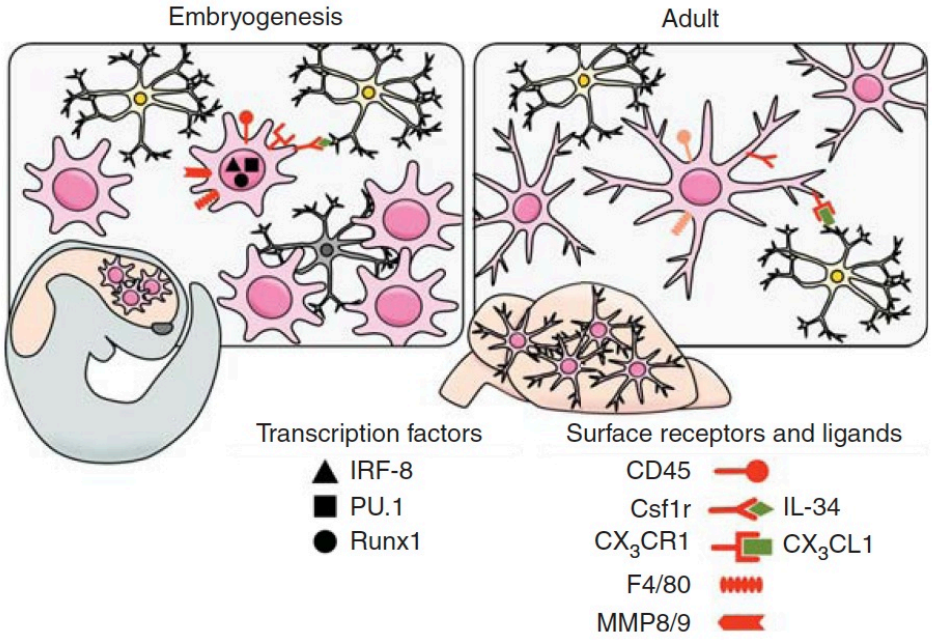

Figure 2 Markers and morphology of embryonic and adult microglia (Ginhoux and Prinz, 2015)
Embryonic microglia (left) show an activated and amoeboid phenotype. During adulthood microglia (right) exhibit small and delineated processes that actively survey the brain parenchyma. They also interact with local neighboring neurons. All transcription factors (black), receptors (red) and precursor stages are illustrated for each developmental stage.

The chemokine receptor Colony stimulating factor 1 receptor (CSF-1R) is a tyrosine kinase transmembrane receptor mainly expressed by myeloid cells including microglia. CSF1R-/- mice lack microglia and epidermal Langerhans cells (Ginhoux and Merad, 2010; Ginhoux et al., 2006), but also exhibit broad myelo-suppression, impacting peripheral cells including macrophages, HSCs, osteoclasts and mast cells (Cornelis et al., 2005). A ligand for CSF-1R is the colony stimulating factor 1 (CSF-1), which is a critical factor for the proliferation, differentiation and survival of myeloid cells (Greter et al., 2012). Mice with a frameshift mutation in the csf1 gene ($csf1^{op/op}$ mice) also display greatly reduced macrophage and monocyte populations in various tissues that lead to severe developmental deficits (Jenkins and Hume, 2014); the mutation also promotes disease phenotypes such as osteopetrosis (Dai et al., 2002). CSF-1 expression is influenced by many factors: irradiation increases its production, PU.1 acts as a repressor for CSF-1, and also Estrogen (Tamoxifen) leads to higher CSF-1 levels (Ginhoux and Jung, 2014). In contrast to CSF-1R-/- mice, the $csf\text{-}1^{op/op}$ mice only show slightly reduced microglia populations, suggesting the occurrence of another ligand for the receptor within the brain. This resulted in the discovery of Interleukin 34 (IL-34) as alternative ligand for the CSF-1R. Even though CSF-1 and IL-34 bind to different regions of the CSF-1R, they both promote comparable regulation of CSF-1R signaling. IL-34 binds with high affinity *in vitro* (Garceau et al., 2010) and can also promote survival and proliferation of human monocytes (Lin et al., 2008). In contrast to CSF-1, IL-34 is not involved in the embryonic development of microglia, but it influences microglial homeostasis in the adult. Still, IL-34 and CSF-1 do not completely phenocopy each other's expression, which may hint towards compensatory mechanisms between them (Wang et al., 2012).

Another important cytokine receptor expressed on microglia is the fractalkine receptor or Cx_3Cr1. Its expression is restricted to the macrophage population, therefore microglia are the only cells in the CNS that express Cx_3Cr1 (Jung et al., 2000). Its only known ligand, fractalkine or Cx_3CL1, is produced by neurons (Kim et al., 2011) and can be found in a membrane bound form or as

a secreted variant (Hughes et al., 2002; Kierdorf et al., 2013c). Cx_3Cr1 is often used as specific marker for microglia in the healthy CNS (Jung et al., 2000).

1.3 Development of Microglia

The precise origin of microglia and their precursors in embryonic development has long been a subject of debate. Pío del Río-Hortega discovered microglia in 1919 and proposed for the first time that microglia are of mesodermal origin and could possibly derive from meningeal macrophages infiltrating the brain during embryonic development (Del Rio-Hortega, 1932). Amoeboid microglia were detected in fetal mouse and rat brains early in development at E11.0 (Ashwell, 1990, 1991). The identification of embryonic Mac-1 $(CD11b)^+$ cells as microglial progenitors in the developing brain was further supported by their high proliferative potential in a CSF-1-dependent manner when plated on an astrocyte monolayer (Alliot et al., 1991). Concurrent with the establishment of embryonic circulation, macrophage-like cells were found in blood vessels and in the embryonic mesenchyme in rat embryos from E10.5 (Sorokin et al., 1992). Alliot *et al*. also described the appearance of microglia ($F4/80^+CD11b^+$ cells) in the brain rudiment of mice and rats even as early as E8.0 and their high proliferative capacity from E9.5 until 2 weeks postnatally (Alliot et al., 1999). At E9.5, CX_3CR1^+ cells were detected in the cephalic mesenchyme, which subsequently infiltrated the neuroepithelium at E10.5 (Mizutani et al., 2012). Strikingly, these microglia progenitors in the developing brain phenotypically resembled yolk sac (YS) macrophages (Alliot et al., 1999; Ginhoux et al., 2010; Mizutani et al., 2012). Altogether, these studies specified the early genesis of microglia in the developing brain that preceded the initiation of fetal liver and bone marrow (BM) hematopoiesis and was concurrent with the emergence of YS hematopoiesis (Waisman et al. 2015).

Early reports already proposed in 1999 that YS macrophages could be the progenitors of microglia. Pessac *et al*. documented the presence of potential microglial progenitors ($F4/80^+CD11b^+$) in the YS and adjacently in the brain rudiment, with their numbers increasing dramatically from E9.5 until two

weeks after birth (Alliot et al., 1999). In agreement with these studies, in zebrafish embryos, macrophage-like cells appeared at an early stage in the YS, before the emergence of other leukocytes, and subsequently colonized the cephalic mesenchyme (Herbomel et al., 1999). Only recently, with the advances of newly available fate-mapping models that allowed the tracing of YS progenitors, the unique ontogeny of microglia was definitely established (Ginhoux et al., 2010; Hoeffel et al., 2015; Kierdorf et al., 2013a; Schulz et al., 2012a). Ginhoux *et al*. used a lineage-tracing model to label YS progenitors including YS macrophages by making use of Runx1 transcription factor. With this inducible system, they could show that adult microglia arise unequivocally from YS macrophages that seed the mouse brain at E9.5, where they proliferate *in situ* and are maintained throughout adulthood (Ginhoux et al., 2010). Kierdorf *et al*. subsequently identified the precursors of the primitive YS macrophages/microglia. They found c-kit^{+} erythromyeloid progenitors (EMP) in the yolk sac at E8 that differentiated into CD45^{+}c-kit^{lo}CX$_3$CR1^{-} early precursors before their maturation and migration into the developing brain as CD45^{+}c-kit^{-}CX3CR1^{+} cells (Kierdorf et al., 2013b). More recently, Hoeffel *et al*. extended the characterization of YS EMPs and identified two waves of EMP that arise sequentially in the YS: an early wave of EMPs derived from primitive hematopoiesis that only differentiate locally in blood islands of the extra-embryonic YS and at a later wave of E8.5 EMPs derived from definitive hematopoiesis, which then either develop locally into YS macrophages or migrate to seed the fetal liver following the establishment of blood circulation from E9.0 (Hoeffel et al., 2015). These fetal liver precursors will eventually also generate adult hematopoietic stem cells in the BM. After E12.5, the fetal liver becomes the major hematopoietic organ during embryonic development (Ginhoux and Jung, 2014). However, this study clearly showed that all microglia arise from YS macrophages deriving during the early wave of EMPs.

In contrast to other adult or embryonic macrophage populations, the development of YS macrophages is unique in that these cells bypass a monocyte stage (Takahashi et al., 1989a, b). YS macrophages seed the brain and other tissues through the blood circulation, which develops gradually from

E8.5-E10 (McGrath et al., 2003). Notably, at this early developmental stage, the generation of monocytes and other myeloid cells in the fetal liver has not commenced (Naito et al., 1990). Thus YS macrophages constitute evidently an independent lineage and arise before the development of other myeloid cells that differentiate from definitive HSCs. This is also reflected by the fact that the development of YS macrophages is independent of c-Myb (Fig. 3), a transcription factor critical for HSCs and their progeny, but relies on the transcription factor PU.1, a transcription factor crucial for other tissue macrophages (Schulz et al., 2012b).

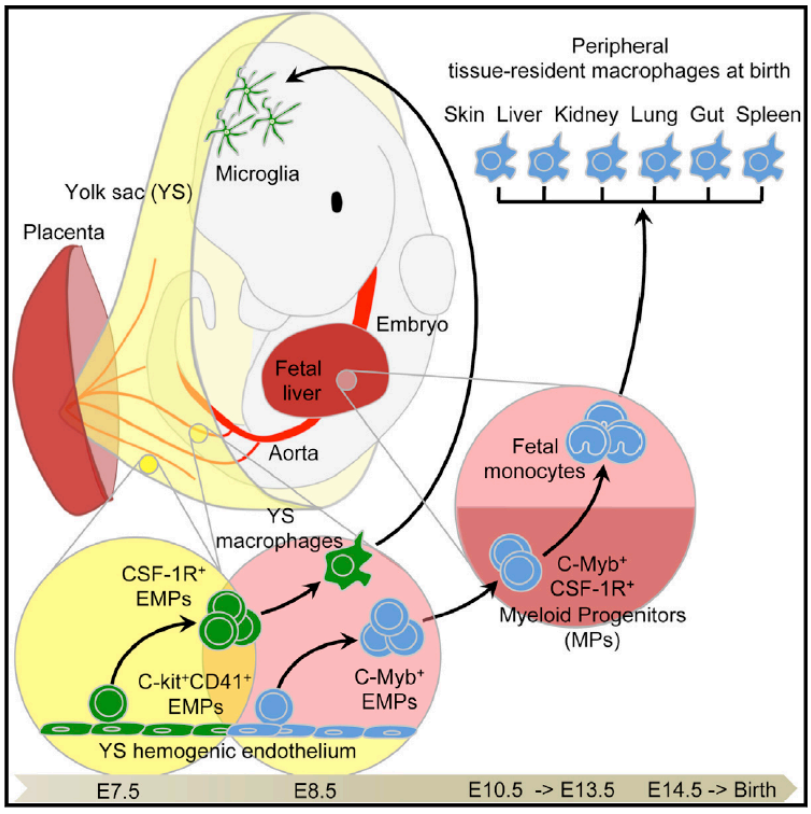

Figure 3 Microglia are unique tissue macrophages (Hoeffel et al., 2015) Other than most tissue macrophages microglia arise only from early yolk sac progenitors resulting from the first wave of primitive hematopoiesis (yellow circle). Fetal liver macrophages do not contribute tot he microglia

n steady state. Thereby microglia are CSF-1R dependent, but c-Myb independent.

It is important to note that microglia have a unique origin compared to other macrophages. Even though YS macrophages seed all tissues at mid-gestation in the developing embryo, they are not essential for the generation

of adult tissue-resident macrophages as they are later substituted by fetal monocytes that differentiate into tissue macrophages able to self-renew into adulthood (Hoeffel et al., 2015). The only exception is microglia. The reason for the absence of a fetal monocyte contribution to the microglial progenitor pool could lie in the lack of access to the developing brain. At around E13.5, when fetal monocytes start to colonize most embryonic tissues, there is only a negligible influx of fetal monocytes into the brain, which coincides with the formation of the blood brain barrier (BBB) (Daneman et al., 2010).

Under physiological conditions microglia self-renew locally independently of circulating peripheral precursors. Already at birth highly proliferative microglia are present in the CNS and are not replenished by a perinatal wave of myeloid progenitors (Ginhoux et al., 2010). Early studies describing macrophage-like cells in the developing embryo lead to the concept that microglia arise during embryonic development and seed the developing brain before birth. However, studies addressing microglia turnover during inflammation or after BM transplantation suggested that microglia could arise from BM-derived progenitors such as blood monocytes that infiltrate the inflamed brain.

1.4 Microglia Depletion as Research Model

The advantages and disadvantages of the various microglia ablation models will be discussed here. Microglia ablation systems allow studying their development, and their role during CNS homeostasis, and during neurodegenerative and neuroinflammatory conditions. Further, this system can be used to address the most important general questions: How important is the existence of microglia inside the adult CNS? Which main functions do they process throughout life span?

1.4.1 Full Deletion of Single Genes in Mice

Genetic models of microglia-deficient mice carrying mutations in genes critical for their development, such as PU.1, CSF-1R and transforming growth factor beta (TGF-β1) (Butovsky et al., 2014; Ginhoux et al., 2010; Kierdorf et al., 2013c), are not useful as these mice rarely survive into adulthood and have pleiotropic defects in organs other than the brain (McKercher et al., 1996; Scott et al., 1994). For example, in addition to the absent microglia, mice lacking CSF-1R exhibit severely reduced macrophage populations and display multiple developmental defects such as osteoporosis. In another example, TGFβ1-deficient mice display drastic changes in the development of microglia (Butovsky et al., 2014), but also develop multi-organ autoimmune disease at early age (Shull et al., 1992).

To circumvent such developmental defects, genetic tools and pharmacologic inhibitors have been used to successfully deplete microglia. Importantly, although effective depletion of microglia can be achieved with different depletion schemes, such depletion is only transient as microglia always reconstitute their own niche rapidly after being depleted.

1.4.2 Conditional Genetic Deletion Models

In 2005, a mouse line that allows the expression of a suicide gene out of the herpes simplex virus (HSV), the thymidine kinase (TK), under the myeloid specific promoter CD11b (Heppner et al., 2005) was generated. Treatment of these CD11b-HSVTK mice with ganciclovir (GCV) results in rapid elimination of $CD11b^+$ myeloid cells, including microglia. As elimination of all CD11b-expressing cells leads to rapid mortality in these animals, the authors used a BM chimera strategy where BM from wild type (WT) mice was grafted into irradiated CD11b-HSVTK host mice Alternatively, to circumvent massive BBB damage, they administered GCV intra-cerebroventricularly (i.c.v.). After two weeks 90% of microglia were depleted, but treatment also resulted in the

death of these mice, possibly due to the myelotoxicity of the GCV. In this model, peripheral $CCR2^{+}$ cells - most likely $Ly6C^{hi}$ monocytes - repopulate the microglia compartment within two weeks after treatment termination. Importantly, the i.c.v. treatment compromises the integrity of the BBB locally, also enabling peripheral cells to enter the brain parenchyma. Concomitant with the ablation, temporary astrocyte activation was reported, but neurons remained unchanged in terms of number and morphology (Grathwohl et al., 2009).

For a more specific *in vivo* manipulation of microglia, the *Cx$_3$Cr1^{creER}* animals were generated. CX_3CR1 is a chemokine receptor, which is highly expressed by microglia. Importantly, this Cre recombinase is tamoxifen-inducible, which allows for microglia-specific targeting: even though CX_3CR1 is also expressed by other myeloid cells and precursors in the BM (Geissmann et al., 2010), Cre expression is lost over time in the short-lived CX_3CR1^{+} myeloid cells in contrast to the long-lived and self-renewing microglia, that exhibit permanent recombination (Goldmann et al., 2013; Yona et al., 2013). For microglia ablation, the *Cx$_3$Cr1^{creER}* were crossed to the inducible diphtheria toxin receptor (iDTR) mice, resulting in *Cx$_3$Cr1^{creER}:iDTR* mice. Using the iDTR strain in another model to deplete oligodendrocytes, we were able to show that diphtheria toxin (DTx) can pass through the BBB (Buch et al., 2005; Gritsch et al., 2014; Locatelli et al., 2012). The advantage of this new mouse model is that DTx can be injected intra-peritonially and one can omit the preparation of BM chimeras and therefore avoid BBB damage. The disadvantage of this system is that it requires the use of tamoxifen (TAM). Treatment of mice with TAM may lead to an immunomodulatory phenotype as shown by the suppression of the autoimmune disease experimental autoimmune encephalomyelitis (EAE) (Elloso et al., 2005), however, our previous studies showed no such direct effect (Yogev et al., 2012). Like others, I was able to show a specific and long-lasting recombination in microglia in *Cx$_3$Cr1*^{CreER} reporter mice (Goldmann et al., 2013; Yona et al., 2013). Here, I will examine the depletion efficiencies using the *Cx$_3$Cr1^{creER}*: iDTR system (Fig. 4) and the consecutive tissue response to microglia ablation.

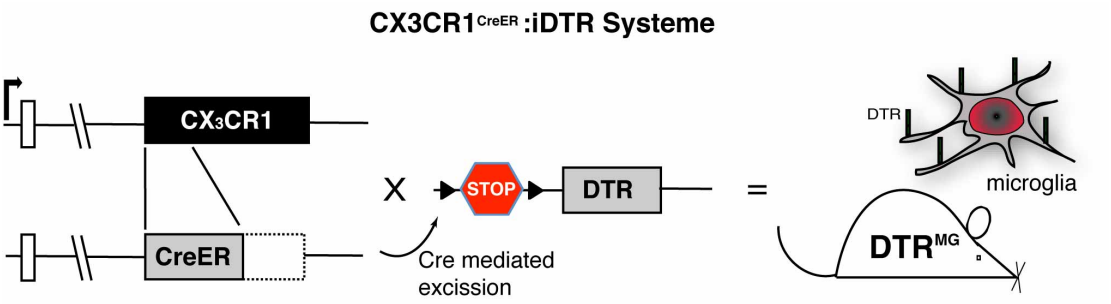

Figure 4 Cx_3Cr1^{creER}:iDTR System (adapted from (Yona et al., 2013))
The activation of the inducible Cx_3Cr1^{creER} with TAM leads to a Cre- mediated excision of the STOP cassette upstream of the diphtheria toxin receptor (DTR). After 6 weeks the receptor is expressed on microglia surface specifically.

1.4.3 Pharmacological Treatment for Microglia Ablation

Next to genetic depletion, there are also other possibilities to ablate microglia in the CNS. Pharmacological treatment of mice with a reagent inhibiting CSF-1R signaling (PLX3397) resulted in ~99% ablation of microglia. Nevertheless, stopping the treatment was followed by a fast repopulation of microglia within 5 days (Elmore et al., 2014). This model was used to study the source of the repopulating microglia. Two days after termination of treatment, it was found that CNS intrinsic microglia precursors transiently expressed the neural marker *nestin*, and gave rise to new microglia in the brain parenchyma.

1.5 Aim of the Study

Microglia are known as the CNS resident macrophages that have important functions such as tissue maintainance, phagocytosis of cellular debris and immunesurveillance. However, the mechanisms by which microglia fulfill their functions still remain elusive, most likely due to the lack of markers and tools to specifically target microglia. The Cx_3Cr1^{CreER} mouse line, published for the first time in 2013 (Yona et al., 2013), pioneered the way for microglia specific targeting. The iDTR system in combination with the Cx_3Cr1^{CreER} allows for the microglia specific ablation upon Dtx administration in adult mice *in vivo*.

In this thesis I will test the microglia ablation efficiency and, consequently, the impact of the depletion on tissue integrity and the self-maintenance of microglia. The objectives of this thesis are three fold: studying microglia replacement in adult mice; exploring potential microglial progenitors and clarifying the need for microglia within the CNS. Furthermore, I hope to discover additional microglia functions, which could be manipulated, to reduce the severity of CNS-related inflammatory diseases.

2 Materials and Methods

2.1 Chemicals and Biological Material

Chemicals (Table 1) were purchased from Fluka Chemie (Switzerland), Carl Roth (Karlsruhe), AppliChem (Darmstadt), Sigma-Aldrich (Steinheim) or Merck Millipore (Darmstadt) unless stated otherwise. Solutions were prepared with double destilled water (ddH_2O).

Soultions and chmicals used in cell culture were produced sterile by working under a sterile hood (Heraeus, Germany).

Name of chemical	Supplier
β-Mercaptoethanol (β-ME)	Fluka Chemie GmbH, Switzerland
Acetone	Merck Millipore, Darmstadt
Agarose, electrophoreses grade	Biozym LE Agarose, Hess. Oldendorf
Bovine serum albumine (BSA)	Sigma-Aldrich, Steinheim
BromodesoxyUridin (BRDU)	Sigma-Aldrich, Steinheim
Calcium chloride	Sigma-Aldrich, Steinheim
Chloroform	Merck Millipore, Darmstadt
Citric acid	Fluka Chemie GmbH, Switzerland
Diethylpyrocarbonate (DEPC)	AppliChem, Darmstadt
Dithiothreitol (DTT)	AppliChem, Darmstadt
dNTPs	Pharmacia Biotech, USA
Ethanol, abs.	AppliChem, Darmstadt
Ethidium bromide	Sigma-Aldrich, Steinheim
Ethylendiamine tetraacetate (EDTA)	Fluka Chemie GmbH, Switzerland
Fetal calf serum (FCS)	Boehringer Mannheim GmbH, Mannheim
Ficoll 400	Amersham Pharmacia, Freiburg
Glacial acetic acid	Fluka Chemie GmbH, Switzerland

Hydrochloric acid (37%)	Merck, Darmstadt
Isopropanol	AppliChem, Darmstadt
Magnesium chloride	Sigma-Aldrich, Steinheim
Magnesium chloride **Natrium Chlorid**	Sigma-Aldrich, Steinheim
Olive Oil	MP Biomedicals,
Percoll	Sigma-Aldrich, Steinheim
Potassium acetate	Fluka Chemie GmbH, Switzerland
Potassium chloride	Merck Millipore, Darmstadt
Proteinase K	Roche, Switzerland
Red Taq	Sigma-Aldrich, Steinheim
Sodium azide	Fluka Chemie GmbH, Switzerland
Sodium chloride	AppliChem, Darmstadt
Sodium citrate	Fluka Chemie GmbH, Switzerland
Sodium dodecyl sulfate	AppliChem, Darmstadt
Sodium hydrogencarbonate	Fluka Chemie GmbH, Switzerland
Sodium hydroxide	Fluka Chemie GmbH, Switzerland
Tamoxifen	Sigma Aldrich, Steinheim
Tris base	Fluka Chemie GmbH, Switzerland
Tris/ HCl	AppliChem, Darmstadt

Table 1: Chemicals

2.2 Molecular Biology

2.2.1 Isolation of Genomic DNA

Tail biopsy (0,1 cm) or cells were lysed over night (o/n) at 56°C in lysis buffer (10 mM Tris-HCl, pH 8; 10 mM EDTA; 150 mM NaCl; 0.2% (w/v) SDS; 400 mg/ml proteinase K). After cooling down to roomtemperature, an equal volume of isopropanol was added, mixed by inverting and centrifuged with full speed to precipitate the DNA. The Pellet was washed with 70% (v/v) EtOH, again precipitated and air tried to get rid of residual EtOH. DNA was finally

resuspended in water or TE buffer (10 mM Tris-HCl, pH 8; 1 mM EDTA) and solved at 56°C for 1 hour.

2.2.2 Polymerase Chain Reaction (PCR)

PCR was used to screen mice for the presence of targeted alleles or transgenes, which are detected with specific primer (Table 2) to amplify fragments for sequencing. The REDTaq®Ready Mix™ PCR Reaction Mix (Sigma-Aldrich) was used as cycling reagent and the reactions were performed in either the T3000 Thermocycler (Biometra, Göttingen, Germany) or the Primus96 mashine (PEQLAB, Erlangen, Germany) with the annealing temparatures mentioned in the Table 2 below.

Name of primer	Sequence (5'-3')	$T_{Ann.}$° C	Direction
Universal Cre fw	GGA CAT GTT CAG GGA TCG CCA GGC G	58°C	sense
Universal Cre rev	GCA TAA CCA GTG AAA CAG CAT TGC TG	58°	anti-sense
Actin fw	TGT TAC CAA CTG GGA CGA CA	58°C	sense
Actin rev	GAC ATG CAA GGA GTG CAA GA	58°C	anti-sense
CX3CR1cre fw	CCT CTA AGA CTC ACG TGG ACC TG	58°C	sense
CX3CR1cre rev wt	GAC TTC CGA GTT GCG GAG CAC	58°C	anti-sense
CX3CR1cre spec rev	GCC GCC CAC GAC CGG CAA AC	58°C	anti-sense
Rosa26 FA	AAA GTC GCT CTG AGT TGT TAT	60°C	sense
Rosa26 RA	GGA GCG GGA GAA ATG GAT ATG	60°C	anti-sense
Rosa26 SpliAcB	CAT CAA GGA AAC CCT GGA CTA CTG	60°C	anti-sense
IL-1R1 32	CTAGTCTGGTGGAACTTACATGC	58°C	sense
IL-1R1 33	AACTGAAAGCTCAGTTGTATACAGC	58°C	anti-sense

Table 2: Primer for PCR

2.2.3 Agarose Gel Electrophoresis

Agarosegels were prepared in percentage of 0.8% - 2% (w/v) in 1x TAE buffer with the DNA intercalating substance ethidium bromide (0.5 mg/ml). In a

gelelectrophoresis the DNA fragments were separated by size, which were compared to the GeneRuler 100bp Plus DNA Ladder (Thermo Scientific).

2.2.4 RNA Isolation

RNA was either prepared from whole brain tissue using the TRIzol reagent (Invitrogen), Lysing Matrix D tubes (MP Biomedicals) and a tissue ruptor (MP FastPrep®-24), or was prepared from FACS-sorted microglia with the RNeasy® Plus Micro Kit (Qiagen) following manufacturer's guidelines.

2.2.5 Quantitative Real Time PCR

cDNA was synthesized out of 200- 1000ng of RNA using SuperscriptII (invitrogen). Quantitative Realtime PCR was messured in an AB StepOnePlus Real Time PCR "Thermocycler" (life technologies™) with using SYBR green (Qiagen). All Primers were purchased from Qiagen, as described on their homepage: http://www.qiagen.com/products/pcr/quantitect/primerassays.aspx.

2.2.6 Next Generation Sequencing

The different microglia samples were FACS sorted (FACS Aria) and immediately centrifuged down for 15 min and 400 x g. RNA was isolated with the RNeasy® Plus Micro Kit (Qiagen) according to the manufacturer's instructions. RNA amounts were measured by Q-bit 2.0 fluorometer (Life Technologies) and the quality was assessed on a Bioanalyzer (Agilent) using a High sensitivity chip. Samples with a RNA integrity number (RIN) > 8 were used for library preparation with TrueSeq® RNA Sample Prep v2 Kit (Illumina) according to the manufacturers' manual. Library size distribution was assessed on a Bioanalyzer 2100 using a High Sensitivity DNA Chip (Agilent). Sequencing was performed on a MiSeq using a MiSeq Reagent Kit v3 resulting in resulting in 8 - 14 million reads per sample.

2.3 Cell biology

2.3.1 Preparation of Single Cell Suspension from CNS Tissue

Mice were anesthetized and perfused with NaCl and organs were excised out. Brains were either fixed with 4% of PFA for histology, were snap frozen in liquid nitrogen for RNA preparation, or were digested according to manufacturer's guidelines supplied in the MACS tissue dissociation kit Papain (Miltenyi Biotec). The tissue homogenate was loaded on a 30:70% Percoll gradient for enrichment of CNS infiltrates.

2.3.2 Cell Counting

Cells were counted with a Neubaur cell counter and total cells numbers were calculated according to manufactorers guidelines.

2.3.3 Flow Cytometry

Specificity	Clone	Supplier
Biotin Lineage Kit	145-2C11; RA3-6B2; RB6-8C5; M1/70; TER-119	BD Pharmingen (#559971)
CD11b	M1/70	eBioscience (#25-0112)
CD45	104	eBioscience (#17-0454)
CD86/B7.2	GL1	Pharmingen (#553691)
F480	BM8	eBioscience (#12-4801)
GR1	RB6-8C5	BD Bioscience (#553129)
Ly6C	AL-21	BD Bioscience (#560594)
MHCII	M5/114.15.2	eBioscience (#12-5321)
SA- APC-ef780		eBioscience (#47-4317)

Table 3: FACS antibodies

Single-cell suspensions for Fluorescence-activated cell sorting (FACS) were stained with surface antibodies purchased from eBioscience, BD Pharmingen or Biolegend and used according to the manufacturer's protocol. Samples were acquired with FACS Canto II and sorted with FACS AriaII.

2.3.4 Magnetic Cell Sorting and FACS Sorting

Distinct cell populations were sorted from homogenous cell suspensions by magnetic cell sorting (MACS; Miltenyi Biotec, Bergisch Gladbach, Germany). In principle, all cells of a population were labeled with specific antibody-coupled microbeads (10 µl beads, 90 µl PBS/0,5% BSA per 10^7 cells) and separated on MS MACS columns in a magnetic field. In FACS sorting the cells are labeled wih flurochrome-coupled antibodies that are detectected by the lasers of a FACSAriaII (BD) and sorted into 15 ml falcons according to the marker expression.

2.4 Histological Analysis and Immunohistochemistry

For vibratome sections, tissues were fixed over night with 4% PFA and embedded in 2% agarose and cut sagittally at 40μm. The sections were stained aver night with primary antibodies (Table 4) to iba1 (rabbit, Wako), GFP (rabbit, abcam), GFAP (rabbit, DAKO), BrdU (mouse, Roche). After washing with PBS the sections were incubated with secondary antibodies (Table 5) for 1 hour at room temperature. The TSA^{TM}-Kit Cyanine 3 System (Perkin & Elmer) was used to enhance the staining intensity, when needed. TUNEL Assay (Roche) was performed according to manufactorers guidelines. For DAB stainings Biotinylated antibodies were used, which were coupled to Horseradish preoxidases (HRPs) according to Table 4 below. DAB was supplied by Sigma (#D5905). And slices were embedded in Vectahield containing Dapi (Vector). Images were acquired with a Zeiss sp5 or sp8 confocal microscope or an Olympus ix81 fluorescence microscope and further processed with ImageJ64 and Adobe Illustrator CS4. For 3D reconstructions, at least 20 stacks were takenin a range of 20mm in a 63x magnification.

Primary antibodies	specificity	Supplier (Cat. No#)
BrdU (α- mouse)	1:500	Roche (#11170376001)
CD11b (α- rat)	1:200	Abcam (#ab8879)
Gfap (α- rabbit)	1:400	DAKO (#20334)
GFP (α- rabbit)	1:5000	Abcam (#ab6551)
Iba (α- rabbit)	1:500	WAKO (#019-19741)
Il-1R1 (α- mouse)	1:400	Abcam (#ab115497)
Ki67 (α- rat)	1:50	DAKO (#7249)
Ki67 (α- rabbit)	1:800	Abcam (#ab16667)
MHCII (α- rat)	1:100	BD (#556999)
NeuN (α- mouse)	1:1000	Chemicon (#MAB377)
Nestin (α- rat)	1:100	Millipore (#MAB353)
Olig2 (α- mouse)	1:200	Millipore (#MABN50)
TUNEL Enzyme	1:10	Roche

Table 4: Primary antibodies

Secondary antibodies	dilution	Supplier (Cat. No#)
α -mouse IgG Alexa488	1:200	Jackson (#115-545-166)
α -rabbit IgG Cy3	1:200	Jackson (#111-165-144)
α -rabbit IgG Cy5	1:200	Jackson (#705-175-147)
α -rat IgG DyLight488	1:200	Jackson (#112-545-167)
Biotinylated α -rabbit IgG	1:400	Vector (#BA-1000)
Streptavidin Cy3	1:200	Jackson (#016-160-084)
Streptavidin HRP	1:400	Vector (#SA-5004)

Table 5: Secondary antibodies

2.4.3 Quantification of Histology

The images were counted blind by two independent people. 20 randomly depicted 20x fields per animal and at least three mice per group were analysed.

2.5 Mouse Experiments

All general handling of mice was performed according to Hogan (Hogan et al., 1987) and Silver (Silver 1995).

2.5.1 Mice

$CX_3CR1^{creERT2}$ (Yona et al., 2013) were bred to iDTR mice (Buch et al., 2005) and R26-YFP reporter mice(Srinivas et al., 2001). All mice were on C57BL/6 background and housed in specific pathogen-free conditions in the animal facility at the University of Mainz. All animal experiments were in accordance with the guidelines of the Central Animal Facility Institution (ZVTE, University of Mainz).

2.5.2 Tamoxifen Treatment

Tamoxifen (TAM; Sigma) was suspended on 37°C in olive oil (MP Biomedicals). 2 mg Tamoxifen was administered s.c. twice on postnatal days 12 and 14.

2.5.3 Diphtheria Toxin Treatment

For microglia depletion, mice were injected intraperitoneally (i.p.) with 500ng diphtheria toxin (DT; Merck Millipore) twice, with a day interval.

2.5.4 Antibody Treatment

The α-CCR2 blocking antibodies (MC-21) and isotype control antibodies (MC-67) were used over five days with one injection of 25 μg a day.

2.5.5 BrdU Feeding

Prior to depletion mice were fed with 0,6 mg BrdU (Sigma) in the drinking water throughout the whole depletion time course.

2.5.6 Intracerebroventricular Treatment with IL-1RA

Mice were anesthetized with i.p. injections of Ketamin (40 mg/kg) and Xylazin (5 mg/kg) and secured in a small animal stereotaxic frame (Kopf instruments). The injection side of the brain was cleaned and opened sorrowful. A small hole was drilled into the scull proximal to the injection side. A stainless-steel guide cannula (11 mm, 24-gauge) was inserted into the third ventricle (2.5 mm post bregma, 3 mm deep). 4 μg of IL-1RA in a total volume of 2 μl was slowly injected into the ventricle over the time of 2 min. To reduce pain the mice were injected with 4mg/kg of Rimadyl®.

2.5.7 Bone Marrow Transplantation

DTR^{MG} mice were lethally irradiated with 9,5 Gray and reconstituted with 5 x 10^6 BM cells from R26-YFP mice (which were crossed to the deleter-Cre so that all BM cells expressed YFP) or C57Bl/6 Ly 5.1 donor animals. Mice were analyzed as detailed in the main text and figure legends.

2.5.8 EAE Induction

Active EAE was induced by immunization with MOG35-55 peptide (amino acid sequence: MEVGWYRSPFSRVVHLYRNGK). The emulsion contains 50μg of the peptide mixed with complete Freud's Adjuvance (CFA) and with 8 mg/ml of *Mycobacterium tuberculosis* H37RA (both supplied by Difco Laboratories, Detroit, Michigan, USA). The mice were immunized subcutaneously into the tail base with 100 μl of the emulsion. They also received 200 ng of Pertussis toxin (Sigma Aldrich, Steinheim, Germany) intraperitoneally on day 1 and day 3 of immunization. Clinical scores of EAE were assessed daily according to the following criteria: 0, no disease; 1, decreased tail tone; 2, partial paralysis or weakness of hind limb; 3, partial hind limb paralysis; 4, full hind limb paralysis: 5, additional paresis of the fore limbs; 6, moribund or dead.

2.6 Bioinformatic Analysis

2.5.9 Statistics

Statistical analysis was performed with Prism Graph Pad (Version 5.0b) and the statistical environment R (Version 3.0.2). The unpaired Student's t test was used and all bar graphs are represented as means ± SD, and significance is expressed as follows: *, $p<0.05$; **, $p<0.01$; ***, $p<0.001$.

2.5.10 NGS Data Anlysis

RNA-sequencing experiments were carried out with the Illumina MiSeq machine, according to manufacturer's instructions. Quality control of the sequenced reads (single end, 51 bp long) was performed with the FastQC tool (http://www.bioinformatics.babraham.ac.uk/projects/fastqc). After inspecting the reports, the raw data have been subject to a quality-filtering step with the fastq_quality_filter tool (http://hannonlab. cshl.edu/fastx_toolkit/, parameters used -Q33 -q20 -p90 -v).

Short reads alignment was performed with UCSC mm10 chosen as the reference genome. The indexes and annotation files were retrieved from Illumina iGenomes (http://cufflinks.cbcb.umd.edu/igenomes.html).

The TopHat gapped aligner version 2.0.10 (combined with Bowtie2, version 2.1.0.0) was run on the input files. Mapping rates were reported between 94 and 96% of the raw reads.

The aligned files were processed with the htseq-count tool (http://www-huber.embl.de/users/anders/HTSeq/doc/count.html), using the annotation file we also used for supporting the alignment. The parameters used are --mode=intersection-strict --stranded=no.

The Bioconductor DESeq package version 1.14.0 was used to perform the differential expression analysis. To fully model the sequencing experimental design, the framework of generalized linear model was adopted for the analysis. MA plots show the comparisons of the three different microglia populations. The raw counts for the genes are normalized by the size factor corresponding to each library size as in the DESeq normalization method, and

then for each gene a combination of M-A values (M = log2 fold change, A = average) is derived and plotted. The False Discovery Rate threshold was set to 0.05 for the entire analysis. The three contrasts between available conditions (BM-originated VS control, BM-originated VS CNS-derived and CNS-derived VS control) generated sets of 4060, 2658 and 711 DE genes, respectively.

Independent filtering was performed on the count table provided as input to DESeq, and the threshold chosen was set according to the databased method developed in the HTS-Filter Bioconductor package (Rau et al., 2013). Sample clustering and principal component analysis (PCA) were performed on the Variance Stabilized Transformed data, after library size normalization as in the DESeq package. The chosen similarity metric was the Euclidean distance. PCA was performed using the 1000 genes showing the highest variability across samples. A permutation test was used to test for differences between distances among the conditions at level 0.05. The test statistic was chosen as the difference of the mean values of the Fisher-transformed correlation coefficients between control samples and, respectively, repopulating microglia and monocyte-derived microglia.

Heatmaps show the standardized Z-score (across samples) for the considered genes. Hierarchical clustering based on the Euclidean distance was applied to the samples and to the genes

3 Results

3.1 Targeting Microglia with the CX_3CR1^{CreER} System

Microglia originate from yolk sac-derived progenitors and seed the developing brain during embryogenesis (Ginhoux et al., 2010; Kierdorf et al., 2013c) Though this developmental aspect of the origin of microglia is understood, controversy still remains as to what extent and from which sources microglia are maintained and replenished in the postnatal steady state. Homeostatic turnover rates of microglia are rather small (Lawson et al., 1992), but some studies suggest that under pathological conditions new microglia are able to arise from BM-derived precursors (Varvel et al., 2012). Because of the specific experimental conditions involved, the interpretation of these findings remain controversial (Ajami et al., 2011)'(Mildner et al., 2007). To better understand the origin of microglia and their self-renewing potential, we used a recently developed mouse line, in which a tamoxifen (TAM)-inducible Cre-recombinase is expressed under the control of the *Cx3cr1* promoter (CX_3CR1^{CreER} mice) (Yona et al., 2013). In order to specifically manipulate microglia cells, but not other cells of the myeloid linage that express CX_3CR1, we took advantage of the inducible nature of the system. When activated by TAM, nuclear translocation of the CreER fusion protein is only transient and recombination occurs only for a limited time period. If cells are analyzed at a later time point, only long-lived cells (e.g. microglia) will still carry Cre-mediated mutations, whereas short-lived cells (e.g. monocytes) will be replaced by non-mutated progenitors (Goldmann et al., 2013). In order to test

the system, CX_3CR1^{CreER} mice were crossed to the YFP reporter strain (Srinivas et al., 2001) and the resulting mice were injected twice with TAM at the age of two weeks, as shown in Figure 5A. Following this treatment, almost all microglial cells expressed eYFP (Fig. 5B), while monocytes/macrophages isolated from blood, BM or spleen did not (Fig. 5C) (Bruttger et al., 2015)

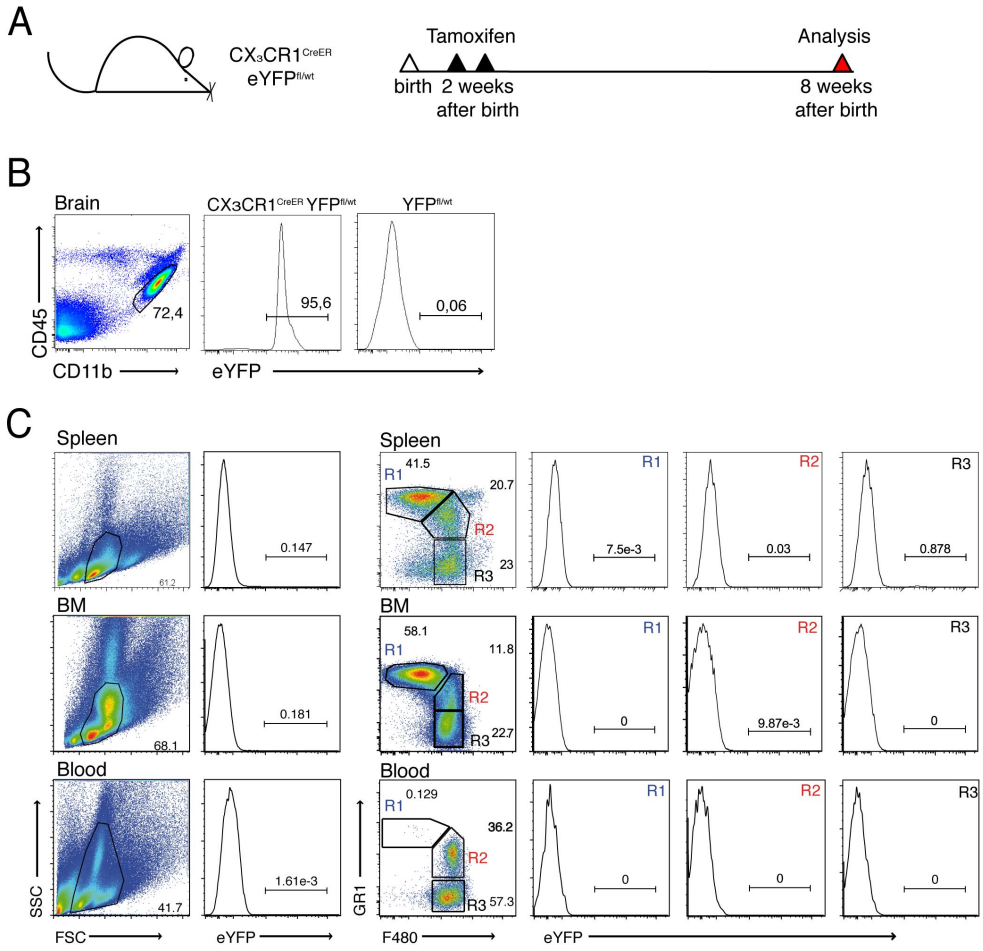

Figure 5: Microglia specific targeting (adapted from (Bruttger et al., 2015))

(A) scheme showing schedule of injection (B) eYFP expression in microglia (C) no eYFP expression in peripheral organs visible

3.1.1 Microglia are Efficiently Depleted using the CX_3CR1^{CreER} System

To employ this system for specific microglia ablation, we crossed CX_3CR1^{CreER} mice to iDTR mice (Buch et al., 2005), generating DTR^{MG} mice. Cre-mediated recombination was also induced in DTR^{MG} mice by TAM injections of two-week-old mice, leading to surface expression of the diphtheria toxin receptor (DTR) by microglia (Fig. 6A). For cell depletion, DTR^{MG} mice were treated with three injections of diphtheria toxin (DT) at the age of eight weeks (white triangles Δ), resulting in around 80 % depletion of microglia three days after DT injection (red triangle Δ), as we could quantify with the Iba1 expression by histology (Fig. 6B and 6C) (Bruttger et al., 2015). Similarly, when analyzed by flow cytometry, we found a significant reduction in the number (total event counts) of $CD45^{int}CD11b^{+}$ microglia cells, both in the brain and spinal cord (Fig. 6D) indicating that the system allows efficient microglia ablation.

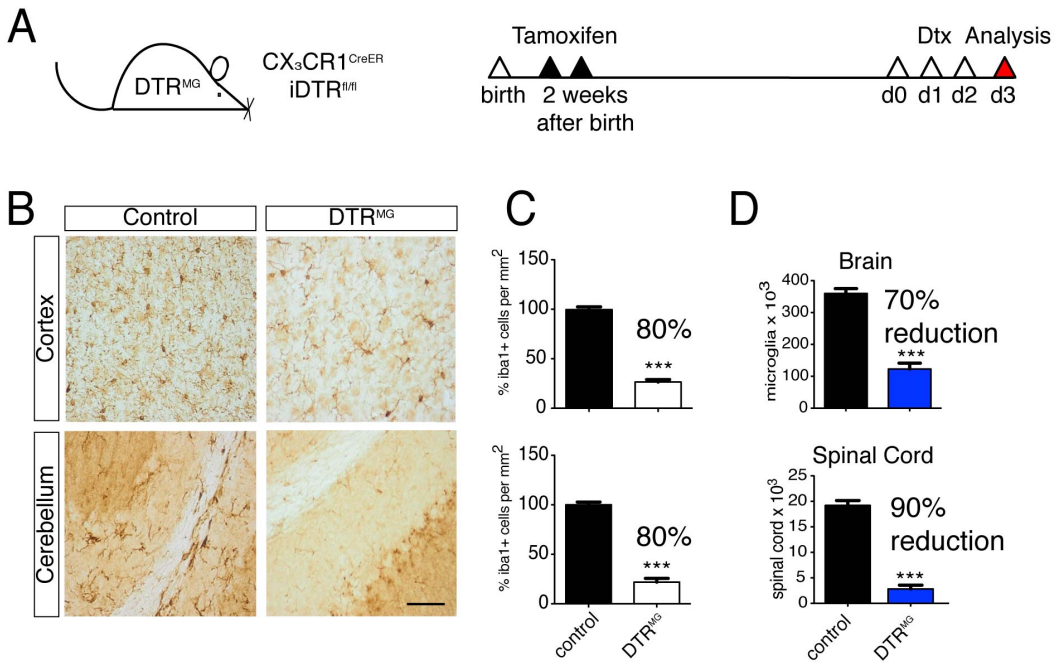

Figure 6: Microglia ablation in a genetic model

(A) scheme for mouse crossing and schedule of injection. Mice are injected 3 times with 500ng Diptheria Toxin (Dtx), each injection was 24 hours appart (B) Iba-1 staining on 40 μm thick vibratom sections (C) Total cell counts (±SEM) of Iba-1+ cells are shown in a bar graph (D) Statistical analysis of total cells counts of $CD45^{int}$ and $CD11b^{hi}$ cells messured by FACS.

3.1.2 Microglia Ablation is Followed by Rapid Repopulation

To complete the evaluation of our microglia ablation scheme, we extended the analysis to days 3, 7 and 14 after the first DT injection (Fig. 7A). We isolated mononuclear cells from brain and spinal cord and analyzed them for the expression of CD45 and CD11b. Microglia are typically characterized as $CD45^{int}$ $CD11b^{+}$ cells, and can be distinguished from infiltrating monocytes/macrophages that express higher levels of CD45 (Ford et al., 1996). However, it has also been reported that once activated, microglia up-regulate CD45 expression, thereby impeding discrimination from macrophages by flow cytometry (Zhang et al., 2002). As described above (Fig. 6B and 6C), DTR^{MG} mice showed a drastic reduction of microglia at day 3

after DT injection (Fig. 7B and 7C). Of note though, the majority of mononuclear cells were microglia, suggesting that the qualitative flow cytometric analysis failed to reveal the full extent of microglia ablation. Instead, quantitative analysis of total cell counts from the microglia gate confirmed a depletion rate of around 80% at day 3 when compared to TAM- and DT-treated control mice (Fig. 7C). When analyzing mice at day 7 after DT application, we noted that a large number of $CD11b^+$ cells in the CNS were $CD45^{high}$, identifying either activated microglia or infiltrating monocytes (Bruttger et al., 2015). However, from day 7 onwards, the total cell number of $CD11b^+$ cells was very similar to that seen in controls (Fig. 7B and 7C). At d14 after DT injection, the numbers of $CD11b^+$ cells, as well as CD45 expression were restored almost to control levels (Fig. 7B-D). CD11b mRNA expression levels measured in whole cortex homogenates mirrored the flow cytometry results

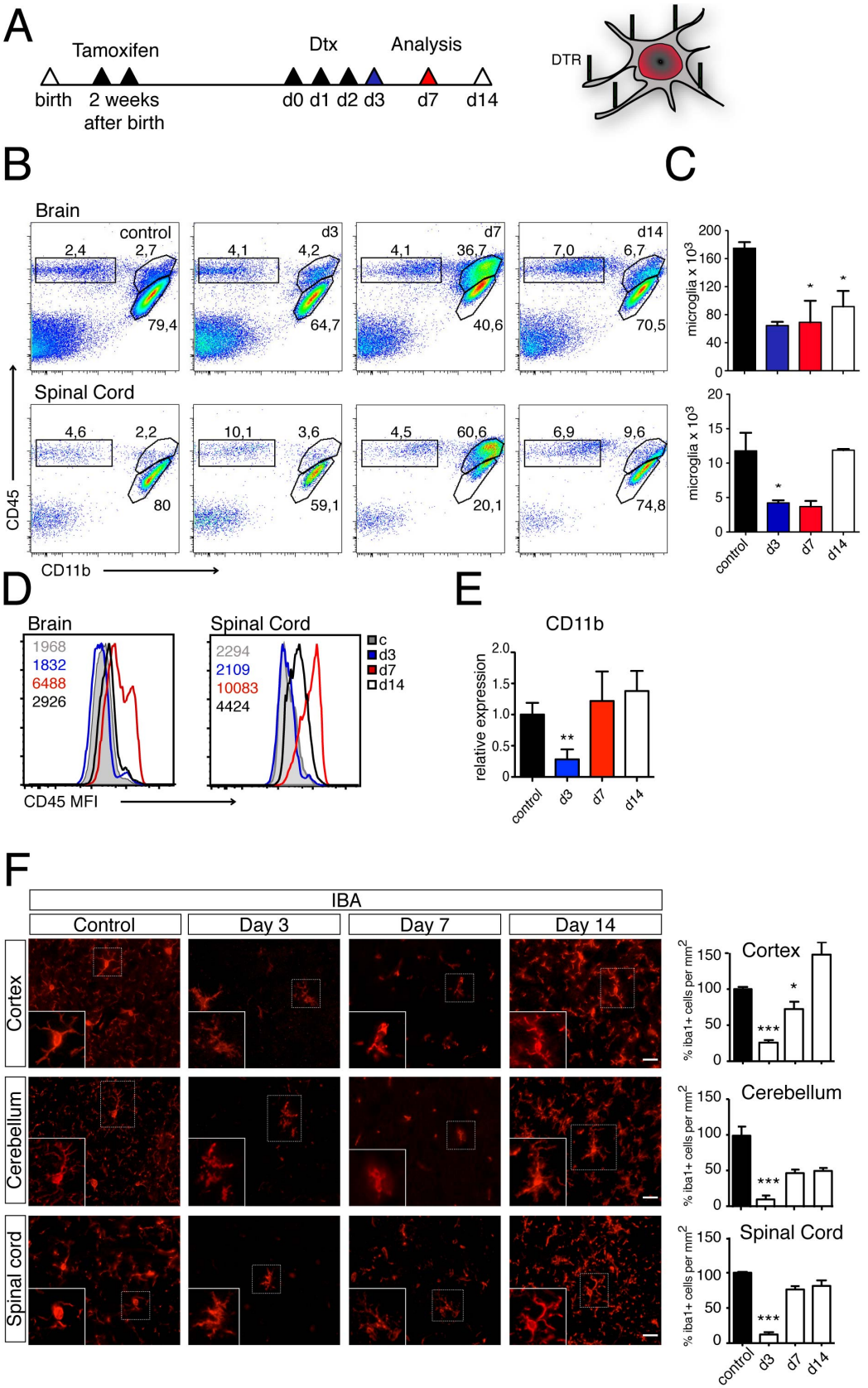

Figure 7: Timecourse of microglia ablation and repopulation (adapted from (Bruttger et al., 2015))

(A) scheme showing the strategy for microglia ablation (B) Representative FACS plots of the brain (upper row) and spinal cord (lower row) are depicted for time course depletion. Dead cells were excluded with a live cell marker and debris by size. (C) The bar graphs depicting total cell counts (±SEM) within the $CD45^{int}$ $CD11b^{hi}$ microglia gate. (D) Control: black bars; day 3: blue bars; day 7: red bars and d14: white bars. A histogram overlay of the mean fluorescence intensity (MFI) of CD45 expression for all time points. (E) mRNA was purified from cortex homogenate and the expression of *cd11b* (±SEM) was quantified by real time PCR relative to the expression of *hprt*. (F) Histological analysis using Iba1 specific antibodies. An example of each time point is shown for Cortex, Cerebellum and Spinal cord (left panel). Scale bars = 20μm. The bar graphs represent the % of iba1+ cells per mm^2 (±SEM) for each region on each time point (right panel). See also Figure S2. Statistical significance (unpaired Student's t test) is indicated as *$p < 0.05$, **$p < 0.01$, and ***$p < 0.001$.

3.1.3 Microglia Depletion Leads to Self Activation, Astrogliosis and Cytokine Storm

The depletion of microglia does not occur without any visible reactions of the cells themselves or of their sourronding environment. Looking closer into the microglia population ($CD45^{int}CD11b^{hi}$) by flow cytometry on days 3 and 7 after DT injection, a higher expression of MHC class II and CD86 was detected (Fig. 8A and B). And also immunohistological analysis of MHC class II and $Iba1^{+}$ cells showed several double possitive cells (Fig. 8C), indicating the activation of the remaining microglia (Bruttger et al., 2015).

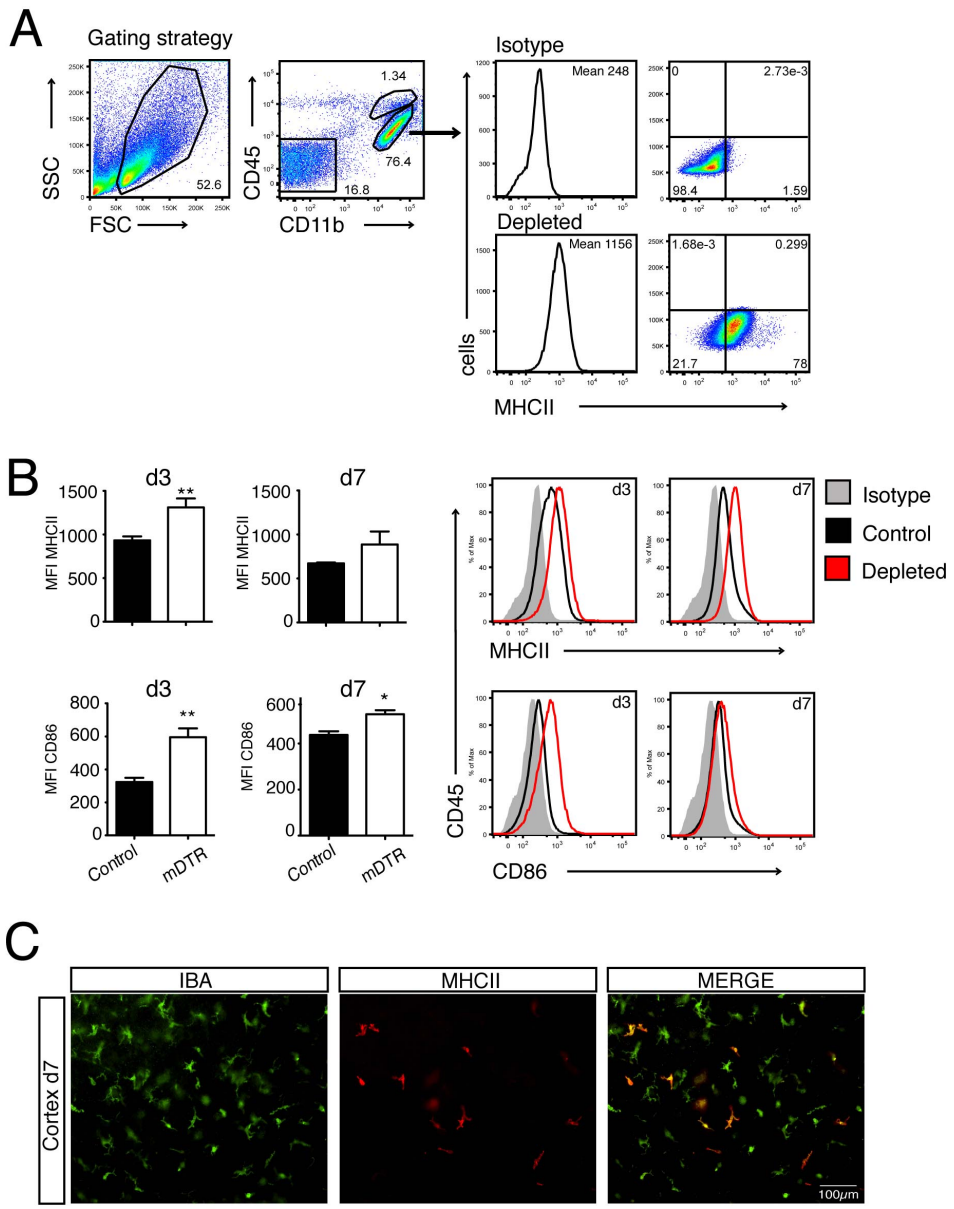

Figure 8: microglia ablation leads to severe side effects in the brain (adapted from (Bruttger et al., 2015))

A) gating strategy for activated microglia analyzed by flowcytometry showing the co-expression of MHCII and CD86 (B) The MFIs (±SEM) of MHCII (upper panel) and CD86 (lower panel) are summarized in the bar graphs for day 3 and day 7 after ablation. Histogram overlays represent one sample for each group in the right panel. The isotype control os shown in gray, the control in black and depleted in red. (C) Immunohistochemical costainings for MHCII and iba1 on day 7. Iba1 in green, MHCII in red and the merge. Scale bars = 100μm.

Not only the microglia themselves showed a response to their ablation, but also the other neighbouring cells inside the CNS were perturbed. Astrocytes

started to upregulate GFAP throughout the depletion time course (Fig. 9A). The mRNA levels of GFAP are significantly elevated on day 3 and continue to rise to a ten fold expression on d14 (Fig. 9C). On the protein level the GFAP expression is significantly changed on day 7 and 14, especially in the cortex and brain stem (Fig. 9A). The quantifications of total GFAP+ cell counts also reflected a significantly higher expression of GFAP (Fig. 9B) (Bruttger et al., 2015).

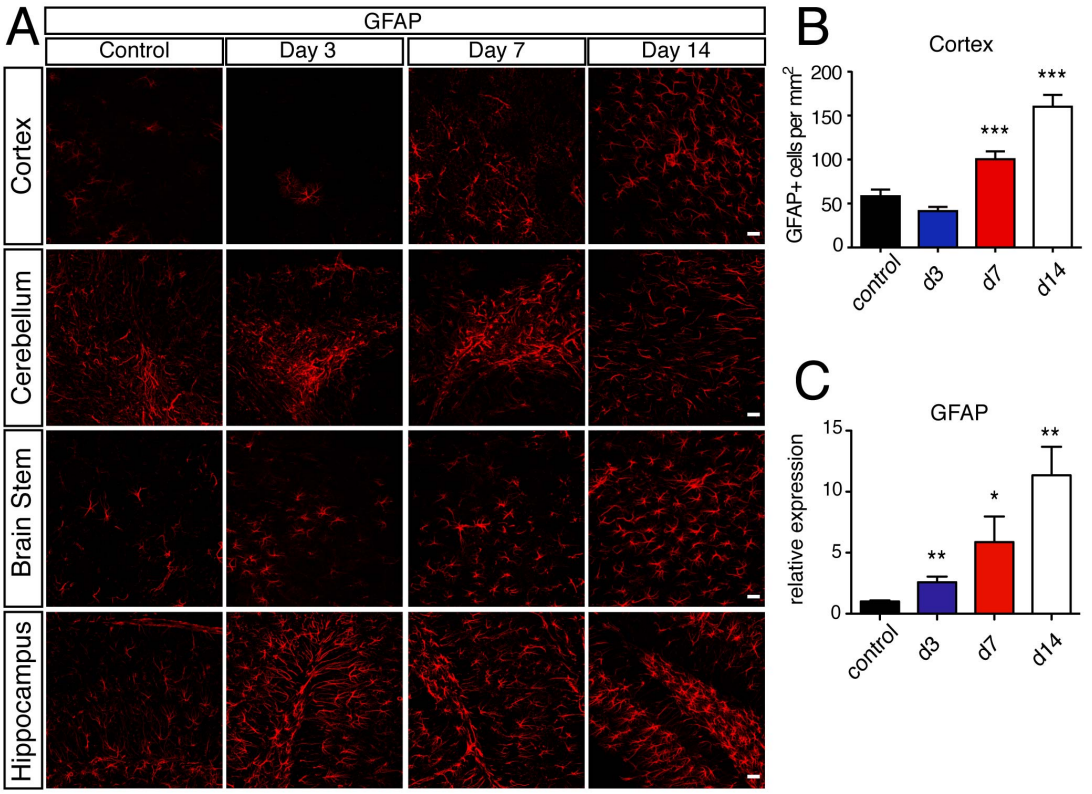

Figure 9: tissue response to microglia ablation (adapted from (Bruttger et al., 2015))

(A) Representative pictures of confocal microscopy of GFAP fluorescence at different time points (control, day 3, day 7 and day 14) for four different brain regions: cortex, cerebluum, brain stem and hippocampus. Scale bars = 20 μm. (B) The total number of GFAP expressing cells in 1 mm^2 (±SEM) of the cortex was determined. The GFAP expression increases significantly on day 7 (2-fold) and on d14 (3-fold). (C) mRNA was extracted from homogenates of the cortex and the relative expression (±SEM) of GFAP was measured normalized to HPRT. A significant increase of GFAP mRNA levels is detectable already on day 3 after depletion and rises constantly over time. Statistical significance (unpaired Student's t test) is indicated as *$p < 0.05$, **$p < 0.01$, and ***$p < 0.001$.

The massive microglia cell death in this genetic model provokes changes in the CNS environment. We detected increased mRNA levels of proinflammatory cytokines, such as TNFα and IL-1β, and chemokines, like CXCL9/10 and CCL2/5/7, and costimulatory molecules in the cortex of microglia depleted animals at all indicated timepoints (Fig. 10). These findings establish that other CNS resident cells, in particular astrocytes, react to the ablation-induced environmental changes inside the CNS (Bruttger et al., 2015).

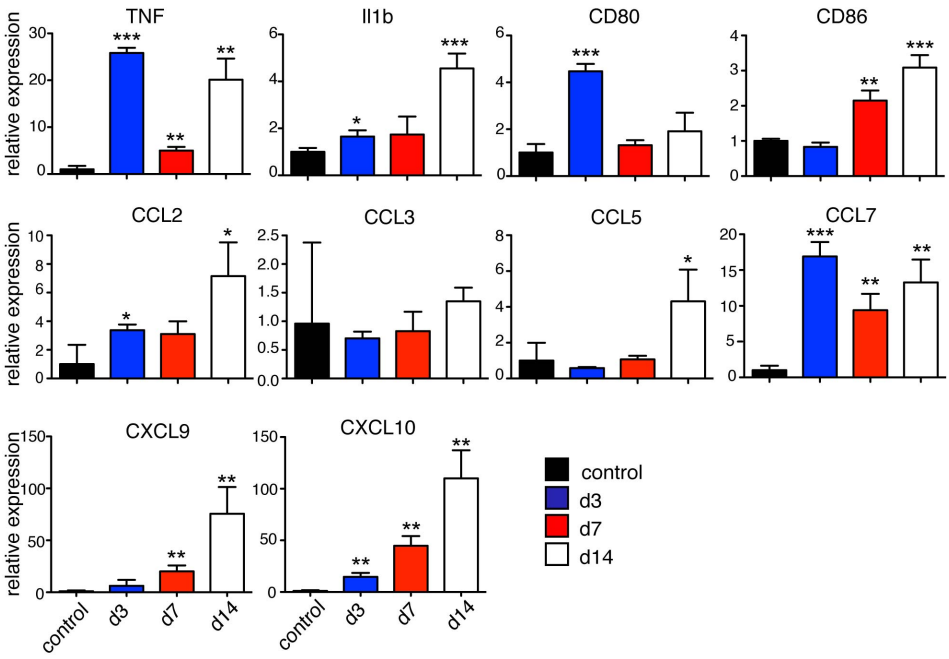

Figure 10: Cytokine storm - dramatic upregulation of proinflammatory cytokines (adapted from (Bruttger et al., 2015))

(A) mRNA was purified from cortex homogenate and the expression (±SEM) of different cytokines, chemokine's and activation markers were quantified by real-time PCR relative to the expression of HPRT (Control: blackbars, day 3: blue bars, day 7: red bars and d14: white bars). Statistical significance (unpaired Student's t test) is indicated as *$p < 0.05$, **$p < 0.01$, and ***$p < 0.001$.

3.2 BM-derived Macrophages Contribute to the Microglia Pool in BM Chimeric Mice

To determine if repopulating brain macrophage originate from a CNS-resident internal pool or from peripheral sources, we employed the DTR^{MG} mice in a BM chimeric system. Lethally irradiated DTR^{MG} mice that had undergone TAM-induced Cre recombination/ DTR expression (Fig. 11A) were reconstituted with BM from eYFP reporter mice (Srinivas et al., 2001). In the resulting mice, the radio-resistant host microglia can be ablated by toxin application and BM-derived peripheral cells can be detected according to their YFP label. Interestingly, following DT treatment of the BM chimeras, all cells in the microglia gate (Fig. 11D and 11F) expressed the YFP transgene (Bruttger et al., 2015).

3.2.1 Cells with BM Origin Repopulate the CNS

Of note an intravenously engrafted BM cell suspension can seed the brain with early hematopoietic precursors without the involvement of a monocyte intermediate (Mildner et al., 2007). We therefore also specifically assessed contributions of monocytes by treating one group of animals with α-CCR2 antibodies (MC-21) following DT injections. This regimen, which depletes circulating $Ly6C^{+}$ monocytes and thus prevents their entry to the brain, as shown in the context of autoimmune CNS inflammation (Mildner et al., 2009), was not sufficient to hinder repopulation. Although the α-CCR2 treatment was effective in itself and $Ly6C^{hi}$ blood monocytes were efficiently ablated (Fig. 11B), the depleted microglia in the CNS were still replaced by BM

macrophages. Treatment with α-CCR2, however, did not alter the percentage (Fig. 11E) or total numbers (Fig. 11C) of monocytes or microglia in the CNS when analyzed 7 days after DT injection. Regardless of whether the mice were treated with α-CCR2 regimen, the majority of microglia expressed YFP (Fig. 11D and 11F) and hence are derived from peripheral BM progenitors (Bruttger et al., 2015).

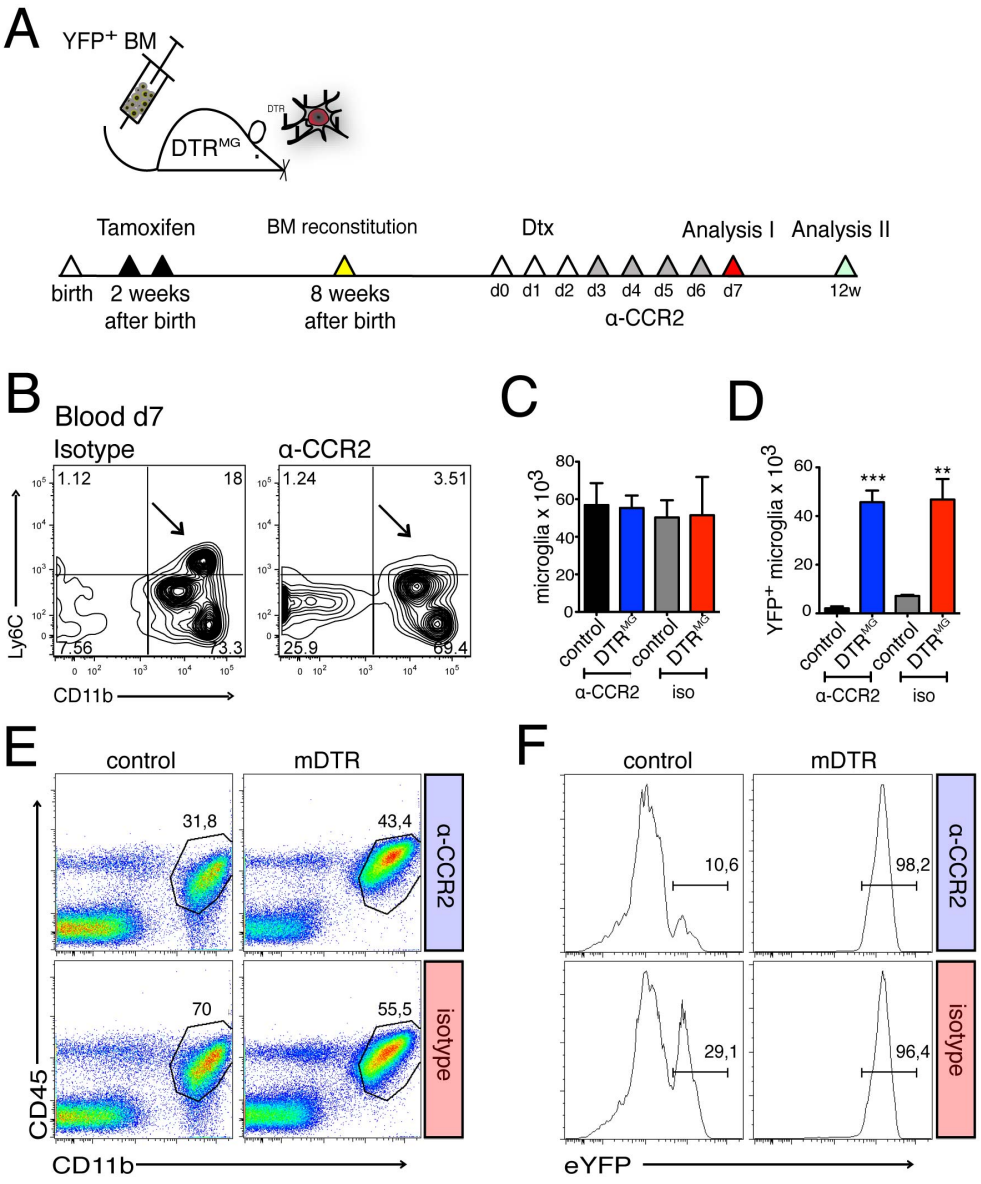

Figure 11: In a BMC model microglia are replaced by bone marrow macrophages (adapted from (Bruttger et al., 2015))

(A) The time scake indicates the required injections for BM reconstitution, microglia depletion and α-CCR2 (clone: MC-21) treatment (B) FACS plots of blood cells are shown for a-CCR2 treated animals in comparison to Isotype treated animals. The existance of CD11b+Ly6Chi monocytes in the blood of animals, pregated on B220- and CD3- cells, are analyzed on day 7 after depletion. (C) The bar graphs of total event counts (±SEM) summarize all FACS results. α-CCR2 treated mice are represented in blue, littermate controls in black, isotype treated animals in red and isotype treated controls in gray bars. (D) Total event counts (±SEM) of $eYFP^+$ cells are summarized according to c. (E) homogenates from DTR^{MG} and control mice at day 7 post-depletion and treated with α-CCR2 or with isotype control antibodies were analyzed by FACS. Representative FACS plots for CD11b and CD45 are shown. (F) Representative histograms showing eYFP expression for the different groups described in e. Statistical significance (unpaired Student's t test) is indicated as *$p < 0.05$, **$p < 0.01$, and ***$p < 0.001$.

3.2.2 BM Macrophages Can Replace Microglia over Long Timeperiod

Looking at a later timepoint in the BM chimeric mice, at 12 weeks after microglia ablation (Fig. 12A), when the brain was fully repopulated, most brain macrophages remained YFP^+ no matter if we analyzed by FACS (Fig. 12B) or Immunohistochemistry (Fig. 12C and 12D). The cells of donor BM origin seem to populate the CNS permanently and possibly take over microglia functions. Finally, we analyzed the distribution of these BM-derived brain macrophages. As can be seen in Figure 12, few YFP^+ cells were detected in control chimeras that did not undergo the ablation (Fig. 12C). When analyzing the cortex by Iba-1 staining (Fig. 12D), we found a normal distribution of microglia in DT-treated non-DTR transgenic control chimeras, while DT-treated DTR^{MG} mice showed less process-forming brain macrophages at day 7. In contrast, the CNS of DTR^{MG} mice largely resembled WT CNS in terms of distribution and morphology of $Iba1^+$ cells at 12 weeks post depletion (Bruttger et al., 2015). Of note the Iba1 staining does not discriminate between microglia and BM-derived brain macrophages. However, similar data were obtained when the sections were analyzed for eYFP expression (Fig. 12C). Other regions such as cerebellum and brain stem showed similar reconstitution kinetics.

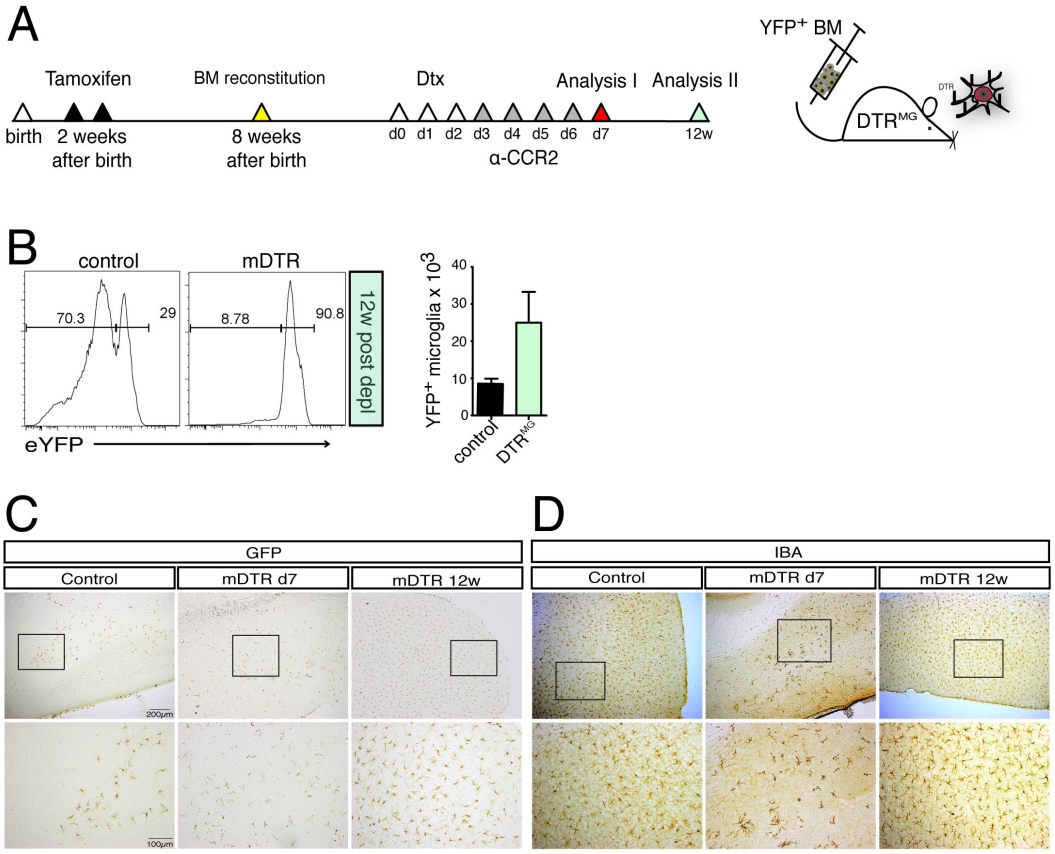

Figure 12: BM macrophages replace the microglia niche over long timeperiod (adapted from (Bruttger et al., 2015))

(A) The time scale indicates the required injections for BM reconstitution, microglia depletion and α-CCR2 treatment. (B) DTR^{MG} mice and controls were reconstituted with $eYFP^+$ BM. After microglia depletion mice were allowed to recover for 12w and brains analyzed by FACS. Cells were pre-gated as $CD11b^{hi}CD45^{int}$. One representative plot displaying eYFP expression is shown. Bar graphs show total cell counts (±SEM) of $eYFP^+$ cells. (C) Brain sections are shown for controls, DTR^{MG} day 7 and DTR^{MG} 12w, stained with antibodies specific to eYFP (left) or Iba1 (right). Two magnifications of the cortex are shown. Scale bars=200μm (upper panel) and 100μm (lower panel). All statistical significance (unpaired Student's t test) is indicated as $*p < 0.05$, $**p < 0.01$, and $***p < 0.001$.

3.2.3 HSCs Can be Excluded as a Peripheral Source of Microglia

Uncommited hematopoetic Stem Cells (HSCs) are the very early progenitor of microglia during development and they were shown to be a possible source for longterm microglia replacement in the context of EAE (Ajami et al., 2011). In order to test wether the HSCs also contribute to the microglia pool after ablation, we took advantage of the DTR^{MG} + eYFP reporter mice whose

microglia do not only express the DT receptor on their surface, but also express YFP upon cre mediated excision of the Stop cassette upstream of the YFP gene. On day 3 after ablation of the microglia according to our normal injection pattern (Fig. 6A), we injected the mice each with 10.000 FACS sorted RFP+ HSCs ($lin^- sca\text{-}1^+ c\text{-}kit^+$) intravenously (Fig. 13A). Indeed, after 28 days we were able to track back RFP^+ cells in the BM compartment (Fig. 13B), whereas we failed to find any RFP^+ cells inside the brain (Fig. 13C). In the CNS, we could exclusively find YFP^+ microglia (Bruttger et al., 2015).

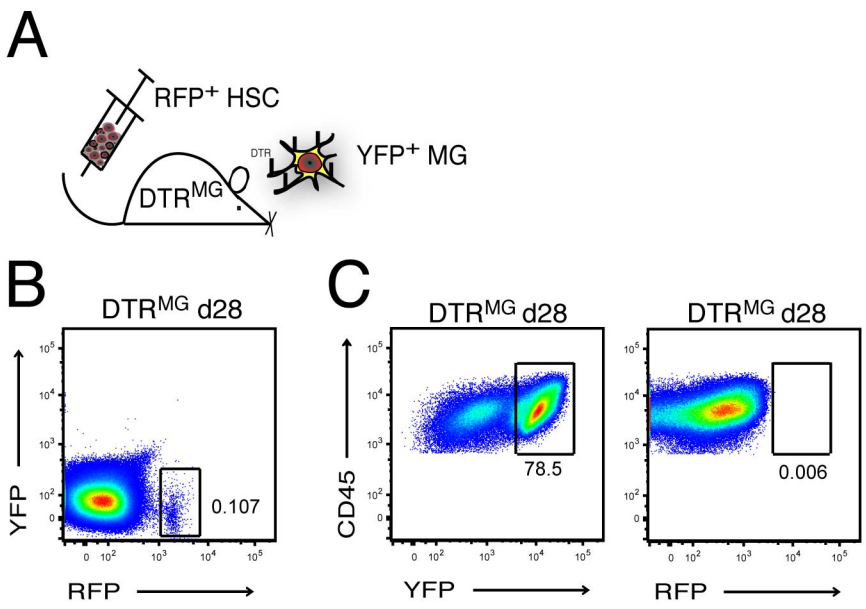

Figure 13: Hematopoetic stem cells can be excluded as microglia progenitors

(A) schematic picture of the injected RFP+ BM cells in DTR^{MG} mice (B) 8 weeks after depletion and consecutive injection of RFP+ BM the RFP+ cells can still be found in the BM of those animals (C) The microglia compartment only consist of YFP+ and YFP- cells, but no RFP signal can be found in the CNS.

3.3 In Absence of Irradiation Microglia Renew Exclusively from Internal Pools

To circumvent the inherent experimental pitfalls of the BM chimeras (Lampron et al., 2012), we next crossed the DTR^{MG} mice to R26-STOP-eYFP reporter mice (Srinivas et al., 2001), resulting in animals that harbor, following TAM injection, microglia that express both eYFP and DTR (Fig. 14A). As shown in Fig. 14B for the cortex, we detected significantly less $eYFP^+$ and $IBA\text{-}1^+$ microglia at day 3 after ablation, whereas by day 7 the cell number as well as the morphologic appearance of these cells reached similar levels to the control animals. Additional flow cytometrical analysis complemented the immunohistological data (Fig. 14C-D). Kinetics of microglia depletion and reconstitution corroborated the earlier experiments (Fig. 14C and 14D). Interestingly, the proportion and absolute numbers of eYFP expressing cells were increased at day 7, indicating that microglia were repopulated from CX_3CR1-positive ($eYFP^+$) cells, most likely microglia, and thus a CNS-resident internal pool. Moreover, both $eYFP^+$ as well as $eYFP^-$ microglia numbers increased by day 7 (Fig. 14E), suggesting that microglia, which had escaped Cre-mediated recombination, contributed in a similar manner to microglia repopulation (Bruttger et al., 2015).

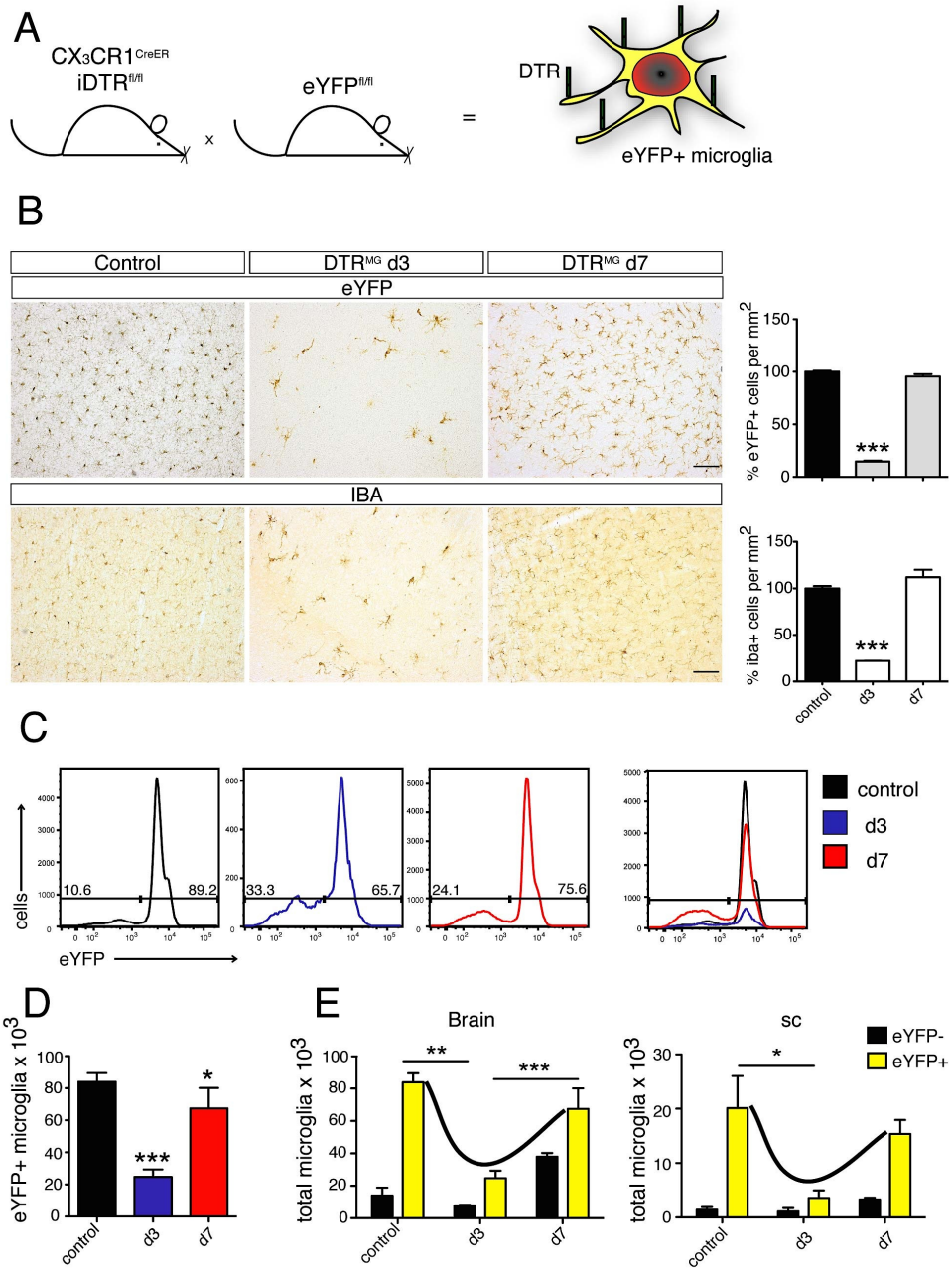

Figure 14: Without irradiation microglia repopulate from internal pools (adapted from (Bruttger et al., 2015))

(A) DTR^{MG} mice crossed to R26 YFP$^{fl/fl}$ mice to obtain litter which express the DTR and eYFP (B) The distribution of total cells was confirmed with immunohistochemical staining for eYFP and Iba1. Microglia cell numbers in the cortex of control, day 3 and day 7 animals were quantitated. Scale bars=100 μm. The cell counts were normalized to the controls and the values are expressed in the bar graphs. (C) Representative FACS histograms for eYFP expression of CNS homogenates pre-gated on microglia (Control: black, day 3: blue, day 7: red). The right panel shows an overlay of all three histograms at the different time points and illustrates the distribution and relation of total cell numbers. (D) Statistical analysis of total cell number (±SEM) of eYFP^{+} microglia represents the average of total cell counts (control: n=3, day 3: n=4, day 7: n=4) (E) The comparison between eYFP^{+} and eYFP^{-} cells clarifies the distribution between the two populations shown for brain and spinal cord. Statistical significance (unpaired Student's t test) is indicated as *$p < 0.05$, **$p < 0.01$, and ***$p < 0.001$.

3.3.1 Clusters of Proliferating Microglia Repopulate the CNS

While analyzing microglia distribution, we noticed that, at the peak of repopulation at around day 7, many microglial cells were found in micro-clusters, defined as a formation of five or more microglial cells within an area of 0.6 mm^2 (Fig. 15A, indicated with arrowheads). The clusters were present in all CNS regions, including cortex, cerebellum, brain stem and dentate gyrus (Fig. 15A). Clusters were first observed on day 7 after depletion but were mostly resolved by day 14 (Fig. 15B). Based on these observations, we investigated whether the repopulating microglia originated from cells escaping ablation and underwent massive proliferation. To follow cell proliferation, mice were fed with BrdU starting from two days prior to depletion until analysis at day 7. When brain slices were stained for BrdU and Iba-1, we observed proliferating microglia as early as day 3 after DT injection (Fig. 15A). At day 7 these cells formed clusters of multiple cells that were $BrdU^{bright}$ (Fig. 15C). In the same figure, there are single $BrdU^{+}$ cells that seem to migrate away from the cluster (Bruttger et al., 2015), suggesting that repopulation of the surrounding tissue originates in there (Fig. 15C).

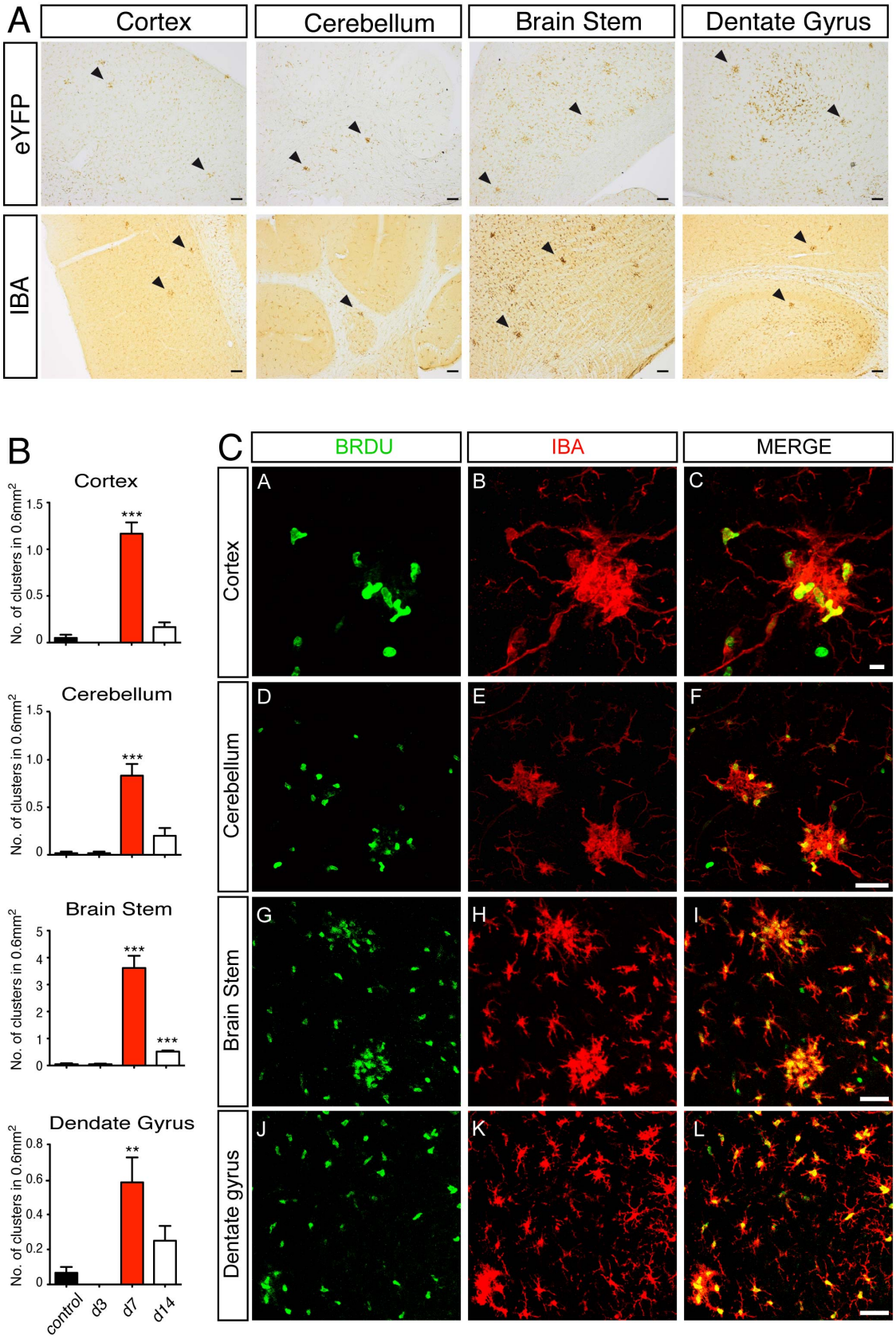

Figure 15: Microglia form clusters of proliferation to reconstitute the CNS (adapted from (Bruttger et al., 2015))

(A) Representative pictures of immunohistochemistry for eYFP (upper panel) and iba1 (lower panel) for the given brain regions. Scale bar=50 μm. The arrowheads highlight a cluster formation (≥5 cells). (B) The total number (±SEM) of clusters per region is represented by the bar graphs. 1 cluster consists of ≥5 microglia cells. (C) Mice were fed with 0.6 mg/ml BrdU in drinking water throughout the depletion time course. Single staining and a merge of fluorescence microscopic pictures of BrdU (green) and iba1 (red) stained sections are shown. Scale bars=10 μm in a-c and 50 μm in d-l. Statistical significance (unpaired Student's t test) is indicated as *$p < 0.05$, **$p < 0.01$, and ***$p < 0.001$.

Finally, at d14, $BrdU^+$ microglia were still detectable in high numbers, however at this late time point were widely distributed in the tissue and no longer organized in clusters (Fig. 16). By co-staining for BrdU and YFP (Fig. 16A), we were able to verify that these clusters consisted exclusively of CNS-resident cells, and that this $eYFP^+$ microglia population was the major source of proliferating cells following DT-mediated ablation (Fig. 16B). These data suggest that after ablation of a large proportion of microglia, the remaining cells rapidly proliferate in order to repopulated microglia-depleted areas (Bruttger et al., 2015).

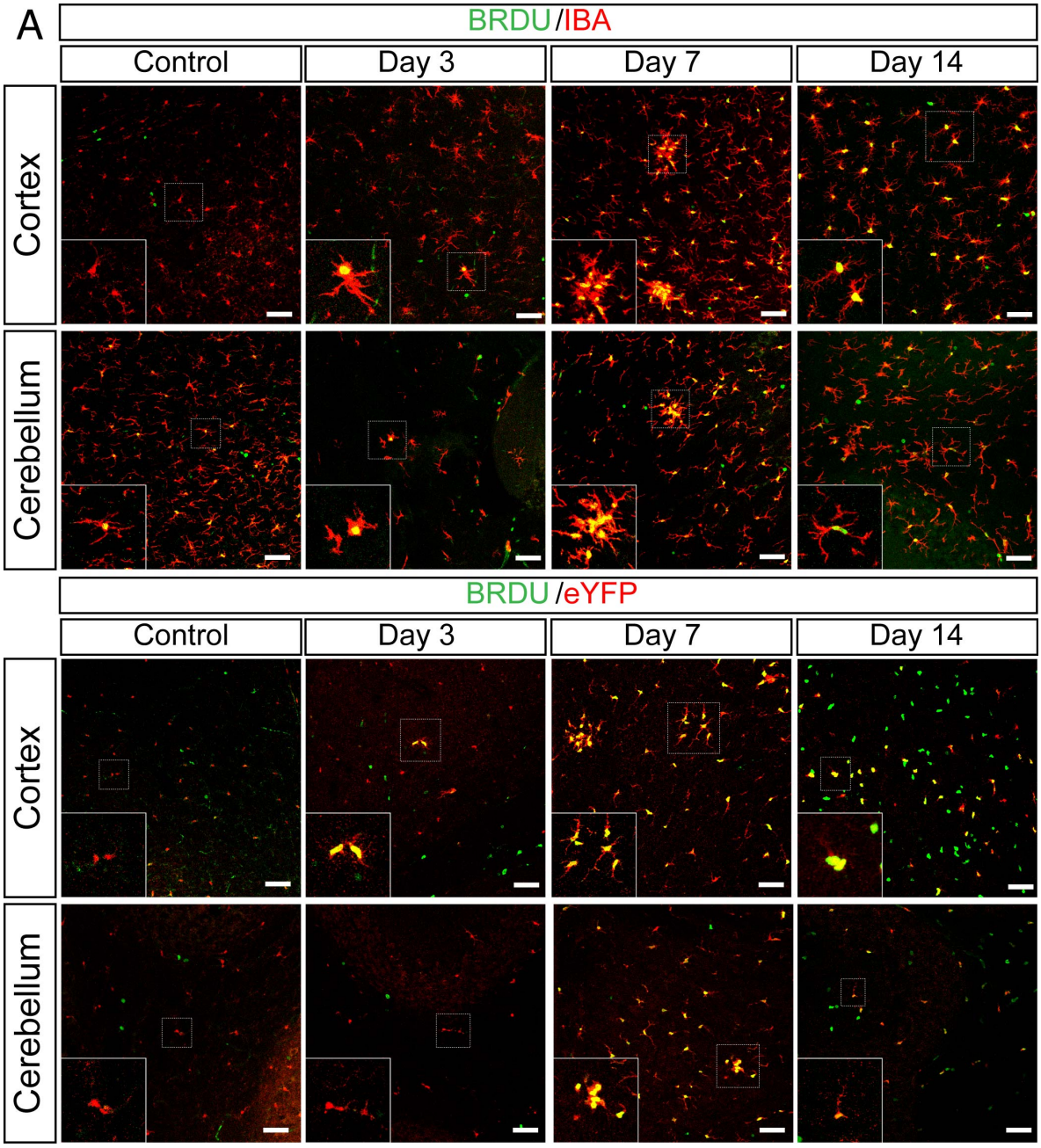

Figure 16: Cluster of proliferation are Iba-1+ and eYFP+ (adapted from (Bruttger et al., 2015))

(A) According to Figure 4C one representative overlay of Iba1 and BRDU co-staining for all time points (control, day 3, day 7, d14) are shown for cortex and cerebellum. Scale bars =20 µm. Magnifications of indicated areas are shown. We observed depletion of Iba1+ cells on day 3, on proliferating clusters day 7 and many double positive cells on d14 present throughout the CNS. (B) Representative overlays of eYFP and BRDU co-staining are shown forthe depicted areas and for all time points (according to a). Scale bars=20 µm. Magnifications of indicated areas are shown.

3.3.2 Newly Repopulated CNS-derived Microglia Display Unaltered Gene Expression Profiles, While BM Macrophages are Distinct

Next, we aimed to characterize the gene expression profile of the newly formed microglia and compare it with the signature of BM macrophages that repopulate the microglia niche in the BM chimeras. To that end, we sorted eYFP^{+} repopulating brain macrophages from either BM chimeric mice as described in Figure 11 (BM origin) or from non-irradiated mice described in Figure 14 (CNS origin) (Bruttger et al., 2015). For comparison, we isolated microglia from control animals, based on their YFP expression out of CD45 and CD11b (microglia gate) (Fig. 17).

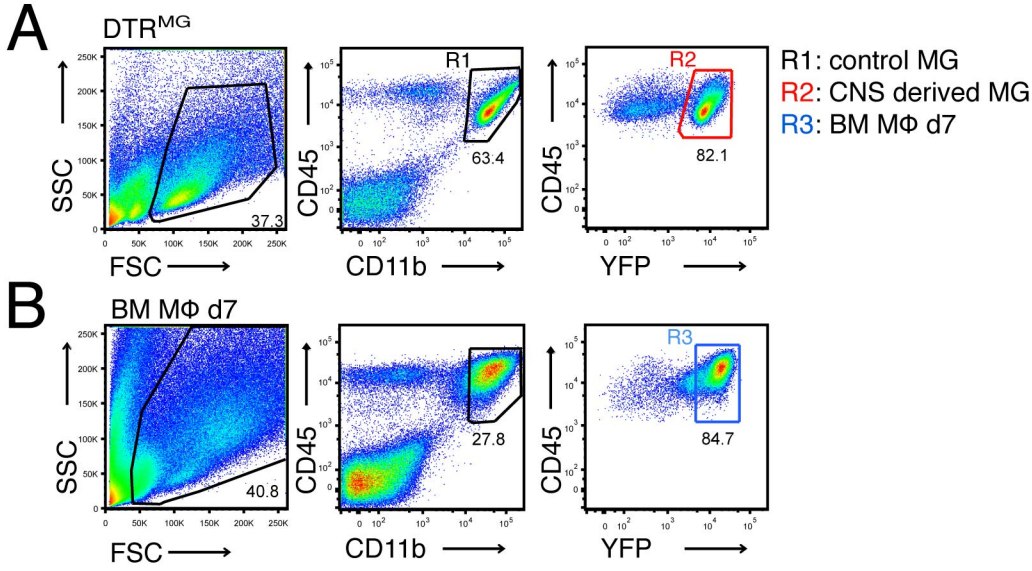

Figure 17: Sorting strategy for different CNS resident microglia populations

(A) gating strategy for microglia out of DTR^{MG} mice and their cre- littermate controls. Microglia out of the R1 gate (black) are wildtype control microglia and gate R2 (red) shows the YFP+ microglia out of a DTR^{MG} mouse. (B) BM derived macrophages in the CNS were also sorted according to their YFP signal seen in gate R3 (blue).

Isolated mRNA from these three microglia populations was subjected to RNA sequencing (Fig. 17). The sequencing data were normalized to the raw counts of each library size in the context of the three different NGS runs. Next, the Bioconductor DESeq package version 1.14.0 was used to perform differential expression (DE) analysis and for an estimation of biological variance. The raw counts for the genes are normalized and plotted in MA-values (M=log2 fold change, A=average) (Fig. 18A). Comparison of the expression profiles of the three brain macrophage populations revealed higher numbers of differentially expressed genes in BM-derived macrophages versus either control (Fig. 18A left panel) or newly generated microglia (Fig. 18A right panel). In contrast, there were fewer differences between CNS-derived and wild type control microglia (Fig. 18A mid panel). Heat map analysis of all DE genes, constructed on the basis of hierarchical clustering of gene expression values, displayed a close relationship across the samples within one biological group. More importantly, the gene expression pattern of control microglia resembled very closely that of CNS-derived repopulating microglia, but differed substantially from the expression pattern found in BM-originated microglia (Fig. 18C). To examine these differences, we plotted the relationship between the three groups using principal component analysis (PCA). The samples within each biological group clustered together (Fig. 18B), confirming reproducibility of the results. In the PCA analysis the distance of control microglia from BM-derived macrophages was significantly greater than that to microglia that originated in CNS-internal pools (Fig. 18B) (Bruttger et al., 2015).

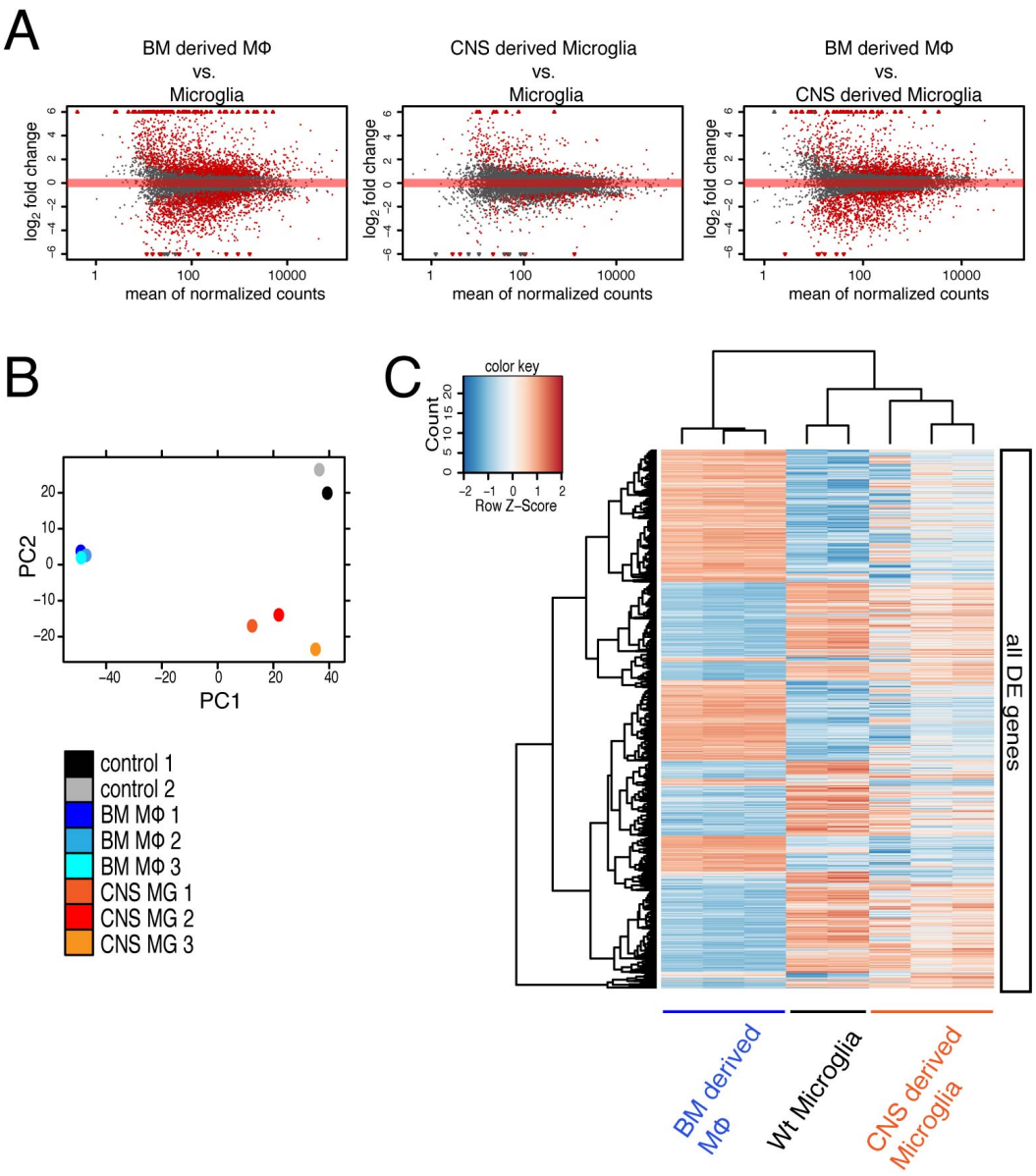

Figure 18: NGS analysis for detailed comparison of the different microglia populations (adapted from (Bruttger et al., 2015))

(A) Plots showing the comparisons of the different microglia populations. The raw counts for the genes are normalized to obtain M-A values (M=log2 fold change, A=average). One dot represents one gene. The differentially expressed (DE) genes are depicted in red (BM-originated microglia vs. controls: 4060 DE genes; BM-originated microglia vs. CNS-derived microglia: 2658 DE genes; CNS-derived vs. control 711 DE genes) (B) The distances between the populations, based on two principal components for the top 1000 DE genes, are shown in the Principal Component Analysis (PCA) plot. The distance between CNS-derived samples and WT microglia is significantly ($p \leq 0.05$) smaller than the distance between BM-originated and WT. Significances are calculated by permutation test. (C) Heat map of all DE genes in FACS-sorted microglia populations. Each row represents one specific gene; the columns represent different samples. The values shown are normalized and standardized by row to show variations across the samples (blue: down regulation; red: up regulation). The dendrogram above the heat map shows the relationship between the different samples based on similar expression levels across the 3 conditions. The dendrogram on the left is constructed on the basis of hierarchical clustering of the DE gene expression.

Similar results were obtained when we analyzed the transcriptome data focusing on the genes included in a so-called MG400 chip, which combines 400 genes characteristic for microglia and macrophages (Butovsky et al., 2014). Heat map analysis of this gene set (data not shown) clearly confirmed the close relation between control and CNS-derived repopulating microglia. In their study Butovsky and colleagues also described 88 genes that are microglia-specific, compared to other macrophage populations (Butovsky et al., 2014). Accordingly, we found 87 of these genes in our analysis of DE genes (Fig. 18A), and a great majority of them were upregulated in control and CNS-derived microglia, when compared to brain macrophages of BM origin. Some of them are depicted in Figure 19B; *p2yr12, mertk, pros1, c1qa, olfml3, entpd1, hexb, and tmem119* were differentially expressed in the gene array (Fig. 19B) and in order to control the validity of the data the experiment was repeated and the different microglia population were validated by qPCR (Fig. 19C). Both experiments produced the same results. The CNS derived microglia show more similar expression patterns to the controls and the day 7 BM MΦ differ in expression. An additional later time point (d28) for BM MΦ still shows a significant difference to the controls in the expression profile of the microglia signature genes (Fig. 19C) whereas over time they show a trend towards gene expression levels of control microglia (Bruttger et al., 2015).

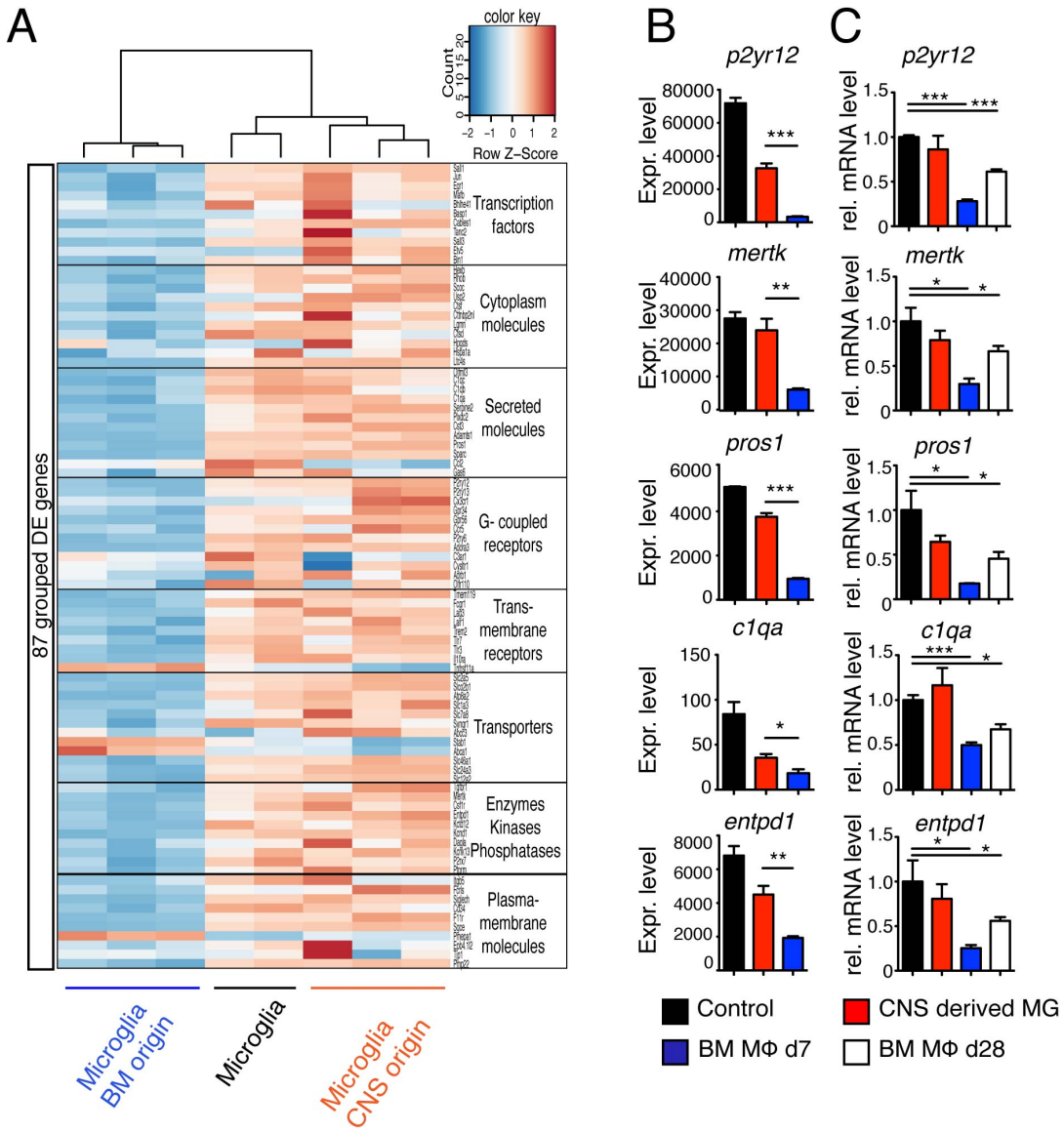

Figure 19: NGS analysis according to MG400 microglia signature genes (adapted from (Bruttger et al., 2015))

(A) Plots showing the comparisons of the different microglia populations. The raw counts for the genes are normalized to obtain M-A values (M=log2 fold change, A=average). One dot represents one gene. The differentially expressed (DE) genes are depicted in red (BM-originated microglia vs. controls: 4060 DE genes; BM-originated microglia vs. CNS-derived microglia: 2658 DE genes; CNS-derived vs. control 711 DE genes) (B) Expression values (±SEM) of the MG signature genes *p2yr12, mertk, pros1, c1qa* and *entpd1* (according to Butosky et al. 2013). (C) qPCR validation (±SEM) of the microglia signature genes. Statistical significance (unpaired Student's t test) is indicated as *$p < 0.05$, **$p < 0.01$, and ***$p < 0.001$.

3.4 Factors that Influence Microglia Repopulation

3.4.1 Nestin is Expressed in Repopulating Microglia

Nestin was discovered in 1985 as a intermediate filament protein which builts a componant of the cytoskeleton (Hockfield and McKay, 1985). During embryogenesis, nestin is expressed by migrating and proliferating cells. In adults one can only find nestin expression in areas of regeneration (Coste et al., 2015). It has been shown recently, that during repopulation microglia start to express the neuronal stem cell marker *nestin* (Elmore et al., 2014).

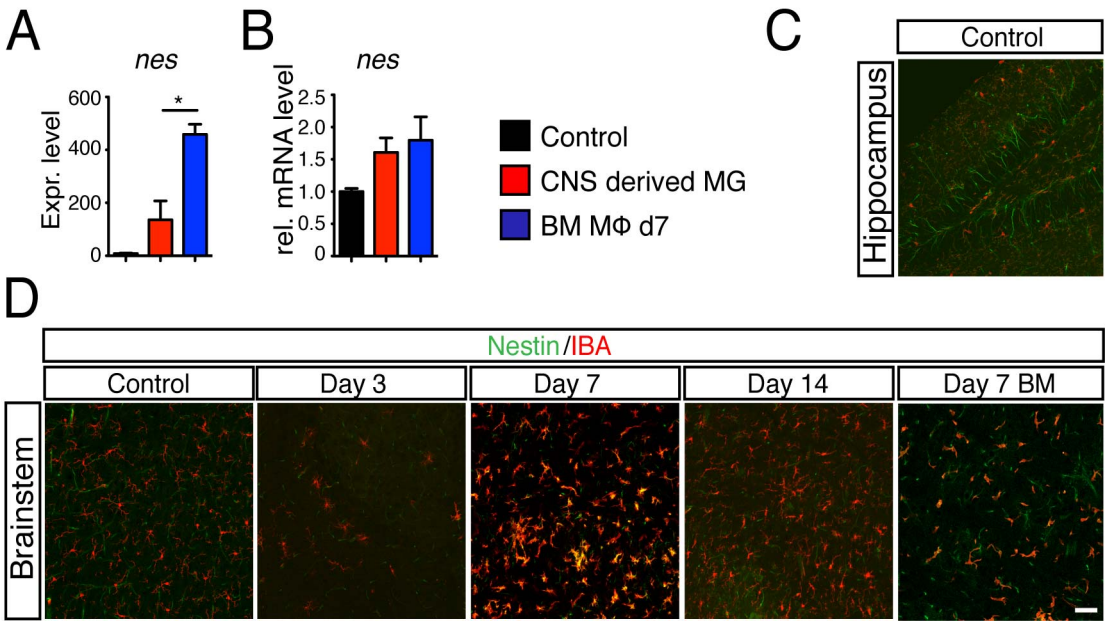

Figure 20: Nestin is expressed in CNS derived microglia and BM macrophages (adapted from (Bruttger et al., 2015))

(A) Expression values (±SEM) and (B) qPCR validation (±SEM) of *nestin* control MG, CNS derived microglia and BM MΦ (C) staining control for nestin antibody shows a proper nestin expression in the hippocampal radial glia (D) Immunohistological analysis of *nestin* and *iba-1* in the brainstem of control, day 3, day 7, d14 and day 7 BM MΦ shows coexpression of nestin and iba-1 in day 7 CNS derived MG and day 7 BM MΦ.Statistical significance (unpaired Student's t test) is indicated as *$p < 0.05$, **$p < 0.01$, and ***$p < 0.001$.

We could confirm Elmore's findings. Detectable amounts of *nestin* RNA can be found in the RNA seq data. Not only the repopulating CNS derived

microglia, but especially the replacing BM macrophages express high amounts of nestin RNA, seen in RNA sequencing and qPCR (Fig. 20A and 20B). Also nestin protein can be visualized by performing nestin and iba-1 immunohistological co-staining, showing that microglia transiently express *nestin*. In control and day 3 animals there is only nestin expression visible in the hippocampus (Fig. 20C) but no coexpression in microglia. On day 7, a strong coexpression was visible, particularly in the clusters of proliferating microglia, but on d14 *nestin* is no longer being expressed by microglia (Fig. 20D). As can be seen in the same figure, the BM macrophages in the CNS also showed strong expression of *nestin* (Bruttger et al., 2015). Taken together, the analyzed gene expression profiles clearly revealed differences between CNS derived microglia and BM MΦ repopulating the brain.

3.4.2 Csf-1 and Its Receptors are Important Players which Differentiate Microglia from BM Macrophages

Microglia, as tissue resident macrophages, share some features with the normal circulating macrophages; they are highly dependent on the transcriptionfactor PU.1 and the Csf-1 receptor (Csf-1R). Knock out animals for PU.1 or Csf-1R lack microglia completly (Ginhoux et al. 2010; Beers et al. 2006). Also in our NGS approach, we are able to find high amounts of Csf-1 and Csf-1R. Exclusively, csf1 and its receptor display its highest expression in the CNS derived microglia (Fig. 21A). The BM MΦ on day 7 and on day 28 also displayed high gene expression of Csf-1 and Csf-1R (Fig. 21A and B), but could never reach the expression level of the control or CNS derived

microglia. Relative gene expression levels in Figure 20B are shown for validation of the NGS data (Bruttger et al., 2015).

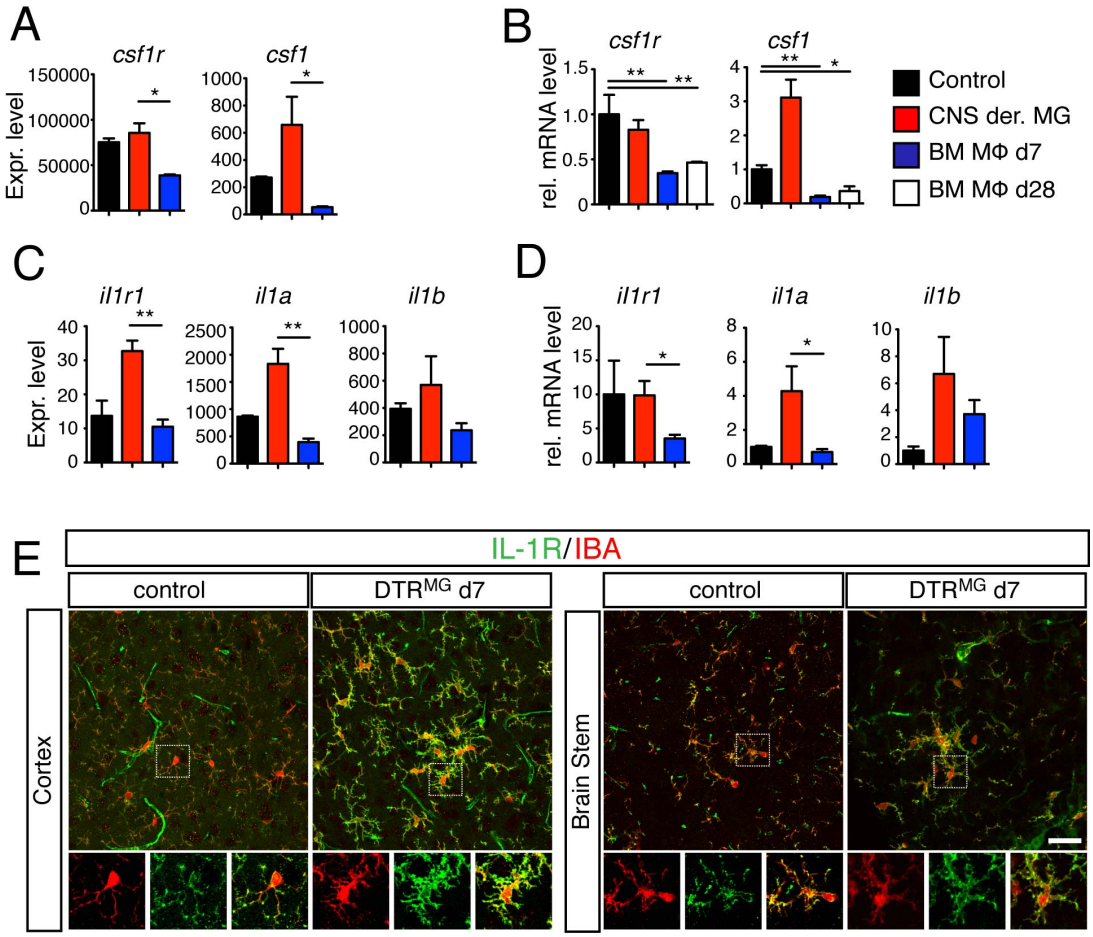

Figure 21: Csf-1 and IL-1α show highest expression in CNS derived microglia (adapted from (Bruttger et al., 2015))

(A) Expression levels (±SEM) of csf-1 and csf-1r messured by NGS and (B) by qPCR. (C) NGS Expression levels (±SEM) of *Il1r1*, *Il1a* and *Il1b* in controls, CNS derived MG and BM MΦ analyzed by NGS or (D) by qPCR. (E) Immunohistochemistry of DTR^{MG} day 7 mice shows $IL\text{-}1R^{+}$ (green) $Iba\text{-}1^{+}$ (red) cells with most prominent expression of IL-1R in the clusters. Scale bars = 40μm. Statistical significance (unpaired Student's t test) is indicated as *$p < 0.05$, **$p < 0.01$, and ***$p < 0.001$.

3.4.3 Microglia Repopulation is Dependent on Interleukin-1 Signaling

The Interleukin-1 signaling pathway is involved in the regulation of several cellular functions such as the induction of cell proliferation and activation (Basu et al., 2002; Pineau and Lacroix, 2007; Pineau et al., 2010). Also in the context of microglia depletion and repopulation we found evidence for the importance of IL-1 signaling. According to the NGS data and their qPCR validation there are two genes, Il-1R1 and Il-1α, which are significantly higher expressed in the CNS derived, repopulating microglia, compared to control microglia and to BM MΦ (Fig. 21C and D). Also immunohistochemistry showed a high expression of IL-1R1, especially in the proliferative clusters exemplarily shown for clusters in the cortex and brain stem (Fig. 21E) (Bruttger et al., 2015).

We further investigate the role of IL-1 signaling on microglia repopulation. To that end, we superimposed our ablation protocol with IL-1 neutralization. We injected DT-treated DTR^{MG} mice twice with soluble IL-1 receptor antagonist (IL-1RA, *Anakinra,* acting as an antagonist of IL-1 signaling) intra-cerebroventricularly (i.c.v.) on day 3 and 4 after depletion and analyzed the mice on day 7 (Fig. 22A). The icv injections of IL-1RA (*Anakinra*) into the third ventricle delayed the repopulation of microglia significantly in the cortex, cerebellum and thalamus (Fig. 22B). The brain stem showed no differences in repopulation, possibly due to inefficient distribution of IL-1RA, when icv injected into the third ventricle, as has previously been shown (Chauhan et al., 2001). In addition, the morphology of the repopulating cells changed dramatically after IL-1RA injections. Specifically, the cells did not acquire the

typical microglia morphology, i.e. ramification, but remained round in shape and lacked an abundance of processes (Bruttger et al., 2015).

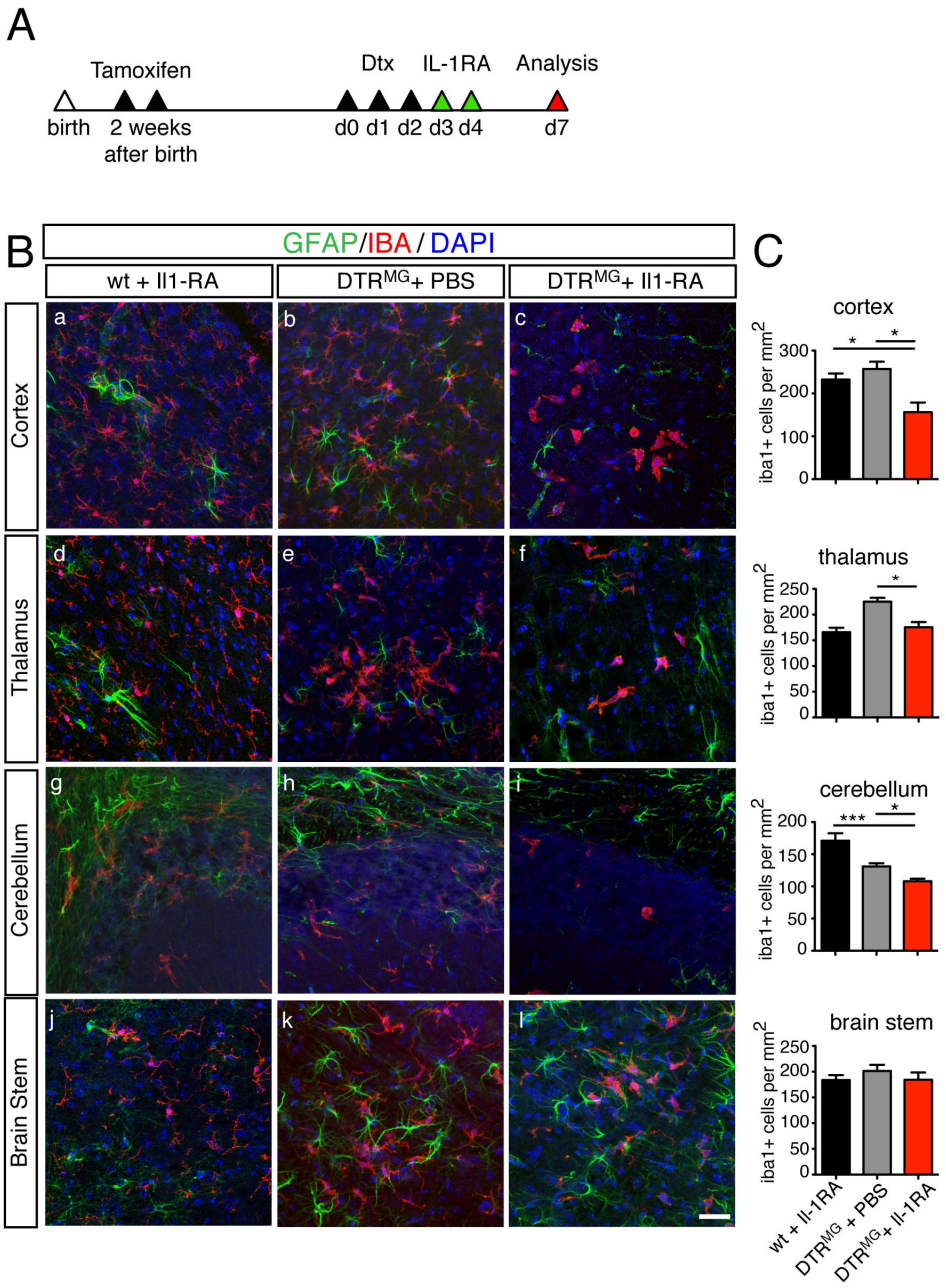

Figure 22: repopulation of DTR^{MG} mice on day 7 is hindered upon IL-1RA i.c.v. treatment (adapted from (Bruttger et al., 2015))

(A) Time schedule for TAM, Dtx and IL-1RA injection (B) Immunohistochemistry of CNS vibratome slices of controls + IL-1RA icv, DTR^{MG} mice + PBS icv. and DTR^{MG} mice + IL-1RA icv. were co-stained for Iba-1 (red), GFAP (green) and Dapi (blue). Scale bars = 40μm. (C) Quantification of total microglia numbers (±SEM) in controls + IL-1RA icv., DTR^{MG} mice + PBS icv. and DTR^{MG} mice + IL-1RA icv. in 5 mice per group (n=5) representative for the cortex. Statistical significance (unpaired Student's t test) is indicated as *$p < 0.05$, **$p < 0.01$, and ***$p < 0.001$.

The quantifications resulted in a significantly lower amount of counted microglia and therefore showed less repopulation in IL-1RA treated animals (Fig. 22C). Astrocytes did not show differences in GFAP expression across the brain regions in the different samples (Fig. 22B).

3.4.4. IL-1RA Blockade Effects Microglia Proliferation early after i.c.v. Treatment

Similar to previous experiments, we icv injected DT-treated DTR^{MG} mice twice with IL-1RA antibodies on day 3 and day 4 after depletion, fed them with BRDU additionally, and analyzed the mice on d5. In all the examined brain regions (cortex, cerebellum, thalamus and brain stem), we found significantly reduced numbers of Iba-1^{+} cells in the IL-1RA-treated mice, compared to PBS-treated controls (Fig. 23B and 23C), after microglia depletion (Bruttger et al., 2015).

Legend of Figure 23:

(A) Time schudule for TAM, Dtx and IL-1RA injections (B) Immunohistochemistry for Iba-1 (red) and BrdU (green) of DTRMG d5 mice fed with BrdU during depletion time course shows smaller number of Iba-1+ cells in cortex, cerebellum, thalamus and brain stem. Scale bars = 40 µm. (C) Quantification of the Iba-1+ cells counted in the indicated brain regions. Statistical significance (unpaired Student's t test) is indicated as *$p < 0.05$, **$p < 0.01$, and ***$p < 0.001$.

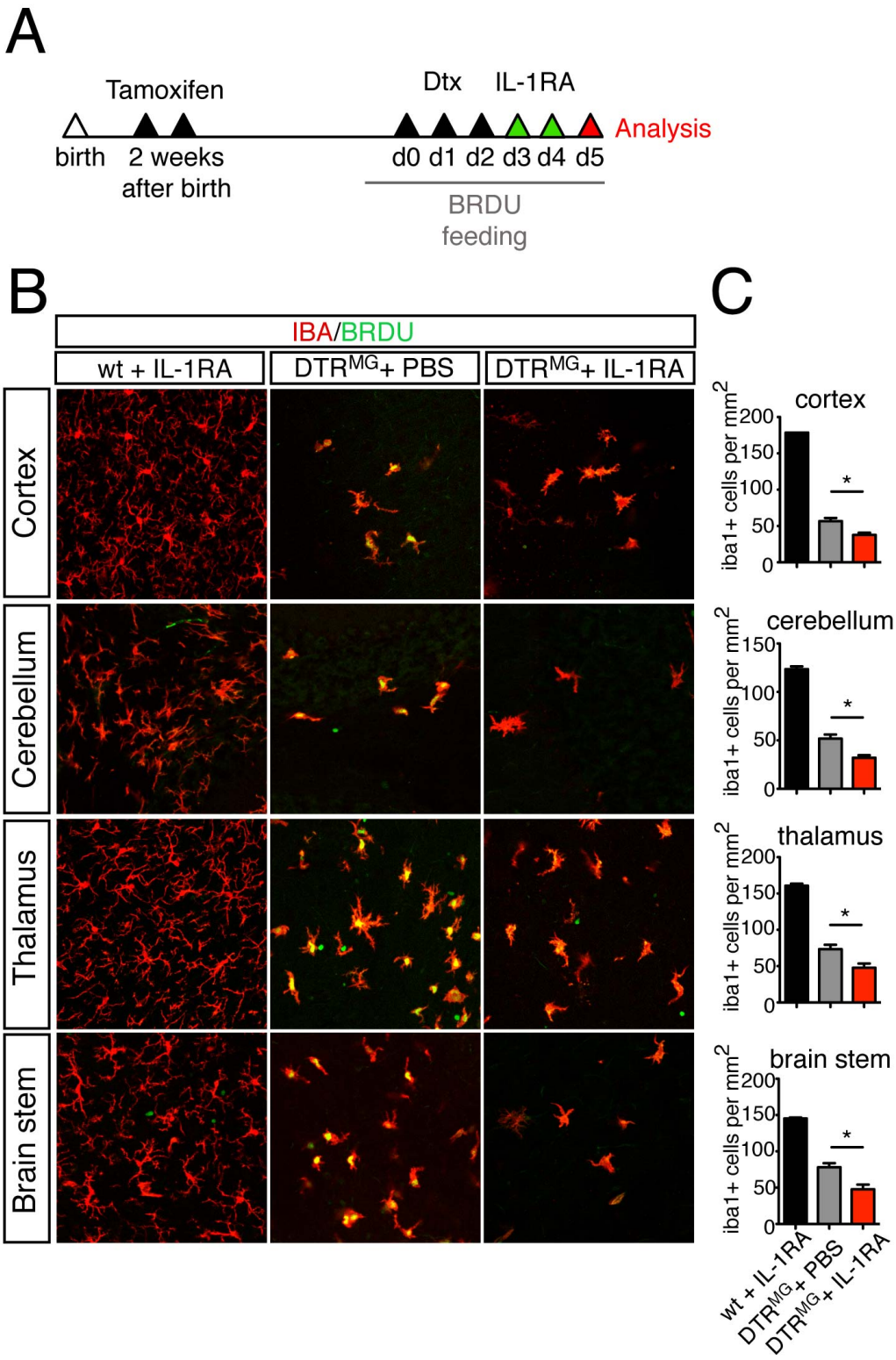

Figure 23: Blockade of IL-1R signaling leads to reduced proliferation and microglia reconstitution after depletion (adapted from (Bruttger et al., 2015))

Analysis of proliferation of the repopulating microglia revealed differences in BrdU labelling (BrdU is not expressed!) across the samples (Fig. 23). As expected, microglia in the controls treated with IL-1RA did not incorporate BrdU. In line with previous experiments (Fig. 15C), the depleted and PBS-treated mice showed BrdU incorporation in Iba-1^{+} cells. After depletion and IL-1RA treatment the microglia are not positive for BrdU, indicating that IL-1RA treatment abrogates proliferation of microglia in the context of depletion. Similar results were obtained by histology, using antibodies specific for Ki67: IL-1RA-treated animals displayed significantly less CD11b^{+}Ki67^{+} cells than controls (Fig. 24C and 24D) (Bruttger et al., 2015).

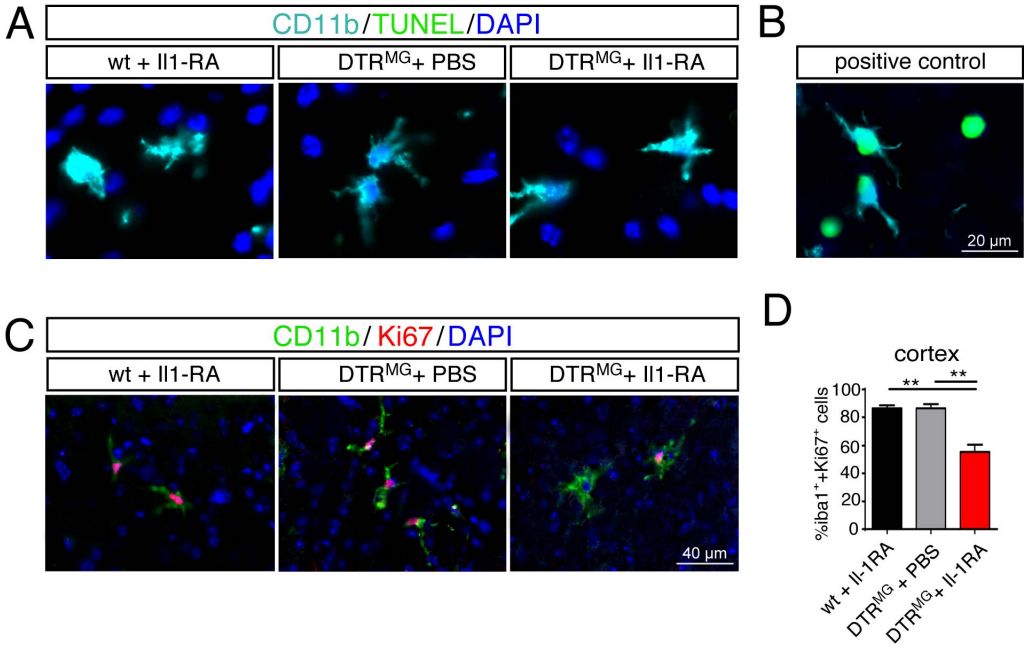

Figure 24: Ki67 expression in repopulating microglia after IL-1RA treatment is blocked, but TUNEL is not

Immunohistochamistry for CD11b (blue), TUNEL (green) and dapi (dark blue) in the perifrontal cortex of control mice + Il-1RA icv, DTR^{MG} mice + PBS icv and DTR^{MG} mice + Il-1RA icv (B) staining control for TUNEL (green) (C) Immunohistochemical stainings for CD11b and Ki67 also in the perifrontal cortex of the mice described in B. (D) Quantification (±SEM) of iba1^{+} Ki67^{+} cells Statistical significance (unpaired Student's t test) is indicated as *$p < 0.05$, **$p < 0.01$, and ***$p < 0.001$.

In order to exclude an effect of IL-1RA on apoptosis of microglia or on other brain cells we performed two different kinds of experiment. With a TUNEL assay we looked for apoptotic cells inside the treated brains. In non of the three different groups and in non of the brain regions we could detect a positive TUNEL signal (Fig. 24A), but in the positive control we found TUNEL+ cells (Fig. 24B). The absence of TUNEL positive cells in the samples suggested that IL-1RA treatment did not provoke apoptosis of microglia and it did not induce apoptosis of other resident brain cells (Bruttger et al., 2015).

3.4.5 Impact of Depletion and IL-1RA Treatment on Other Brain Cells

The impact of IL-1RA treatment on other brain cells was further controled by histology for Astrocytes and Oligodendrocytes. The numbers of $GFAP^+$ and $Olig2^+$ cells remained stable and therefore revealed no influence of IL-1RA on oligodendrocyte precursors and mature oligodendrocytes. (Fig. 25A and 25B).

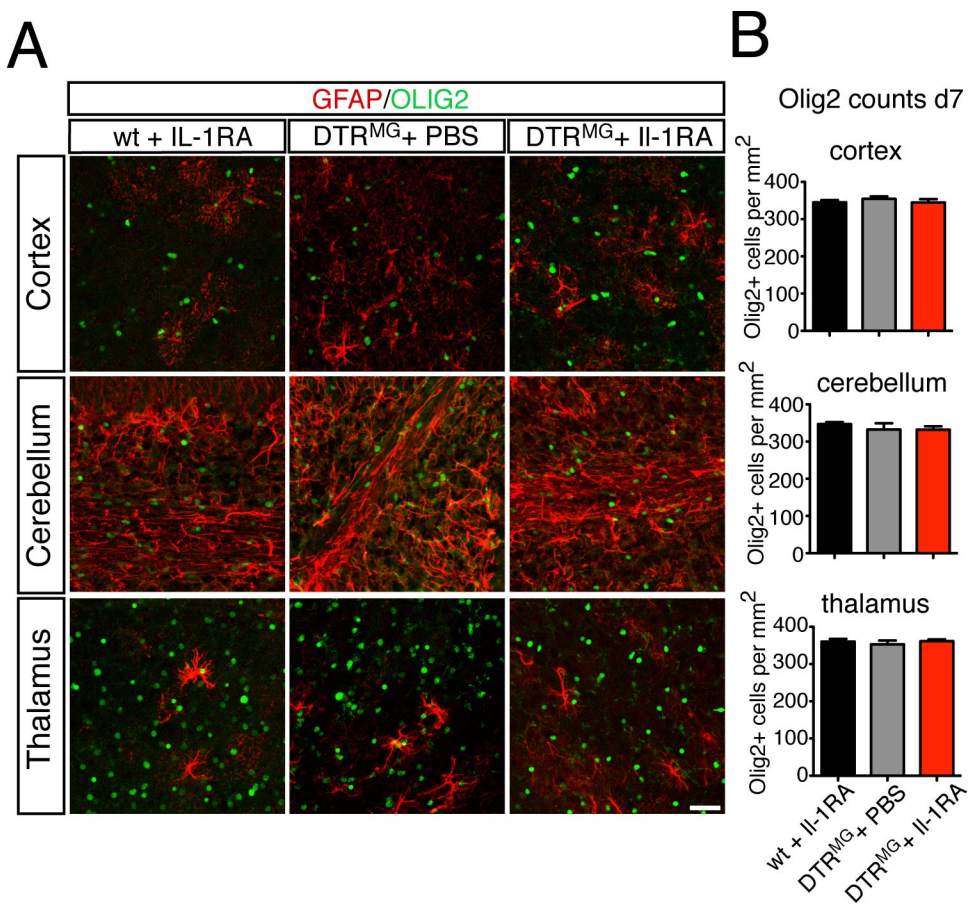

Figure 25: Impact of IL-1RA i.c.v. treatment to other brain resident cells (adapted from (Bruttger et al., 2015))

(A) According to the 3 different treatments of Figure 19 immunohistological stainings for GFAP and Olig2 are shown for cortex, cerebellum and thalamus. Scale bars =20 µm. Representative pictures for the region specified are depicted. (B) Total numbers (±SEM) of Olig2+ cells were counted on 20x magnification in 10 fields per slice and in 2-3 slices per animal. Statistical significance (unpaired Student's t test) is indicated as *$p < 0.05$, **$p < 0.01$, and ***$p < 0.001$.

3.4.6 IL-1R1 Deletion in Microglia Effects Microglia Maintenance

IL-1R1 was previously thought to exert all actions of IL-1, and for decades the field of inflammation has used *il1r1*$^{-/-}$ mice originally generated by targeting deletion of exon 1 and 2 (Glaccum et al., 1997; Labow et al., 1997)). However, a recent study found that an alternative promoter upstream of exon 3 leads to the expression of a truncated signaling receptor named IL-1R3 (Qian et al.,

2012), which is thought to account for IL-1R1-independent IL-1 actions that we have previously identified in glial cells (Andre et al., 2006). We have therefore generated a new mouse line (*il1r1fl/fl*), in which exon 5 is flanked with *LoxP* sites, thus allowing deletion of the three known IL-1 receptor isoforms. We crossed the IL-1R1^{FL} mice to the CX_3CR1-Cre^{ERT2} mice and induced the deletion of IL-1R1 specifically in microglia by injecting the mice with tamoxifen using the same protocol as used for inducing the iDTR allele in Figure 1. These mice were termed IL-1R1^{MG}.

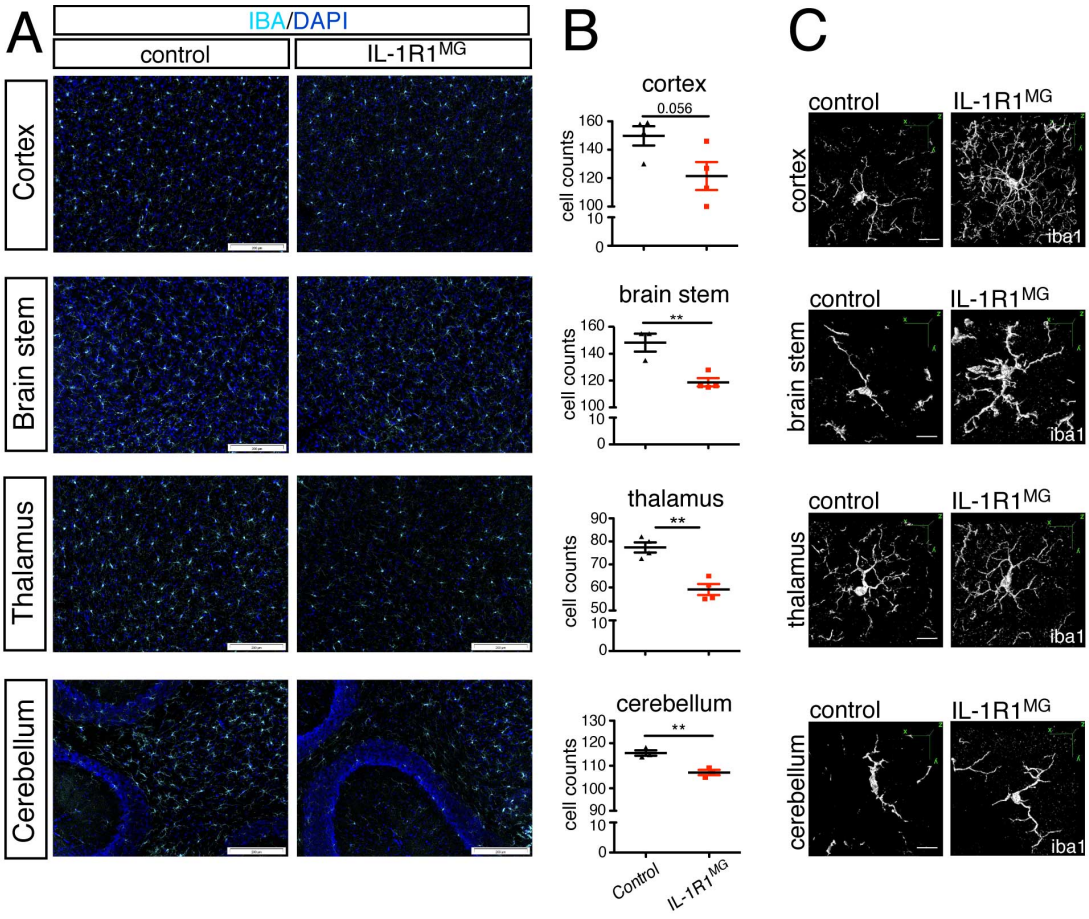

Figure 26: IL-1R1^{MG} mice show reduced microglia numbers (adapted from (Bruttger et al., 2015))

(A) IL-1R1^{MG} mice show a different abundance of microglia throughout the tissue compared to control animals seen in cortex, brain stem, thalamus and cerebellum of 3 months old mice. Scale bars = 200μm. (B) In the quantification of the total cell numbers (±SEM) 10 fields per slice and 2-3 slices per animal were counted on a 20x magnification. (C) IL-1R1^{MG} to control animals a 3D reconstruction of single iba-1^{+} cells taken from each brain region are shown. Scale bars = 20 μm.

Microglia of the IL-1R1^{MG} mice show abnormal distribution (Fig. 26A), resulting in reduced iba-1^{+} cell numbers (Fig. 26B) in cortex, brain stem, thalamus and cerebellum. Furthermore, IL-1R1 deficient microglia showed atypical morphology as demonstrated in three-dimensional reconstructions of confocal *z*-stacks. Specifically, the IL-1R1 deficient microglia have more processes, which appear thicker and more branched (Fig. 26C). Taken together, our results demonstrate that the conditional deletion oft he IL-1R1 distrubs microglia maintenance in the steady state (Bruttger et al., 2015).

3.4.7 Disease Onset of EAE is Delayed in IL-1R^{MG} mice

In another *in vivo* functional assay we assessed the role of IL-1R1 on microglia in an experimental model of Multiple Sclerosis (MS). Here, we found that the IL-1R1^{MG} animals develop similar disease severity but the disease onset is delayed compared to littermate control animals (Fig. 27).

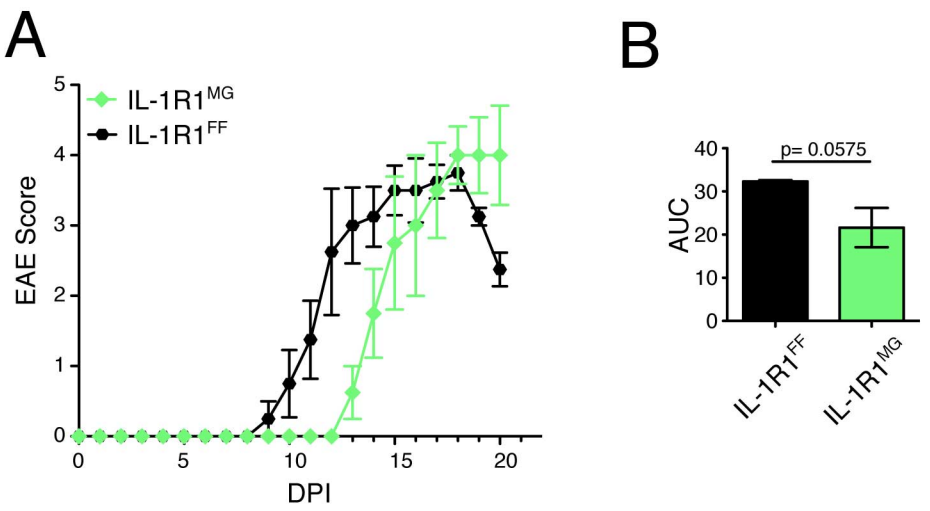

Figure 27: IL-1R1^{MG} mice show delayed onset of EAE

(A) Representative EAE plot for IL-1R1^{MG} mice (green) and controls (black). (B) Quantification (±SEM) for the area under the curve (AUC) for the two different groups. Statistical significance (unpaired Student's t test) is indicated as *p < 0.05, **p < 0.01, and ***p < 0.001

Taken together, our findings suggest that once microglia are ablated, they have the ability to repopulate the various brain regions within a short time window of a few days. On the one hand, the source for this replacement can be CX_3CR1^+ cells residing within the CNS, most likely microglial cells, or on the other hand, it can be BM derived cells. Although we show that BM-derived cells are able to repopulate the CNS in BM chimeras after microglia ablation, the gene expression profile of these cells still suggests that these cells are not proper microglia. The uniqueness of the CNS microglia population is reflected by the dependence on and by the higher expression profile of the Csf-1r and of the IL-1R.

4 Discussion

4.1 Microglia specific targeting

Microglia are tissue resident macrophages of the brain that develop from early yolk sac progenitors (Ginhoux et al., 2010), (Kierdorf et al., 2013c) and exhibit self-renewing potential, comparable to other macrophages found in spleen, liver or pancreas (Schulz et al., 2012b). Lung, peritoneal and BM macrophages are also maintained locally without the contribution of circulating monocytes under steady state conditions (Hashimoto et al., 2013) (Yona et al., 2013). In contrast, intestinal CX_3CR1^+ macrophages are constantly replenished by $Ly6C^{hi}$ blood monocytes (Varol et al., 2009), most likely due to their localization in the gut, an organ characterized by ongoing mild inflammation due to the luminal micro flora and its products. During CNS inflammation (e.g. during EAE) monocytes are recruited to the brain, but only transiently. Once the inflammation is resolved, they migrate back out of the brain and therefore they do not contribute to the microglial pool over time (Ajami et al., 2007)(Jenkins et al., 2011).

Recently, CX_3CR1^{CreER} mice were presented as a novel tool allowing targeting of microglia. A specific and long-lasting recombination in microglia was shown in *Cx3Cr1*^{CreER}:YFP reporter mice (Yona et al., 2013) (Goldmann et al., 2013). The use of these tamoxifen-inducible Cre lines allow for microglia-specific targeting (see Figure 4, introduction). CX_3CR1 is a chemokine receptor, also known as the fractalkine receptor, and is highly expressed by microglia. Even though CX_3CR1 is also expressed on other myeloid cells, including their precursors in the BM (Geissmann et al., 2010), Cre expression is lost over time after tamoxifen treatment in the short-lived CX_3CR1^+ myeloid cells due to high turnover rates. In contrast, the long-lived and self-renewing microglia express the Cre and remain stably recombined (Goldmann et al., 2013; Yona et al., 2013). Even though the brain is an immune privileged organ, peripheral immune cells can influence it, especially under inflammatory conditions. Yet deficits in the peripheral myeloid compartment could affect the CNS (Dantzer

et al., 2008), therefore a precise functional analysis of microglia needs to be carried out with caution, particularly when using knockout mice that affect both peripheral and CNS myeloid cells. To solve this problem, we used the iDTR mouse model. In another model for oligodendrocyte ablation with the MogiCre:iDTR system, oligodendrocytes were depleted successfully, indicating that the DTx can pass through the BBB (Buch et al., 2005; Gritsch et al., 2014; Locatelli et al., 2012).

4.2 Cx_3Cr1^{CreER}:iDTR System: A Model for Genetic Depletion of Microglia

The microglia specific CX_3CR1^{CreER} line was crossed to iDTR animals (Buch et al. 2005). Here, we made use of this system to express a toxin receptor specifically on microglia (DTR^{MG} mice), allowing us to efficiently ablate these cells (>90%) by systemic administration of DT (Fig. 28). We demonstrated that following ablation, the microglia compartment could be rapidly replenished from an intrinsic pool within seven days. Furthermore, in our repopulation model we observed a high number of dividing microglia clusters, which appeared shortly after ablation and resolved once the microglia compartment had been replenished. After only two weeks the microglia compartment regained normal numbers, distribution and morphology (Bruttger et al., 2015). However, the question still remains whether the newly replenished microglia re-establish proper function.

The advantage of this new mouse model is that DTx can be injected intraperitonially (i.p.) and there is no need for preparation of BM chimeras, resulting in very specific and effective microglia ablation (Bruttger et al., 2015). The disadvantage of this system is that it requires the use of TAM (Waisman, 2015). Treatment of mice with TAM may lead to an immunomodulatory phenotype as shown by the suppression of EAE (Elloso et al., 2005) but our previous studies showed no such direct effect (Yogev et al., 2012). In addition, recent reports have described an unexpected biological activity of the DTR in

mice upon inducible expression on conventional dendritic cells (van Blijswijk et al., 2015). However, we could not detect any biological activity for the DTR in our *Cx$_3$Cr1*^{CreER}:DTR system.

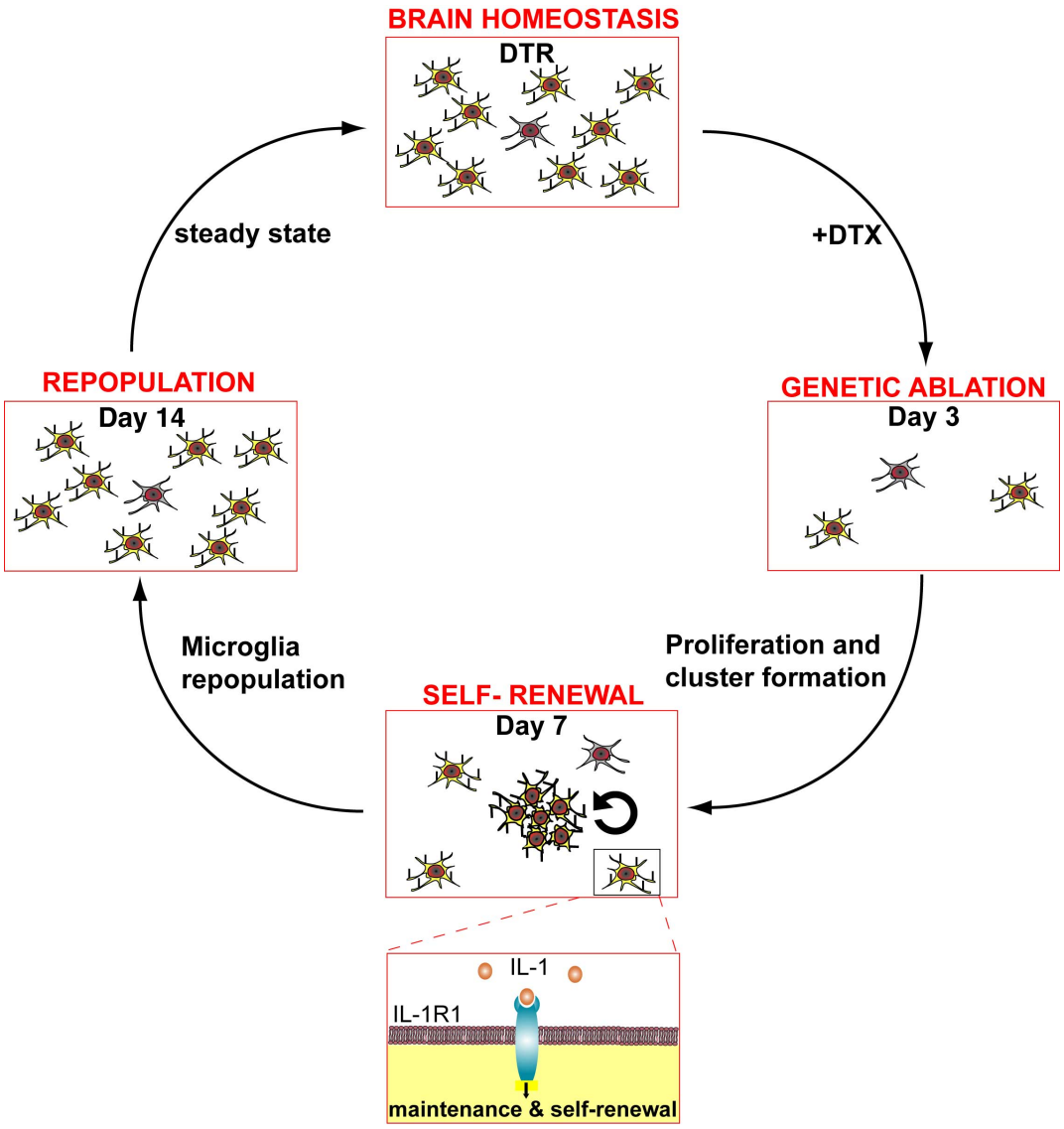

Figure 28 Timecourse of Microglia Depletion and Repopulation (adapted from (Bruttger et al., 2015)
Microglia are efficiently depleted with the *Cx$_3$Cr1*^{CreER}:iDTR system. On day 3 the depletion rate is 90%, but on day 7 already the population is restored. Here we observe clusters of proliferating microglia that highly express the IL-1R1 on their surface. On day 14 all cells are distributed normally again.

4.3 The CD11b-HSVTK System

In the CD11b-HSVTK system microglia are depleted by local application of ganciclovir. Peripheral CCR2^{+} cells, most likely Ly6C^{hi} monocytes, repopulate the whole compartment within only two weeks after treatment termination. The *Cx$_3$Cr1*^{CreER}:iDTR system has several advantages over the CD11b-HSVTK system. Since CD11b also targets many peripheral macrophages and monocytes, the ganciclovir must be administered locally by i.c.v. injection (Waisman, 2015). Importantly, the i.c.v. treatment is a highly invasive procedure that compromises the BBB locally, enabling peripheral cells to enter the brain parenchyma (Fig. 29). Concomitant with the ablation, temporary astrocyte activation has been reported, but neurons remained unchanged in terms of number and morphology (Grathwohl et al., 2009). Whether they still function properly is yet to be determined.

4.4 Pharmacological Depletion of Microglia

In contrast to genetic tools, the pharmacological administration of the CSF-1R inhibitor PLX3397 leads to full microglia deletion (>99%). The advantage of this method is that the drug can be administered in the chow, and can therefore be used to treat any mouse strain (see Figure 2). Furthermore, the BBB remains intact after treatment, as assessed by Evans Blue straining (Elmore et al., 2014). However, this inhibitor is not specific for CSF-1R, as it also inhibits three other kinases: FLT3, PDGFR and KIT (Chitu et al., 2012; Thompson ML1, 2015). In addition, systemic treatment with CSF-1R inhibitor leads to broad myelo-suppression, impacting macrophages, HSCs, osteoclasts and mast cells (Cornelis et al., 2005). Potential peripheral microglia progenitors (like Ly6C^{+} and CX3CR1^{+} cells) in the BM and blood would be similarly affected.

Two major differences between the various models used for microglia depletion are the behavioral changes upon ablation and the tissue response

following depletion. Interestingly, the DTR^{MG} mice do not show any obvious pathological or behavioral phenotype after microglia ablation, although detailed neurological tests still need to be performed. In line with this, CSF-1R inhibition (Elmore et al., 2014) did not affect brain volume, cognition or motor function, as measured with the elevated plus maze, open field, Barnes maze, rotarod or contextual fear conditioning. In contrast, Parkhurst *et al*. (Parkhurst et al., 2013) describes deficits in motoric learning as a result of reduced dendritic spine formation and elimination due to a change in the composition of NMDA and AMPA receptors, which leads to altered biochemical and electrophysiological properties of synapses. Their mice presented multiple learning deficits after microglia ablation in the absence of any obvious CNS tissue alterations even during microglia repopulation. A plausible explanation can be given by considering the different TAM injection patterns to induce the Cx_3Cr1^{CreER}. Parkhurst et al. activate the Cre in younger mice (p1-p3) than we do (p12-14), which might influence the different outcomes of microglia phenotypes. In the former case, synaptogenesis is still occurring, and so by depleting microglia early on, one could expect a secondary effect on the neuronal network, as measured with various behavioral studies. Later on in development, microglia continue to survey synaptic formation, and upon neuronal damage they can strip the synapses from these cells (Kettenmann et al., 2013). Considering the tissue response after microglia ablation, in contrast to the Parkhurst study, we could detect a massive increase in cytokine (TNFα and IL-1β) and chemokine (CCL2, CCL3, CCL5) production (Bruttger et al., 2015), similar to what was observed with CSF-1R inhibition (Fig. 29). Even only a slight disturbance of CNS homeostasis is known to provoke astrocyte activation. Thus, as microglial ablation results in a massive disturbance of the steady state, the source of this cytokine storm is most likely the astrocytes, which showed clear signs of continuous activation, as evidenced by up-regulation of GFAP and S100 expression. However, Parkhurst et al. (Parkhurst et al., 2013) did not observe or report this astrogliosis and the cytokine storm phenomenon.

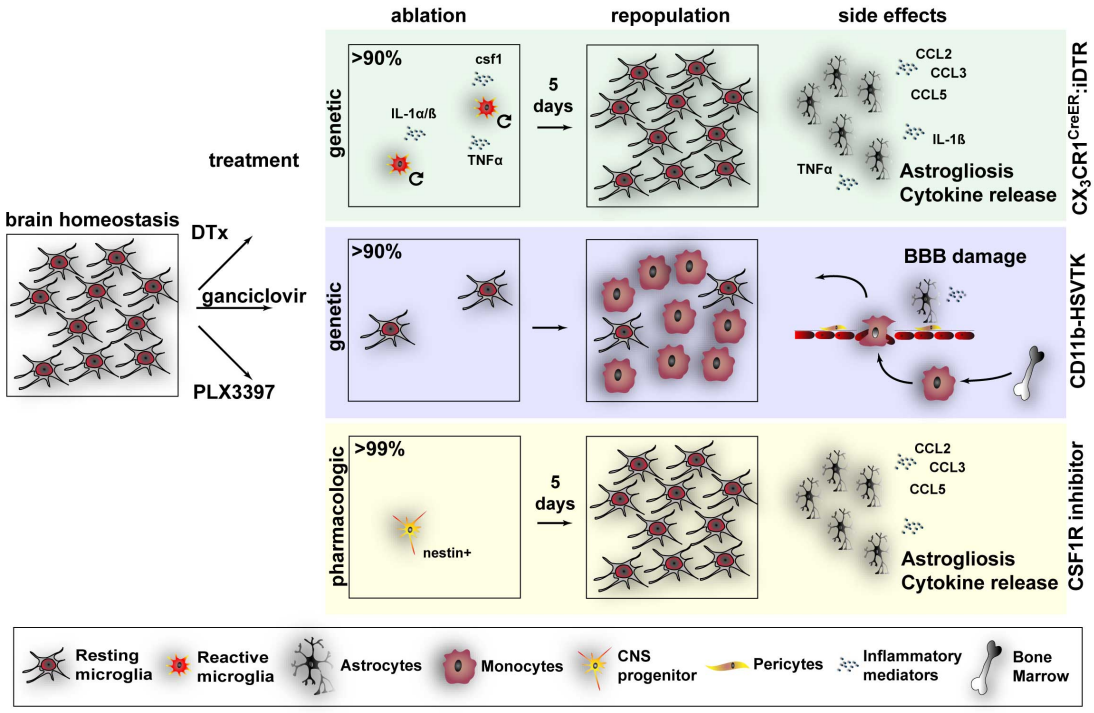

Figure 29 Different Models to ablate Microglia (adapted from(Waisman, 2015))
Two genetic depletions models are shown: the CD11b-HSVTK System (blue) and the *Cx$_3$Cr1*^{CreER}:iDTR system. And a pharmacological depletion system functions through CSF1R inhibition (yellow).

4.5 Microglia Repopulation

In steady state, microglia are quiescent with very little turnover (Lawson et al., 1992). However, when required, these cells can exert massive proliferation, while seeding the CNS during embryonic development (Ginhoux et al., 2010) or during CNS inflammation (Gomez-Nicola et al., 2013) for example. In our repopulation model we observed many clusters of BrdU-incorporating microglia, suggesting their high proliferative capacity. Most likely, the trigger for microglia proliferation is the massive cell death that occurs after ablation, or it is the sensing of the empty niche, possibly mediated by changes of IL-34 and Csf-1 levels. The very same mechanisms might also be ongoing in the brain during steady state, but at a much slower rate difficult to visualize. In our depletion system, the clusters of proliferating microglia were observed after

ablation exclusively in non-irradiated mice (CNS-derived progenitors). No clusters of proliferating microglia were found after depletion in the BM-chimeric system (peripheral progenitors) at any of the analyzed time points (Bruttger et al., 2015). The cells replacing microglia after depletion are derived from CNS intrinsic precursors, but under inflammatory conditions or after irradiation, BM precursors can also give rise to microglia (Ajami et al., 2007; Bruttger, 2015). These peripheral progenitors most likely entered the unprotected CNS as an artifact of irradiation, at the time when BM was engrafted. We injected RFP labeled HSCs i.v. directly after microglia depletion, and after 28 days we could not find RFP+ cells inside the CNS, whereas we were able to track the RFP+ cells in the BM. This experiment was totally devoid of irradiation. This suggests that under steady state conditions the HSCs can be excluded as microglia progenitors. Three major elements contribute to BMT-associated artifact: flooding of the circulation with hematopoietic stem cells, damage to the BBB and irradiation-induced abrogation of the proliferative capacity of CNS resident cells. Corroborating earlier findings (Ajami et al., 2011), the result of the α-CCR2 treatment showed that BM progenitors filling up the microglia niche are not monocytes. These new microglia are able to masquerade as ‘original’ microglia, they exhibit a ramified shape with long processes, and are indistinguishable from intrinsic microglia cells by morphology. However, their genetic profile differs from that of YS-derived microglia and they cannot fully restore the microglia compartment over time, even though BM-derived microglia reside in the brain for at least 12 weeks (Bruttger et al., 2015). What remains an open question is whether over a longer period of time, these newly engrafted microglia acquire full characteristics of embryonically-derived microglia, including function and self-maintenance, or if in the long run CNS resident microglia or precursors of microglia, yet to be discovered, will outnumber the transplanted cells. Indeed, one could speculate whether BM precursors could be utilized in the future for gene therapy in diseases in which microglia are dysfunctional. One could consider replacing genetically damaged microglia with BM precursors after a short period of eradication of the faulty cells. Another approach in microglia

replacement and maturation could be to change environmental factors in the brain(Waisman, 2015). Lately it was shown that microglia maturation and activation during health and disease strongly depend on microbiotic composition (Erny, 2015), which would be fairly easily accessible for treatment of microglia-mediated inflammatory or neuropsychiatric diseases.

Although we demonstrated that without irradiation microglia are repopulated from those highly proliferative CNS internal pools, our data could not determine whether the “new microglia” arise from the residual non-depleted microglia cells, or an alternative source of yet to be defined progenitors. In both cases the new cells would need to be very similar to microglia, as they all express either eYFP or CX_3CR1(Waisman, 2015).

4.6 Microglia Progenitors vs. Self-maintenance

Recently, a new microglia progenitor was characterized by *nestin* expression (Elmore et al., 2014). For a long time it was believed that the brain had limited capacity for regeneration and tissue repair. This remains true for most of the CNS cell types, but some studies challenged this view by showing that many types of glia cells are able to self-maintain locally. Not only oligodendrocyte progenitors can establish their own homeostatic proliferation after depletion (Hughes et al., 2013; Robins et al., 2013), but in fact microglia can also be stimulated to proliferate after pharmacological (Elmore et al., 2014) or genetic ablation (Bruttger et al., 2015). Both studies showed with immunohistological methods that the repopulating cells were $BrdU^+$ and $Ki67^+$. Elmore et al. (2013) showed that cell repopulation occurs rapidly and that the microglia express *nestin*, which is a marker for neuroepithelial stem cells, although it can also be expressed on macrophages as described below. These results suggested the existence of a microglia progenitor within the CNS, since their model resulted in >99% microglia depletion (Waisman, 2015). They compared the *in vivo* situation to the *in vitro* generation of microglia using embryonic stem cells (ESC) that first develop into neurons, and after taking away the

neuronal growth factors they develop into microglia (Beutner et al., 2010). Even though we had similar results (Bruttger et al., 2015), we claim that the entire microglia compartment is rebuilt from the remaining 5-10% microglia cells after ablation. Interestingly, the intrinsically repopulated microglia transiently express nestin. Additionally, the BM-derived microglia that repopulate the brain after irradiation and depletion also express *nestin*. *Nestin* expression by microglia was previously shown, for example, in the early stages of optic nerve injury(Wohl et al., 2011) and traumatic brain injury (Kaya et al., 1999), which points towards the fact that *nestin* may be required for proliferation rather then serving as a stem cell marker. Importantly, as we used the promoter of CX_3CR1 as a cell fate mapping system(Bruttger et al., 2015), we show that all repopulating cells are fate-map positive, indicative of a need for CX_3CR1 expression by the progenitor cells. Alternatively, the CNS environment might trigger *nestin* expression on myeloid cells, irrespective of their origin. The question of the existence of a pre-determined microglia progenitor cell within the brain is not yet conclusively resolved and needs to be further investigated.

4.7 Distinct RNA-Seq Profiles of Different Microglia Populations

In our study, the global transcriptome analysis revealed that the repopulated microglia derived from CNS intrinsic precursors, have a gene expression pattern comparable to that of WT microglia, whereas the BM-derived brain macrophages show a different pattern. This was reflected in the so-called microglia signature genes *P2yr12*, *Mertk*, *Pros1*, *C1qa*, *Olfml3*, *Entpd1*, *Hexb*, and *Tmem119*. They were expressed similarly in WT and CNS-derived microglia, whereas the expression was decreased in BM-derived macrophages (Bruttger et al., 2015). These findings confirm earlier observations that reported differential gene expression patterns of microglia (from different brain regions) compared to peripheral monocytes and other tissue-resident macrophages (Butovsky et al., 2014). Based on these findings

(Butovsky et al., 2014), BM-derived brain macrophages show gene expression patterns similar to peripheral myeloid cells. Even though the BM-derived cells are exposed to the CNS environment, and acquire microglia morphology, they retain a gene expression profile that discloses their separate origin. For example, CSF-1 and CSF-1R, two molecules known to be critical for microglia development and maintenance, are also highly expressed in WT and CNS-derived microglia, whereas their expression is decreased in BM-derived macrophages. Further work is needed to unravel the functional differences between the different microglia populations.

4.8 Impact of Interleukin-1 on Microglia

Two other genes, Interleukin-1 receptor type I (IL-1R1) and Interleukin-1α (IL-1α) are higher and therefore differentially expressed in CNS derived microglia, whereas the BM MΦ display low expression values. This result suggests that microglia partially depend on Interleukin-1 signaling (Bruttger et al., 2015) and therefore describes a new, and thus far unknown factor for microglia maintenance (Fig. 28). Strikingly, the *in vivo* IL-1Ra (*Anakinra*) treatment could delay the repopulation event by affecting proliferation. Taken together, these results suggest an essential role for IL-1 signaling in the physiological maintenance of microglia. Although we neutralized IL-1α by IL-1Ra treatment, we could not completely block the repopulation of the microglia. This could stem from different reasons, or combinations of them: First, the half-life of the drug IL-1Ra is only 4 to 6 hours (Akash et al., 2013); in addition, the access of the drug to all brain regions was incomplete when injected i.c.v. in one specific region. Interestingly, the conditional deletion of the IL-1R1 in IL-1R1^{MG} mice show reduced microglia numbers under steady state throughout various brain regions. The microglia morphology in IL-1R1^{MG} mice is atypical and differs substantially from WT microglia. The former show an over-ramified morphology with multiple processes, which are thicker and more branched (Bruttger et al., 2015). This is a possible side effect due to the presence of

less microglia, since the microglia present must survey more of their microenvironment. It might also be interesting to see if the microglia in such a model have an effect on synaptic stripping or an overall effect on the neuronal network. In a recently published study, microglia of mice kept under germfree conditions showed a similar morphology to the IL-1R1^{MG} mice, which even persisted in inflammation. The authors suggested that these microglia maintain an immature phenotype (Erny, 2015). The immaturity of the microglia in IL-1R1^{MG} mice could also explain the delayed disease onset after EAE induction. Without IL-1R1 expression they might need longer until they are primed for proper functionality. Once the disease started, it reached similar overall maximum scores to wild type controls. In steady state conditions, IL-1 signaling in the CNS seems to play an essential role in proliferation of neural stem cells (Garcia-Ovejero et al., 2013). We could also describe an effect of IL-1 signaling in microglia proliferation. Additionally, microglia specific IL-1 signaling participates in CNS immunity in terms of affecting disease outcome in EAE (Bruttger et al., 2015).

Already the development of new fate-mapping techniques helped to elucidate the ontogeny of microglia during embryonic development. Moreover, the use of CX_3CR1^{CreER} mice enabled us to specifically target microglia for DT-mediated cell ablation in adult mice and to study its consequences for CNS homeostasis. However, the mechanisms by which these unique cells are maintained in the adult CNS are still not clear. This study provides evidence for microglia displaying a very high proliferative capacity. The rapid repopulation of microglia after ablation emphasizes the indispensable role of these cells to maintain tissue integrity in the steady state (Waisman, 2015). The consequences of microglia being absent for longer periods of time remain elusive. Thus CNS integrity and function, under conditions of long-term removal of microglia or of genes expressed by microglia, still need to be investigated. By doing so, this may also help to clarify the exact functions of microglia under homeostatic conditions or in synaptic support. Preliminary results could be obtained by analyzing the microglia specific knock out of IL-1R1. Moreover, our study delivers yet another example for the self-

maintenance of tissue-resident macrophage populations that do not require the contribution of external progenitors. Hence, our depletion system is a valuable tool for observing the physiology of microglia *in vivo*.

5 Summary

The development of new fate mapping techniques helped to elucidate the ontogeny of microglia during embryonic development. Microglia precursors arise during the primitive hematopoiesis at E7.5 and develop into early progenitors found in the yolk sac at E9.5. From there they migrate through the circulation to the CNS parenchyma between E10.5-E13.5, where they persist throughout adulthood. However, the mechanisms by which these unique cells are maintained in the adult CNS still remain elusive.

In this study, we describe the *Cx$_3$Cr1*^{CreER}:iDTR system, a genetic model that allows for specific, conditional ablation of microglia in adult mice. With the help of this new genetic model we were able to deplete microglia with at least 90% efficiency. Surprisingly, the depletion was followed by rapid repopulation of the microglia compartment. The repopulation relied on CNS-resident cells, independent of bone-marrow-derived precursors, whereas the existence of a certain pre-determined microglia progenitor within the CNS is not yet completely proven. During the repopulation process, microglia formed clusters of highly proliferative cells that migrated away until normal microglia numbers were reestablished and steady state distribution was achieved. The trigger for the rapid repopulation is not yet clear, but could be driven by local progenitors in response to IL-1R signaling, since proliferating microglia expressed high levels of the interleukin-1 receptor (IL-1R), and treatment with an IL-1R antagonist during the repopulation phase impaired microglia proliferation. Furthermore, according to other tissue resident macrophages, microglia also demonstrate their potential for efficient self-renewal without the contribution of peripheral myeloid cells.

6 Zusammenfassung

Die Entwicklung neuer Fate-mapping- Techniken hat dazu beigetragen die Ontogenese von Mikroglia während der embryonalen Entwicklung weiter aufzuklären. Mikrogliale Vorläuferzellen entstehen während der primitiven Hämatopoese am embryonalem Tag E7.5 und entwickeln sich weiter zu frühen Vorläuferzellen, die an Tag E9.5 im Dottersack zu finden sind. Von hier aus wandern sie zwischen Tag E10.5-E13.5 durch das Blut zum ZNS, wo sie bis zum Erwachsenenalter verharren. Die Mechanismen, durch die diese einzigartigen Zellen im erwachsenen ZNS aufrechterhalten bleiben sind allerdings noch ungeklärt.

In dieser Studie beschreiben wir das *Cx$_3$Cr1*^{CreER}:iDTR System, ein genetisches Model zur spezifischen und konditionalen Depletion von Mikroglia in erwachsenen Mäusen. Die Depletionseffizienz der Mikroglia Population in diesem Model lag dabei bei mindestens 90%. Überraschenderweise hatte diese Depletion eine schnelle Repopulation des mikroglialen Kompartimentes zur Folge. Diese Repopulation geschah unabhängig von den myeloiden Vorläufern des Knochenmarks und basiert grundlegend auf ZNS-eigenen Zellen. Allerdings konnte die Existenz von bestimmten vorgeprägten Mikroglia-Vorläuferzellen im erwachsenen ZNS noch nicht vollständig bewiesen werden. Jedoch werden während des Repopulationsvorgangs zahlreiche Zellkonglomerate von sich teilenden Mikroglia gebildet. Von diesen Zellkonglomeraten ausgehend wandern die einzelnen Zellen in das Gewebe, bis die normale Zellzahl und Verteilung von Mikroglia wieder erreicht ist. Der Auslöser für diese schnelle Repopulation ist noch unklar, könnte jedoch durch lokale Vorläuferzellen in Antwort auf Interleukin-1 Rezeptor (IL-1R) Signalisierung erfolgen, da sich teilende Mikroglia große Mengen des IL-1R exprimieren. Zudem beeinträchtigt die lokale Behandlung mit einem IL-1R Antagonisten während der Repopulationsphase die Teilungsrate der Mikroglia. Analog zu anderen Gewebsmakrophagen konnten Mikroglia zudem ihr Potential für effiziente Selbsterneuerung demonstrieren, ohne von peripheren myeloiden Zellen abhängig zu sein.

7 References

Ajami, B., Bennett, J.L., Krieger, C., McNagny, K.M., and Rossi, F.M. (2011). Infiltrating monocytes trigger EAE progression, but do not contribute to the resident microglia pool. Nat Neurosci *14*, 1142-1149.

Ajami, B., Bennett, J.L., Krieger, C., Tetzlaff, W., and Rossi, F.M. (2007). Local self-renewal can sustain CNS microglia maintenance and function throughout adult life. Nat Neurosci *10*, 1538-1543.

Akash, M.S., Rehman, K., and Chen, S. (2013). IL-1Ra and its delivery strategies: inserting the association in perspective. Pharmaceutical research *30*, 2951-2966.

Allen, N.J., and Barres, B.A. (2009). Neuroscience: Glia - more than just brain glue. Nature *457*, 675-677.

Alliot, F., Godin, I., and Pessac, B. (1999). Microglia derive from progenitors, originating from the yolk sac, and which proliferate in the brain. Brain Res Dev Brain Res *117*, 145-152.

Alliot, F., Lecain, E., Grima, B., and Pessac, B. (1991). Microglial progenitors with a high proliferative potential in the embryonic and adult mouse brain. Proceedings of the National Academy of Sciences of the United States of America *88*, 1541-1545.

Andre, R., Moggs, J.G., Kimber, I., Rothwell, N.J., and Pinteaux, E. (2006). Gene regulation by IL-1beta independent of IL-1R1 in the mouse brain. Glia *53*, 477-483.

Ashwell, K. (1990). Microglia and cell death in the developing mouse cerebellum. Brain Res Dev Brain Res *55*, 219-230.

Ashwell, K. (1991). The distribution of microglia and cell death in the fetal rat forebrain. Brain Res Dev Brain Res *58*, 1-12.

Ballabh, P., Braun, A., and Nedergaard, M. (2004). The blood-brain barrier: an overview: structure, regulation, and clinical implications. Neurobiology of disease *16*, 1-13.

Basu, A., Krady, J.K., O'Malley, M., Styren, S.D., DeKosky, S.T., and Levison, S.W. (2002). The type 1 interleukin-1 receptor is essential for the efficient activation of microglia and the induction of multiple proinflammatory mediators in response to brain injury. The Journal of neuroscience : the official journal of the Society for Neuroscience *22*, 6071-6082.

Baumann, N., and Pham-Dinh, D. (2001). Biology of oligodendrocyte and myelin in the mammalian central nervous system. Physiol Rev *81*, 871-927.

Beutner, C., Roy, K., Linnartz, B., Napoli, I., and Neumann, H. (2010). Generation of microglial cells from mouse embryonic stem cells. Nat Protoc *5*, 1481-1494.

Bjartmar, C., Hildebrand, C., and Loinder, K. (1994). Morphological heterogeneity of rat oligodendrocytes: electron microscopic studies on serial sections. Glia *11*, 235-244.

Bruttger, J., Karram, K., Wortge, S., Regen, T., Marini, F., Hoppmann, N., Klein, M., Blank, T., Yona, S., Wolf, Y.*, et al.* (2015). Genetic Cell Ablation Reveals Clusters of Local Self-Renewing Microglia in the Mammalian Central Nervous System. Immunity *43*, 92-106.

Buch, T., Heppner, F.L., Tertilt, C., Heinen, T.J., Kremer, M., Wunderlich, F.T., Jung, S., and Waisman, A. (2005). A Cre-inducible diphtheria toxin receptor mediates cell lineage ablation after toxin administration. Nature methods *2*, 419-426.
Butovsky, O., Jedrychowski, M.P., Moore, C.S., Cialic, R., Lanser, A.J., Gabriely, G., Koeglsperger, T., Dake, B., Wu, P.M., Doykan, C.E., *et al.* (2014). Identification of a unique TGF-beta-dependent molecular and functional signature in microglia. Nat Neurosci *17*, 131-143.
Chauhan, N.B., Siegel, G.J., and Lichtor, T. (2001). Distribution of intraventricularly administered antiamyloid-beta peptide (Abeta) antibody in the mouse brain. Journal of neuroscience research *66*, 231-235.
Chitu, V., Nacu, V., Charles, J.F., Henne, W.M., McMahon, H.T., Nandi, S., Ketchum, H., Harris, R., Nakamura, M.C., and Stanley, E.R. (2012). PSTPIP2 deficiency in mice causes osteopenia and increased differentiation of multipotent myeloid precursors into osteoclasts. Blood *120*, 3126-3135.
Cornelis, S., Bruynooghe, Y., Van Loo, G., Saelens, X., Vandenabeele, P., and Beyaert, R. (2005). Apoptosis of hematopoietic cells induced by growth factor withdrawal is associated with caspase-9 mediated cleavage of Raf-1. Oncogene *24*, 1552-1562.
Coste, C., Neirinckx, V., Gothot, A., Wislet, S., and Rogister, B. (2015). Are neural crest stem cells the missing link between hematopoietic and neurogenic niches? Frontiers in cellular neuroscience *9*, 218.
Dai, X.M., Ryan, G.R., Hapel, A.J., Dominguez, M.G., Russell, R.G., Kapp, S., Sylvestre, V., and Stanley, E.R. (2002). Targeted disruption of the mouse colony-stimulating factor 1 receptor gene results in osteopetrosis, mononuclear phagocyte deficiency, increased primitive progenitor cell frequencies, and reproductive defects. Blood *99*, 111-120.
Daneman, R., Zhou, L., Kebede, A.A., and Barres, B.A. (2010). Pericytes are required for blood-brain barrier integrity during embryogenesis. Nature *468*, 562-566.
Dantzer, R., O'Connor, J.C., Freund, G.G., Johnson, R.W., and Kelley, K.W. (2008). From inflammation to sickness and depression: when the immune system subjugates the brain. Nat Rev Neurosci *9*, 46-57.
Davalos, D., Grutzendler, J., Yang, G., Kim, J.V., Zuo, Y., Jung, S., Littman, D.R., Dustin, M.L., and Gan, W.B. (2005). ATP mediates rapid microglial response to local brain injury in vivo. Nat Neurosci *8*, 752-758.
Davalos, D., Grutzendler, J., Yang, G., Kim, J.V., Zuo, Y., Jung, S., Littman, D.R.
Elloso, M.M., Phiel, K., Henderson, R.A., Harris, H.A., and Adelman, S.J. (2005). Suppression of experimental autoimmune encephalomyelitis using estrogen receptor-selective ligands. J Endocrinol *185*, 243-252.
Elmore, M.R., Najafi, A.R., Koike, M.A., Dagher, N.N., Spangenberg, E.E., Rice, R.A., Kitazawa, M., Matusow, B., Nguyen, H., West, B.L., and Green, K.N. (2014). Colony-stimulating factor 1 receptor signaling is necessary for microglia viability, unmasking a microglia progenitor cell in the adult brain. Neuron *82*, 380-397.
Erny, D.H.d.A., Anna Lena; Jaitin, Diego; Wieghofer, Peter; Staszewski, Ori; David, Eyal; Keren-Shaul, Hadas; Mahlakoiv, Tanel; Jakobshagen, Kerstin; Buch, Thorsten; Schwierzeck, Vera; Uternöhlen, Olaf; Chun, Eunyoung; Garrett, Wendy; McCoy, Kathy; Diefenbach, Andreas; Staeheli, Peter; Stecher, Bärbel; Amit, Ido; Prinz, Marco (2015). Host microbiota constantly control maturation and function of microglia in the CNS. Nat Neurosci *18*, 965-977.

Ford, A.L., Foulcher, E., Lemckert, F.A., and Sedgwick, J.D. (1996). Microglia induce CD4 T lymphocyte final effector function and death. The Journal of experimental medicine *184*, 1737-1745.
Garceau, V., Smith, J., Paton, I.R., Davey, M., Fares, M.A., Sester, D.P., Burt, D.W., and Hume, D.A. (2010). Pivotal Advance: Avian colony-stimulating factor 1 (CSF-1), interleukin-34 (IL-34), and CSF-1 receptor genes and gene products. Journal of leukocyte biology *87*, 753-764.
Garcia-Ovejero, D., Arevalo-Martin, A., Navarro-Galve, B., Pinteaux, E., Molina-Holgado, E., and Molina-Holgado, F. (2013). Neuroimmmune interactions of cannabinoids in neurogenesis: focus on interleukin-1beta (IL-1beta) signalling. Biochemical Society transactions *41*, 1577-1582.
Geissmann, F., Manz, M.G., Jung, S., Sieweke, M.H., Merad, M., and Ley, K. (2010). Development of Monocytes, Macrophages, and Dendritic Cells. Science *327*, 656-661.
Ginhoux, F., Greter, M., Leboeuf, M., Nandi, S., See, P., Gokhan, S., Mehler, M.F., Conway, S.J., Ng, L.G., Stanley, E.R.*, et al.* (2010). Fate mapping analysis reveals that adult microglia derive from primitive macrophages. Science *330*, 841-845.
Ginhoux, F., and Jung, S. (2014). Monocytes and macrophages: developmental pathways and tissue homeostasis. Nat Rev Immunol *14*, 392-404.
Ginhoux, F., and Merad, M. (2010). Ontogeny and homeostasis of Langerhans cells. Immunology and cell biology *88*, 387-392.
Ginhoux, F., and Prinz, M. (2015). Origin of Microglia: Current Concepts and Past Controversies. Cold Spring Harbor perspectives in biology *7*.
Ginhoux, F., Tacke, F., Angeli, V., Bogunovic, M., Loubeau, M., Dai, X.M., Stanley, E.R., Randolph, G.J., and Merad, M. (2006). Langerhans cells arise from monocytes in vivo. Nature immunology *7*, 265-273.
Glaccum, M.B., Stocking, K.L., Charrier, K., Smith, J.L., Willis, C.R., Maliszewski, C., Livingston, D.J., Peschon, J.J., and Morrissey, P.J. (1997). Phenotypic and functional characterization of mice that lack the type I receptor for IL-1. Journal of immunology *159*, 3364-3371.
Goldmann, T., Wieghofer, P., Muller, P.F., Wolf, Y., Varol, D., Yona, S., Brendecke, S.M., Kierdorf, K., Staszewski, O., Datta, M.*, et al.* (2013). A new type of microglia gene targeting shows TAK1 to be pivotal in CNS autoimmune inflammation. Nat Neurosci *16*, 1618-1626.
Gomez-Nicola, D., Fransen, N.L., Suzzi, S., and Perry, V.H. (2013). Regulation of microglial proliferation during chronic neurodegeneration. The Journal of neuroscience : the official journal of the Society for Neuroscience *33*, 2481-2493.
Grathwohl, S.A., Kalin, R.E., Bolmont, T., Prokop, S., Winkelmann, G., Kaeser, S.A., Odenthal, J., Radde, R., Eldh, T., Gandy, S.*, et al.* (2009). Formation and maintenance of Alzheimer's disease beta-amyloid plaques in the absence of microglia. Nature neuroscience *12*, 1361-1363.
Greter, M., Lelios, I., Pelczar, P., Hoeffel, G., Price, J., Leboeuf, M., Kundig, T.M., Frei, K., Ginhoux, F., Merad, M., and Becher, B. (2012). Stroma-derived interleukin-34 controls the development and maintenance of langerhans cells and the maintenance of microglia. Immunity *37*, 1050-1060.
Gritsch, S., Lu, J.N., Thilemann, S., Wortge, S., Mobius, W., Bruttger, J., Karram, K., Ruhwedel, T., Blanfeld, M., Vardeh, D.*, et al.* (2014). Oligodendrocyte ablation triggers central pain independently of innate or adaptive immune responses in mice. Nat Commun *5*.

Hashimoto, D., Chow, A., Noizat, C., Teo, P., Beasley, M.B., Leboeuf, M., Becker, C.D., See, P., Price, J., Lucas, D*., et al.* (2013). Tissue-resident macrophages self-maintain locally throughout adult life with minimal contribution from circulating monocytes. Immunity *38*, 792-804.
Heppner, F.L., Greter, M., Marino, D., Falsig, J., Raivich, G., Hovelmeyer, N., Waisman, A., Rulicke, T., Prinz, M., Priller, J*., et al.* (2005). Experimental autoimmune encephalomyelitis repressed by microglial paralysis. Nature medicine *11*, 146-152.
Herbomel, P., Thisse, B., and Thisse, C. (1999). Ontogeny and behaviour of early macrophages in the zebrafish embryo. Development *126*, 3735-3745.
Hockfield, S., and McKay, R.D. (1985). Identification of major cell classes in the developing mammalian nervous system. The Journal of neuroscience : the official journal of the Society for Neuroscience *5*, 3310-3328.
Hoeffel, G., Chen, J., Lavin, Y., Low, D., Almeida, F.F., See, P., Beaudin, A.E., Lum, J., Low, I., Forsberg, E.C*., et al.* (2015). C-Myb(+) erythro-myeloid progenitor-derived fetal monocytes give rise to adult tissue-resident macrophages. Immunity *42*, 665-678.
Hughes, E.G., Kang, S.H., Fukaya, M., and Bergles, D.E. (2013). Oligodendrocyte progenitors balance growth with self-repulsion to achieve homeostasis in the adult brain. Nat Neurosci *16*, 668-+.
Hughes, P.M., Botham, M.S., Frentzel, S., Mir, A., and Perry, V.H. (2002). Expression of fractalkine (CX3CL1) and its receptor, CX3CR1, during acute and chronic inflammation in the rodent CNS. Glia *37*, 314-327.
Jenkins, S.J., and Hume, D.A. (2014). Homeostasis in the mononuclear phagocyte system. Trends in immunology *35*, 358-367.
Jenkins, S.J., Ruckerl, D., Cook, P.C., Jones, L.H., Finkelman, F.D., van Rooijen, N., MacDonald, A.S., and Allen, J.E. (2011). Local macrophage proliferation, rather than recruitment from the blood, is a signature of TH2 inflammation. Science *332*, 1284-1288.
Jung, S., Aliberti, J., Graemmel, P., Sunshine, M.J., Kreutzberg, G.W., Sher, A., and Littman, D.R. (2000). Analysis of fractalkine receptor CX(3)CR1 function by targeted deletion and green fluorescent protein reporter gene insertion. Mol Cell Biol *20*, 4106-4114.
Kaya, S.S., Mahmood, A., Li, Y., Yavuz, E., and Chopp, M. (1999). Expression of nestin after traumatic brain injury in rat brain. Brain Res *840*, 153-157.
Kettenmann, H., Hanisch, U.K., Noda, M., and Verkhratsky, A. (2011). Physiology of Microglia. Physiol Rev *91*, 461-553.
Kettenmann, H., Kirchhoff, F., and Verkhratsky, A. (2013). Microglia: new roles for the synaptic stripper. Neuron *77*, 10-18.
Kierdorf, K., Erny, D., Goldmann, T., Sander, V., Schulz, C., Perdiguero, E.G., Wieghofer, P., Heinrich, A., Riemke, P., Holscher, C*., et al.* (2013). Microglia emerge from erythromyeloid precursors via Pu.1- and Irf8-dependent pathways. Nat Neurosci *16*, 273-280.
Kierdorf, K., and Prinz, M. (2013). Factors regulating microglia activation. Frontiers in cellular neuroscience *7*, 44.
Kim, K.W., Vallon-Eberhard, A., Zigmond, E., Farache, J., Shezen, E., Shakhar, G., Ludwig, A., Lira, S.A., and Jung, S. (2011). In vivo structure/function and expression analysis of the CX3C chemokine fractalkine. Blood *118*, e156-167.

Koizumi, S., Shigemoto-Mogami, Y., Nasu-Tada, K., Shinozaki, Y., Ohsawa, K., Tsuda, M., Joshi, B.V., Jacobson, K.A., Kohsaka, S., and Inoue, K. (2007). UDP acting at P2Y6 receptors is a mediator of microglial phagocytosis. Nature *446*, 1091-1095.

Labow, M., Shuster, D., Zetterstrom, M., Nunes, P., Terry, R., Cullinan, E.B., Bartfai, T., Solorzano, C., Moldawer, L.L., Chizzonite, R., and McIntyre, K.W. (1997). Absence of IL-1 signaling and reduced inflammatory response in IL-1 type I receptor-deficient mice. Journal of immunology *159*, 2452-2461.

Lampron, A., Lessard, M., and Rivest, S. (2012). Effects of myeloablation, peripheral chimerism, and whole-body irradiation on the entry of bone marrow-derived cells into the brain. Cell transplantation *21*, 1149-1159.

Lawson, L.J., Perry, V.H., and Gordon, S. (1992). Turnover of resident microglia in the normal adult mouse brain. Neuroscience *48*, 405-415.

Lin, H., Lee, E., Hestir, K., Leo, C., Huang, M., Bosch, E., Halenbeck, R., Wu, G., Zhou, A., Behrens, D.*, et al.* (2008). Discovery of a cytokine and its receptor by functional screening of the extracellular proteome. Science *320*, 807-811.

Locatelli, G., Wortge, S., Buch, T., Ingold, B., Frommer, F., Sobottka, B., Kruger, M., Karram, K., Buhlmann, C., Bechmann, I.*, et al.* (2012). Primary oligodendrocyte death does not elicit anti-CNS immunity. Nat Neurosci *15*, 543-550.

McGrath, K.E., Koniski, A.D., Malik, J., and Palis, J. (2003). Circulation is established in a stepwise pattern in the mammalian embryo. Blood *101*, 1669-1676.

McKercher, S.R., Torbett, B.E., Anderson, K.L., Henkel, G.W., Vestal, D.J., Baribault, H., Klemsz, M., Feeney, A.J., Wu, G.E., Paige, C.J., and Maki, R.A. (1996). Targeted disruption of the PU.1 gene results in multiple hematopoietic abnormalities. Embo J *15*, 5647-5658.

Mildner, A., Mack, M., Schmidt, H., Bruck, W., Djukic, M., Zabel, M.D., Hille, A., Priller, J., and Prinz, M. (2009). CCR2+Ly-6Chi monocytes are crucial for the effector phase of autoimmunity in the central nervous system. Brain : a journal of neurology *132*, 2487-2500.

Mildner, A., Schmidt, H., Nitsche, M., Merkler, D., Hanisch, U.K., Mack, M., Heikenwalder, M., Bruck, W., Priller, J., and Prinz, M. (2007). Microglia in the adult brain arise from Ly-6ChiCCR2+ monocytes only under defined host conditions. Nat Neurosci *10*, 1544-1553.

Miller, R.H. (2002). Regulation of oligodendrocyte development in the vertebrate CNS. Progress in neurobiology *67*, 451-467.

Mizutani, M., Pino, P.A., Saederup, N., Charo, I.F., Ransohoff, R.M., and Cardona, A.E. (2012). The fractalkine receptor but not CCR2 is present on microglia from embryonic development throughout adulthood. J Immunol *188*, 29-36.

Naito, M., Takahashi, K., and Nishikawa, S. (1990). Development, differentiation, and maturation of macrophages in the fetal mouse liver. J Leukoc Biol *48*, 27-37.

Nimmerjahn, A., Kirchhoff, F., and Helmchen, F. (2005). Resting microglial cells are highly dynamic surveillants of brain parenchyma in vivo. Science *308*, 1314-1318.

Paolicelli, R.C., Bolasco, G., Pagani, F., Maggi, L., Scianni, M., Panzanelli, P., Giustetto, M., Ferreira, T.A., Guiducci, E., Dumas, L.*, et al.* (2011). Synaptic Pruning by Microglia Is Necessary for Normal Brain Development. Science *333*, 1456-1458.

Parkhurst, C.N., Yang, G., Ninan, I., Savas, J.N., Yates, J.R., 3rd, Lafaille, J.J., Hempstead, B.L., Littman, D.R., and Gan, W.B. (2013). Microglia Promote Learning-Dependent Synapse Formation through Brain-Derived Neurotrophic Factor. Cell *155*, 1596-1609.
Pineau, I., and Lacroix, S. (2007). Proinflammatory cytokine synthesis in the injured mouse spinal cord: multiphasic expression pattern and identification of the cell types involved. The Journal of comparative neurology *500*, 267-285.
Pineau, I., Sun, L., Bastien, D., and Lacroix, S. (2010). Astrocytes initiate inflammation in the injured mouse spinal cord by promoting the entry of neutrophils and inflammatory monocytes in an IL-1 receptor/MyD88-dependent fashion. Brain, behavior, and immunity *24*, 540-553.
Prinz, M., and Priller, J. (2014). Microglia and brain macrophages in the molecular age: from origin to neuropsychiatric disease. Nature reviews. Neuroscience *15*, 300-312.
Qian, J., Zhu, L., Li, Q., Belevych, N., Chen, Q., Zhao, F., Herness, S., and Quan, N. (2012). Interleukin-1R3 mediates interleukin-1-induced potassium current increase through fast activation of Akt kinase. Proceedings of the National Academy of Sciences of the United States of America *109*, 12189-12194.
Rau, A., Gallopin, M., Celeux, G., and Jaffrezic, F. (2013). Data-based filtering for replicated high-throughput transcriptome sequencing experiments. Bioinformatics *29*, 2146-2152.
Robins, S.C., Villemain, A., Liu, X.H., Djogo, T., Kryzskaya, D., Storch, K.F., and Kokoeva, M.V. (2013). Extensive regenerative plasticity among adult NG2-glia populations is exclusively based on self-renewal. Glia *61*, 1735-1747.
Salzer, J.L. (2003). Polarized domains of myelinated axons. Neuron *40*, 297-318.
Samokhvalov, I.M., Samokhvalova, N.I., and Nishikawa, S. (2007). Cell tracing shows the contribution of the yolk sac to adult haematopoiesis. Nature *446*, 1056-1061.
Schulz, C., Gomez Perdiguero, E., Chorro, L., Szabo-Rogers, H., Cagnard, N., Kierdorf, K., Prinz, M., Wu, B., Jacobsen, S.E., Pollard, J.W.*, et al.* (2012a). A Lineage of Myeloid Cells Independent of Myb and Hematopoietic Stem Cells. Science.
Schulz, C., Gomez Perdiguero, E., Chorro, L., Szabo-Rogers, H., Cagnard, N., Kierdorf, K., Prinz, M., Wu, B., Jacobsen, S.E., Pollard, J.W.*, et al.* (2012b). A lineage of myeloid cells independent of Myb and hematopoietic stem cells. Science *336*, 86-90.
Scott, E.W., Simon, M.C., Anastasi, J., and Singh, H. (1994). Requirement of Transcription Factor Pu.1 in the Development of Multiple Hematopoietic Lineages. Science *265*, 1573-1577.
Shull, M.M., Ormsby, I., Kier, A.B., Pawlowski, S., Diebold, R.J., Yin, M.Y., Allen, R., Sidman, C., Proetzel, G., Calvin, D.*, et al.* (1992). Targeted Disruption of the Mouse Transforming Growth Factor-Beta-1 Gene Results in Multifocal Inflammatory Disease. Nature *359*, 693-699.
Sierra, A., Encinas, J.M., Deudero, J.J., Chancey, J.H., Enikolopov, G., Overstreet-Wadiche, L.S., Tsirka, S.E., and Maletic-Savatic, M. (2010). Microglia shape adult hippocampal neurogenesis through apoptosis-coupled phagocytosis. Cell stem cell *7*, 483-495.
Sorokin, S.P., Hoyt, R.F., Jr., Blunt, D.G., and McNelly, N.A. (1992). Macrophage development: II. Early ontogeny of macrophage populations in brain, liver, and lungs of rat embryos as revealed by a lectin marker. Anat Rec *232*, 527-550.

Srinivas, S., Watanabe, T., Lin, C.S., William, C.M., Tanabe, Y., Jessell, T.M., and Costantini, F. (2001). Cre reporter strains produced by targeted insertion of EYFP and ECFP into the ROSA26 locus. BMC developmental biology *1*, 4.
Takahashi, K., Yamamura, F., and Naito, M. (1989a). Differentiation, maturation, and proliferation of macrophages in the mouse yolk sac: a light-microscopic, enzyme-cytochemical, immunohistochemical, and ultrastructural study. J Leukoc Biol *45*, 87-96.
Takahashi, K., Yamamura, F., and Naito, M. (1989b). Differentiation, maturation, and proliferation of macrophages in the mouse yolk sac: a light-microscopic, enzyme-cytochemical, immunohistochemical, and ultrastructural study. J Leukoc Biol *45*, 87-96.
Thompson ML1, J.-A.J., Chartier S, Tsai J, Burton EA, Habets G, Lin PS, West BL, Mantyh PW (2015). Targeting cells of the myeloid lineage attenuates pain and disease progression in a prostate model of bone cancer. Pain.
Trotter, J., Karram, K., and Nishiyama, A. (2010). NG2 cells: Properties, progeny and origin. Brain research reviews *63*, 72-82.
van Blijswijk, J., Schraml, B.U., Rogers, N.C., Whitney, P.G., Zelenay, S., Acton, S.E., and Sousa, C.R.E. (2015). Altered Lymph Node Composition in Diphtheria Toxin Receptor-Based Mouse Models To Ablate Dendritic Cells. J Immunol *194*, 307-315.
Varol, C., Vallon-Eberhard, A., Elinav, E., Aychek, T., Shapira, Y., Luche, H., Fehling, H.J., Hardt, W.D., Shakhar, G., and Jung, S. (2009). Intestinal lamina propria dendritic cell subsets have different origin and functions. Immunity *31*, 502-512.
Varvel, N.H., Grathwohl, S.A., Baumann, F., Liebig, C., Bosch, A., Brawek, B., Thal, D.R., Charo, I.F., Heppner, F.L., Aguzzi, A*., et al.* (2012). Microglial repopulation model reveals a robust homeostatic process for replacing CNS myeloid cells. Proceedings of the National Academy of Sciences of the United States of America *109*, 18150-18155.
Waisman, A.; Ginhoux, F.; Greter, M; Bruttger, J. (2015). Homeostasis of Microglia in the Adult Brain: Review of Novel Microglia Depletion Systems. Trends in immunology.
Wang, Y., Szretter, K.J., Vermi, W., Gilfillan, S., Rossini, C., Cella, M., Barrow, A.D., Diamond, M.S., and Colonna, M. (2012). IL-34 is a tissue-restricted ligand of CSF1R required for the development of Langerhans cells and microglia. Nature immunology *13*, 753-760.
Wohl, S.G., Schmeer, C.W., Friese, T., Witte, O.W., and Isenmann, S. (2011). In Situ Dividing and Phagocytosing Retinal Microglia Express Nestin, Vimentin, and NG2 In Vivo. Plos One *6*.
Yogev, N., Frommer, F., Lukas, D., Kautz-Neu, K., Karram, K., Ielo, D., von Stebut, E., Probst, H.C., van den Broek, M., Riethmacher, D*., et al.* (2012). Dendritic Cells Ameliorate Autoimmunity in the CNS by Controlling the Homeostasis of PD-1 Receptor(+) Regulatory T Cells. Immunity *37*, 264-275.
Yona, S., Kim, K.W., Wolf, Y., Mildner, A., Varol, D., Breker, M., Strauss-Ayali, D., Viukov, S., Guilliams, M., Misharin, A*., et al.* (2013). Fate mapping reveals origins and dynamics of monocytes and tissue macrophages under homeostasis. Immunity *38*, 79-91.
Zhang, G.-X., Li, J., Ventura, E., and Rostami, A. (2002). Parenchymal Microglia of Naïve Adult C57BL/6J Mice Express High Levels of B7.1, B7.2, and MHC Class II. Experimental and Molecular Pathology *73*, 35-45.

Zusso, M., Methot, L., Lo, R., Greenhalgh, A.D., David, S., and Stifani, S. (2012). Regulation of postnatal forebrain amoeboid microglial cell proliferation and development by the transcription factor Runx1. The Journal of neuroscience : the official journal of the Society for Neuroscience *32*, 11285-11298.

Erklärung

Ich versichere, dass ich die von mir vorgelegte Dissertation selbständig angefertigt, die benutzten Quellen und Hilfsmittel vollständig angegeben und die Stellen der Arbeit – einschließlich Tabellen, Karten und Abbildungen -, die anderen Werken im Wortlaut oder dem Sinn nach entnommen sind, in jedem Einzelfall als Entlehnung kenntlich gemacht habe; dass diese Dissertation noch keiner anderen Fakultät oder Universität zur Prüfung vorgelegen hat; dass sie - abgesehen von unten angegebenen Teilpublikationen - noch nicht veröffentlicht worden ist sowie, dass ich eine solche Veröffentlichung vor Abschluss des Promotionsverfahrens nicht vornehmen werde. Die Bestimmungen dieser Promotionsordnung sind mir bekannt. Die von mir vorgelegte Dissertation ist von Herrn Prof. Dr. Ari Waisman betreut worden.

Mainz, im September 2015

Julia Bruttger

9 Publications

Genetic cell ablation reveals clusters of local self-renewing microglia in the mammalian central nervous system

Bruttger J, Karram K., Wörtge S., Regen T, Marini F, Hoppmann N, Klein M, Blank T, Yona S, Wolf Y, Mack M, Pinteaux E, Müller W, Zipp F, Binder H, Bopp T, Prinz M, Jung S and Waisman A

Immunity 2015

Perivascular microglia promote blood vessel disintegration in the ischemic penumbra

Jolivel V, Bicker F, Binamé F, Ploen R, Keller S, Gollan R, Jurek B, Birkenstock J, Poisa-Beiro L, **Bruttger J**, Opitz V, Thal SC, Waisman A, Bäuerle T, Schäfer MK, Zipp F, Schmidt MH.

Acta Neuropathol. 2015

Oligodendrocyte ablation trigger central pain independently of innate or adaptive immune response

Gritsch S, Lu J, Thilemann S, Wörtge S, Möbius W, **Bruttger** J, Karram K, Ruhwedel T, Blanfeld M, Vardeh D, Waisman A, Nave KA, Kuner R.

Nat. Commun. 2014

Homeostasis of Microglia in the Adult Brain: Review of Novel Microglia Depletion Systems

Waisman A, Ginhoux F, Greter M, **Bruttger J**

Trends Immunol. 2015 (*In Press*)